ΠΟΛΥΤΕΧΝΕΙΟ ΚΡΗΤΗΣ
TECHNICAL UNIVERSITY OF CRETE

School of Chemical and Environmental Engineering
TUCrete

PhD Thesis

Production of advanced adsorptive materials based on biochar

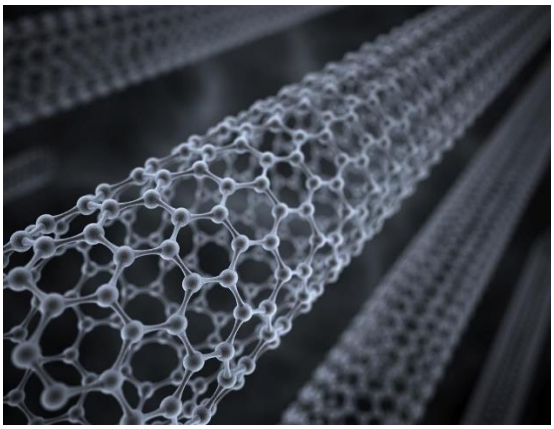

Panagiotis Regkouzas

Supervising committee:

Dr Evan Diamadopoulos, Technical university of Crete

Dr Nikolaos Xekoukoulotakis, Technical University of Crete

Dr Petros Samaras, International Hellenic University

Dr Alexandros Stefanakis, Technical University of Crete

Dr Konstantinos Komnitsas, Technical University of Crete

Dr Stergios Vakalis, University of the Aegean

Dr Dimitrios Gournis, Technical University of Crete

Chania, May 2024

This manuscript is dedicated to my beloved family, who never stopped believing and investing in me during all these years. My deceased father used to quote 'I need to see the evidence that you got it!'. Well dad, this is it! I hope you are having a good time up there and with this you may find some more joy!

Table of Contents

ABSTRACT

Climate change along with the need of CO_2 emissions reduction towards a sustainable way of living in the future has led to the need of reconsidering the linear model that has been followed by humanity so far, thus making a transition into a circular model of resources and waste management. Biochar is a product that is derived from biomass pyrolysis and shows several favourable physicochemical properties, which makes it a good candidate for several applications in different fields. Any type of organic solid waste can be feedstock for biochar production, such as agronomic waste, municipal solid waste, sewage sludge, animal manure, along with other organic industrial wastes. Converting these wastes into biochar changes their initial declaration as "waste" and converts it into resources for new material production. Biochar finds a range of applications, such as soil amendment, adsorptive material, constructed wetland substrate, composting enhancer, energy storage, production of sustainable building materials and solid fuel applications.

This PhD thesis focuses on biochar application as an adsorbent, with the goal to utilize biochar technology to create new advanced and application-targeted adsorptive materials that could be significantly more effective than the conventional ones and can provide a sustainable alternative in difficult-to-manage waste treatment, such as the removal of Emerging Micro-Contaminants from water and wastewater. The produced materials are in total agreement with the principles of circular economy, since a previously consider waste resource is used to create a new material that will be further applied for decontamination purposes. To achieve that, three experimental cycles were implemented to investigate different parameters towards the production of the most effective advanced adsorbent. In the beginning, six different biomasses of agronomic or human derived origin were investigated as feedstocks for biochar production at two pyrolytic temperatures, in order to thoroughly characterize them physicochemically and evaluate their potential for different agronomic and environmental applications. The results of this work showed that higher pyrolytic temperature was more suitable for environmental application of biochar, by providing better carbon stability and more porous structure. Rice Husks was selected as a representative of agronomic waste and Sewage Sludge was selected as a human waste originated biomass to proceed to the next experimental cycle. That involved the production of the nanomaterial Graphene Oxide, which would be further implemented into the two biomasses, in two doses, prior to pyrolysis, resulting to the production of advanced sorptive materials named biochar nanocomposites. The produced samples were physicochemically

characterized, followed by the application of both biochar and biochar nanocomposites as adsorbents for the removal of six Emerging Micro-Contaminants from water and wastewater. Results showed that some biochar nanocomposites could reduce the required amount of adsorption contact time from 60min to 30min, compared to conventional biochar samples, but higher adsorption efficiency was still required, leading to the implementation of the last experimental cycle. That included the implementation of commercially available Carbon NanoTubes into the selected biomasses, leading to the production of CNT-doped biochar nanocomposites. The results concerning the adsorption of the same contaminants from water and wastewater showed that these adsorbents could effectively remove >80% of the pollutants after 5min of contact time, which makes them perfect candidates for filter substrate, used for tertiary water or wastewater decontamination.

Abbreviations

AC: Activated Carbon

AOPs: Advanced Oxidation Processes

BC: Biochar

CNTs: Carbon Nanotubes

EC: Electrical Conductivity

ECs: Emerging Contaminants

EMCs: Emerging Micro-Contaminants

EDs: Endocrine Disruptors

EOP: Exhausted Olive Pomace

EU: European Union

GO: Graphene Oxide

GP: Grape Pomace

MSW: Municipal Solid Waste

OFMSW: Organic Fraction of Municipal Solid Waste

PCPs: Personal Care Products

RH: Rice Husks

SEM: Scanning Electron Microscopy

SS: Sewage Sludge

SSA: Specific Surface Area

STGs: Sustainable Development Goals

UN: United Nations

WTP: Wastewater Treatment Plant

1. Theoretical background

1.1 Biomass pyrolysis

Sustainable waste management is one of the main challenges that environmental engineers face during our times. Under the umbrella of circular economy and sustainability, scientists and engineers started to treat waste as feedstock to produce energy and/or new materials to further minimize the amount of waste that gets disposed of at landfills [Nikolaou et al., 2021]. Biomass is a type of waste that gets generated at high rates of around 250-280Gt per year globally with the biggest percentage of this amount being disposed of in landfills or thrown into the environment. With the continuous and rapid increase of global population the amount of produced waste biomass is going to further elevate, leading to the need of new practises to treat biomass effectively and sustainably [Tiwary et al., 2022]. Biomass waste can be considered anything that originates from living or recently living organisms and can be used to create new products and/or energy. Specifically, some of the main biomass sources are agronomic waste, forestry waste, sub-categories of industrial waste, animal manure, sewage sludge, the organic fraction of municipal solid waste (MSW) and other smaller categories [Ramos et al., 2022]. Thermal/thermochemical techniques can be considered sustainable means of biomass valorisation, providing both new products and energy production and being more environmentally friendly compared to other competitor technologies [Akbarian et al., 2022].

Pyrolysis is one of the main representatives of biomass thermochemical treatment technologies. The main goals of this process are to generate new valuable products, biofuels and thermal/electrical energy, by using low-value and widely available feedstocks, like biomass [Amalina et al., 2022]. The main characteristics of the pyrolysis procedure is that it takes place under anoxic or semi-anoxic (absence of O_2) conditions by providing, usually, N_2 gas and the considerably high operating temperatures (300°C-1200°C) that are needed for biomass decomposition [Tripathi et al., 2016]. The products that are created through the process can be divided into three categories: gaseous (bio-syngas), liquid (bio-oil) and solid (biochar). Pyrolysis conditions, such as biomass type, pyrolysis temperature, residence time, heating rate etc., can be adjusted depending on the most desirable product [Demirbas & Arin, 2002].

Bio-oil is the liquid product of pyrolysis, representing 15-35% of pyrolysis products. It is comprised of a dark-coloured liquid that contains tar and other organic compounds like

oxygenated hydrocarbons [Kan et al., 2016]. Bio-oil is a difficult to manage product due to its contents, low chemical stability and low pH values that make it corrosive and as a result, it should be further treated to create new products, instead of being considered waste. The most difficult to process content of bio-oil is tar, which contains aromatic hydrocarbons, compounds based on O, S, H and N, along with several inorganic compounds, in lower portions [Uddin et al., 2018]. Bio-oil is not so efficient as fuel in its raw form, lacking in calorific value (40-50% of conventional fuels), leading to the need to condense, upgrade and refine it in-situ, after it is generated by the pyrolysis process [Bhoi et al., 2020]. Applying different upgrading techniques, bio-oil can be converted into diesel engine fuel and into several chemical products by adopting chemical treatment methods [Guedes et al., 2018].

Bio-syngas is the gaseous product of pyrolysis and it is comprised of CO, CO_2, CH_4 and in lower ratios of other gases like H_2 and C_2H_4. Bio-syngas is also not generated in high amounts (12-15%), but it can be used directly as fuel to produce thermal or electrical energy and/or cover a large portion of the energy needs of the pyrolysis process itself [Amenaghawon et al., 2021]. Moreover, gases with polluting potential are also generated by the process, such as NO_x, SO_2, H_2S, in lower portions, which can be effectively treated by using proper filtering technology, before releasing them to the atmosphere [Shen et al., 2016]. In order to get the highest possible calorific value of bio-syngas, it is more efficient to collect it after the condensation stage of bio-oil, so that it presents a higher H_2/CO ratio that makes it better as fuel [Lan et al., 2015]. In recent years, researchers found that to create a valuable and sustainable product, it is more efficient to combine the gases straight from the pyrolysis chamber and the gases after bio-oil condensation, resulting to the richest bio-syngas possible, in terms of fuel use [Abou Rjeily et al., 2021].

Biochar is the solid product of biomass pyrolysis and gets generated in the highest portion of 25-45%. It is a porous carbonaceous material that presents several favourable physicochemical properties that make it suitable for several applications in different fields of study [Gao et al., 2020]. Its structure is highly dependable to several pyrolysis conditions like, biomass type, pyrolysis reactor type, pyrolysis temperature, residence time, heating rate and gas supply rate [Buss et al., 2016]. Biochar can be applied to soils as amendment to sequester carbon and improve soil fertility, can be environmentally applied as adsorbent to decontaminate water and soil, can be substrate for constructed wetlands and hydroponics, has been tested as compost process enhancer, can also be used by the capacitor industry as a carbonaceous material and finally it can also be used as solid fuel (charcoal) [Oni et al., 2019]. Biochar has attracted the

interest of several researchers during the last decade due to its unique properties, low cost and the sustainability that defines its production and application. Further information about biochar is available in the upcoming chapter.

1.2 Biochar

Biochar is a rich in organic C material that presents several favourable physicochemical properties compared to the original untreated biomass [Wang & Wang 2019]. When applied as soil amendment for agricultural purposes, it can offer several beneficial properties to the soil and plants. Specifically, it provides a stable C source, which is vital for the micro-biota of the soil by providing them stable food source, it provides macro- and micro- nutrients to the soil increasing its fertility, it makes nutrients more easily available to the plants and prevents nutrient leaching to the soil, increases the water holding capacity of soil leading to lower irrigation needs and provides additional protection to the plants from parasites and diseases [Manolikaki et al., 2016; Enaime & Lübken, 2021]. Moreover, converting biomass into biochar leads to C sequestration and greenhouse effect (in terms of CO_2 emissions) mitigation, by providing a stable carbon source to the soil for more than 100 years, by not being decomposed through time [Nanda et al., 2016]. Additionally, biochar prevents the leaching of heavy metals being present in the feedstock biomass, like in sewage sludge or Municipal Solid Waste (MSW), keeping them in its structure and not making them available to the plants, which protects them from possible toxicity effects [Velli et al., 2021]. One important parameter, though, concerning biochar agronomic application is that it needs an adjustment period (4 to 6 months) at the applied soil, before starting to show its favourable properties [Waqas et al., 2021]. All the above make biochar a suitable organic fertilizer, which might not be as effective as synthetic chemical fertilizers, but it promotes sustainability and the reuse of waste materials towards the production of new valuable products.

Biochar is gathering a lot of attention during the recent years concerning its environmental application as an adsorptive material due to its physicochemical properties that make it suitable for adsorbing organic/inorganic pollutants from water and soil. Specifically, it usually presents high Specific Surface Area (SSA), favourable C content, high porosity and micro-porosity, abundance of surface functional groups and high stability [Wang et al., 2020]. Moreover, it is important to note that there is a small portion of biochar that does not get fully carbonized

during pyrolysis, which provides biochar with some -O containing surface functional groups (carboxylic, hydroxylic and phenolic) that further strengthens biochar adsorptive ability [Abbas et al., 2018]. There are many studies in literature concerning the adsorption of organic or inorganic pollutants on biochar and the involved mechanisms. For inorganic pollutants, like heavy metals, the main adsorption mechanisms are ion exchange, anionic metal attraction, precipitation, cationic metal attraction and physical adsorption, while for organic pollutants the involved mechanisms are electrostatic attraction, polar organic attraction, aromatic and cation -π interactions, hydrophobic interactions, hydrogen bonding, physical adsorption, and partitioning [Ahmad et al., 2014]. Due to this abundance of adsorption mechanisms biochar has the potential to adsorb multiple pollutants, organic and/or inorganic, on the same time, making it a technology that is suitable for soil remediation or water/wastewater treatment purposes.

The physicochemical and structural properties of biochar are strongly dependent on several production parameters. The main parameters that affect biochar properties are the feedstock biomass type, pyrolysis temperature, along with reactor and pyrolysis type, while in lesser extent, reactor heating rate, N_2 supply rate and residence time also play a secondary role concerning the final synthesis of biochar [Dai et al., 2019]. Biomass type is the most important parameter that defines biochar characteristics. There are two main categories regarding biomass origin: agronomic and waste originated biomass. Agronomic biomasses contain higher organic C levels, lower inorganic content in the form of ash, higher calorific value and bulk density, along with lower moisture content, while waste originated biomasses contain high inorganic content, lower C and bulk density levels and less potential for pore development [Leng & Huang, 2018]. Another important factor on biochar characteristics is the operating pyrolysis temperature. Lower pyrolysis temperatures (300-500°C) provide biochar with more graphitic structures, leaving a bigger semi-pyrolyzed portion in its structure, making it a good candidate for agronomic applications, favouring the slow release of nutrients and the interaction of the unpyrolyzed part with soil organic matter [Al-Wabel et al., 2018]. On the other hand, higher pyrolysis temperatures (above 400°C) are more suitable for environmental applications, since biochar shows a more aromatic structure with enhanced porosity and higher SSA, due to the more extended degradation of the organic content of biomass [Tomczyk et al., 2020]. Reactor and pyrolysis type also play a significant role in biochar physicochemical structure. There are several types of pyrolysis (slow, fast and flash pyrolysis, hydro-pyrolysis, microwave-assisted pyrolysis etc.) targeting different pyrolysis products. Slow pyrolysis is the

process that targets on biochar production, providing the highest yields, but biochar can also be produced in lower quantity by the other processes, but it will lack of some favourable characteristics [Ippolito et al., 2020]. Reactor type (fixed bed, rotary-kiln, batch and semi-batch, fluidized-bed and plasma) is also important concerning the heat transfer to the pyrolyzing biomass, biomass yield, produced emissions and biomass carbonization [Gholizadeh et al., 2020]. On the same direction, reactor heating rate, gas supply and residence time also play a secondary role on biochar characteristics. Lower heating rate combined with higher residence time and gas supply result to higher biochar yields and better carbonization [Sakhiya et al., 2020].

1.3 Biochar modification and biochar nanocomposites

The main competitor of biochar in the market of adsorptive materials is activated carbon (AC). AC is also produced by pyrolysis, but usually at higher temperatures and followed by an activation step by supplying steam, CO, CO_2 or compressed air into the pyrolysis chamber, leading to the complete carbonization of biomass, higher porosity and significantly higher SSA [Inyang & Dickenson, 2015]. It is obvious from the above that AC is a higher quality product, but lacks in sustainability compared to biochar, due to the activation part and the use of more resources, while it is more expensive to produce it [Tan et al., 2017]. Biochar technology came to provide a cheaper, more sustainable and still effective solution to the adsorptive material market, but the need to further improve its properties arose, in order to be more antagonistic to AC. As a result, a series of modifications got developed and published in literature that investigated biomass/biochar modifications, prior- or post- pyrolysis, to create either modified biochars or new integrated adsorptive materials based on biochar [Yang et al., 2019].

Surface chemical modification of biochar has attracted a lot of research interest during the recent years. It includes several modification methods such as acidic/alkaline modification and impregnation of metal salts/oxides, each of which targets the development of different characteristics on biochar surface, depending on the desired application [Sizmur et al., 2017]. Acidic modification provides better hydrophilic function of biochar surface and -O containing functional group, while alkaline modification provides higher SSA and creates positive charges on biochar surface helping it to adsorb negatively charged compounds [Rajapaksha et al., 2016]. Metal salts can also be impregnated either to biomass, prior to pyrolysis, or to biochar,

after pyrolysis, which can help with the adsorption of several contaminants through the creation of additional sorption sites [Ahmed et al., 2016]. Another modification process is the treatment of biochar with ferric chloride which results to the formation of γ-Fe_2O_3 nanoparticles and -Fe surface functional groups, making biochar magnetic and favouring its adsorptive abilities towards inorganic contaminants, such as heavy metals [Chin et al., 2021]. Several other methods, physical or chemical, have also been developed and published in literature, but the abovementioned techniques are the most popular and effective.

Another category regarding biochar modification includes the impregnation of functional materials, such as nanomaterials, prior or post pyrolysis on biochar, which does not result in another modified biochar, but to new integrated adsorptive materials based on biochar, called biochar nanocomposites or nanobiochars [Chausali et al., 2021]. These nanomaterials can be graphene, Graphene Oxide (GO), Carbon Nanotubes (CNTs), Chitosan, ZnS nanocrystals, nanoscale zero-valent iron and others. Nanomaterials have gained a lot of scientific interest lately due to their multiple uses in various application fields, their unique physicochemical properties, their thermal and mechanical strength, microporosity and functional groups [Tan et al., 2016]. Biochar nanocomposites present significantly improved physicochemical and structural abilities, such as higher SSA and microporosity, increased pore volume, provision of -O and -C mostly functional groups on their surface, along with additional sorption sites, making them good and advanced sorptive materials for the decontamination of polluted water and wastewater, mostly from organic contaminants [Cheng et al., 2021]. Additionally, Wang et al., 2021 connected biochar nanocomposites and its applications to several of the Sustainable Development Goals (STG) set by the United Nations (UN) to be met by 2030 [UN, 2015], something that highlights the benefits in terms of sustainability that this type of modification provides. Specifically, it contributes to STG 2, 3, 6, 7, 9, 11, 12, 13, 15, as the researchers described in Figure 1.1.

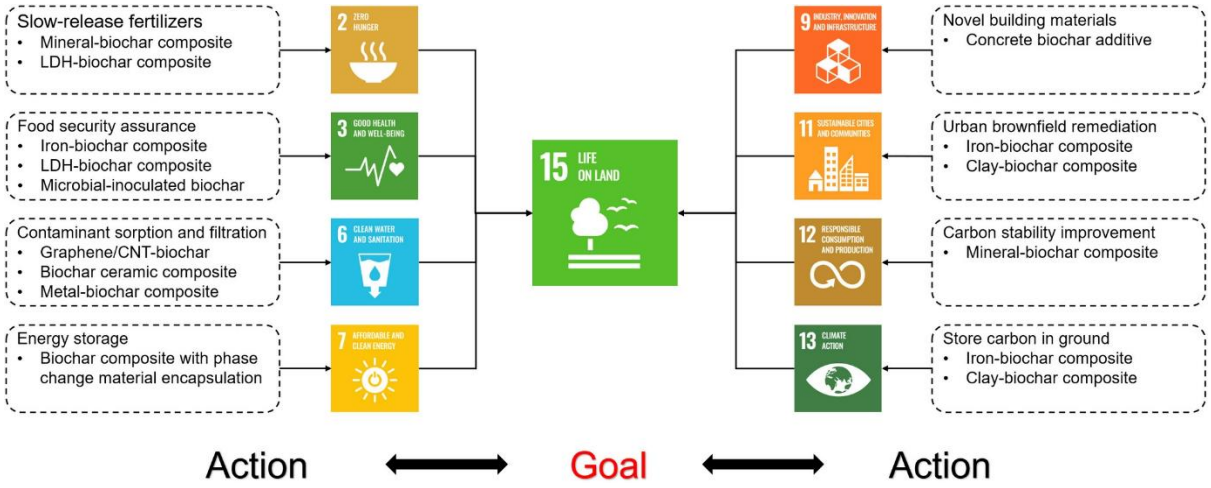

Figure 1.1: Effect of biochar composites application to the Sustainable Development Goals (STGs) set by the EU [Wang et al., 2021]

1.4 Emerging Contaminants (ECs)

Emerging contaminants represent a big family of organic mostly micro-pollutants, which are being increasingly found in WWTP effluents and surface waters during recent years. Their main characteristics are the low concentrations (ng L^{-1} to μg L^{-1}) in which they are being found, along with the inability of conventional wastewater treatment techniques to successfully remove them [Palansooriya et al., 2020]. These contaminants can be pesticides/herbicides, phenols, pharmaceuticals both from human and animal industry, illicit drugs, hormones like estrogens and androgens along with Endocrine Disruptors (EDs), Personal Care Products (PCPs), flame retardants and other minor categories [Richardson & Kimura, 2019]. They may end up in surface waters through various routes, such as WTPs, animal industry, soil leaching, industrial activity, uncontrolled waste disposal,either in their initial form or in the form of their metabolites [Bilal et al., 2019]. When emerging contaminants end up in surface waters and back to the food-chain, they may cause various severe problems to the recipient organisms, the magnitude of which is not yet fully understood. These adverse effects could be cancer formation, mutant-genesis, cell mutations, hormonal and endocrine system disruption, oxidative stress, abnormal physiological processes, development and growth of antibiotic-resistant bacteria and several other partially unknown effects [Sivaranjanee & Kumar, 2021; Gogoi et al., 2018]. Due to the severity of the presence and continuous detection of ECs in wastewater and surface waters, they are monitored and recorded in continuously updating

databases, while the scientific community is working on crating regulations and finding the proper technologies to counterattack this problem [Kumar et al., 2022]. Some of these technologies are methods such as Advanced Oxidation Processes (AOPs) that include ozonation, UV irradiation, Fenton, catalytic/photocatalytic degradation and others, membrane filtration, coagulation and filtration technologies that use adsorptive materials and nanomaterials [Rathi et al., 2021].

2. PhD candidacy experimental description and novelty

In the following chapters, the experimental work of this PhD is presented, divided into three experimental cycles. The first experimental cycle concerns the production of conventional biochar from different biomasses and at different pyrolytic temperatures, with the goal to thoroughly characterize them physicochemically and evaluate their potential for environmental and/or agronomical application. Three waste-originated and three agroindustrial biomasses were selected to produce biochar at two temperatures, characterize and evaluate them, in order to choose the final two that will be used for environmental applications in the following experimental cycles.

In the second experimental cycle, two biomass feedstocks were chosen as a result of the first cycle, Rice Husks (RH) as the agroindustrial biomass that showed the most favourable physicochemical structure for environmental applications as biochar, and Sewage Sludge (SS) as a difficult-to-manage waste that needs alternative solutions concerning its treatment or reuse. These feedstocks were used to produce conventional biochar along with biochar nanocomposites doped with Graphene Oxide (GO), the latter being produced in the laboratory. The produced samples were thoroughly characterized concerning their structural and physicochemical properties and then applied as adsorbents for the removal of six Emerging Micro-Contaminants (EMCs) from water and wastewater.

In the third and last experimental cycle, the same biomasses were used to produce Carbon NanoTube (CNT)-doped biochar nanocomposites, aiming to improve the adsorptive efficiency of the produced materials by adopting a commercial nanomaterial for the enhancement of biochar. The adsorbents of this cycle were proven to be the most effective, leading to the investigation of the mechanisms that were involved in this process, to get valuable insight in the relationship of the adsorbents with the investigated pollutants, so that future biochar nanocomposites can be engineered based on the needs of the applied field.

This PhD thesis includes several novelties, with the most important one being the investigation of EMC adsorption in as close to realistic possible conditions despite the several challenges in terms of initial concentrations (μg/L), while in literature usually higher concentrations are investigated (mg/L). Moreover, the concept of using materials that were previously considered waste to create new sustainable products, which, when further combined with nanomaterials, can be effectively used for water and wastewater decontamination, suggests a novelty of

circular and sustainable concern. Finally, for EMCs being declared hazardous during recent years and being regulated, seeking sustainable technologies based on biochar nanocomposites could be an effective solution to mitigate their environmental problem.

3. Experimental cycle 1. Biochar production from waste biomass: characterization and evaluation for agronomic and environmental applications

ABSTRACT

This chapter focused on the valorization of different types of waste biomass through biochar production at two pyrolysis temperatures (400 and 600°C). The different feedstocks being used included three materials of municipal origin, specifically two types of sewage sludge and the organic fraction of municipal solid waste, and three materials of agroindustrial origin, specifically grape pomace, rice husks and exhausted olive pomace. The scope of the research was to characterize the resulting materials, in order to evaluate their possible uses in agronomic and environmental applications. Biochar characterization included the determination of several physical and chemical parameters, while germination assays were also carried out. Under the investigated conditions, both pyrolysis temperature and feedstock type appeared to significantly affect biochar characteristics, leading to the production of versatile materials, with many different possible uses. Specifically, results implied that biochars of both municipal and agroindustrial origin have the potential to effectively be used in applications including the improvement of soil characteristics, carbon sequestration, the removal of organic and inorganic contaminants from aqueous media, and the remediation of contaminated soil, with the degree of suitability of each material to each specific use being estimated to differ depending on its particular characteristics. For this reason, with these characteristics in mind, before proceeding to larger scale applications a cautious selection of materials should be conducted.

3.1 Introduction

Waste management has become a very important matter during recent years, since waste generation shows a continuously elevating trend causing major environmental implications. There are many categories of waste, where biomass-originated waste materials gained the attention of scientists, both because of their increasing rate of production and because of their potential to be reused to produce energy or manufacture new products with added value [Tripathi et al., 2019]. Biomass wastes are usually divided into two major categories:

agronomic waste that include agronomic residues, forestry waste, agricultural waste and others, along with biological human and animal activity derived waste such as Municipal Solid Waste (MSW), sewage sludge (SS), animal manure and others [Chew et al., 2019].

The continuous increase of wastes has directed global interest to the development of sustainable waste management strategies. One of the most representative examples of rapidly increasing waste production is that of municipal waste (Elkhalifa et al., 2019). In fact, both municipal solid waste (MSW) and sewage sludge (SS) obtained from municipal wastewater treatment plants constitute two priority waste categories which, as a result of the increasing population in urban centers, are continuously generated in large quantities. The importance of these wastes comes not only from their high production rates, but also from their particular composition, since they often contain various potentially toxic elements (e.g. potentially toxic metal(loid)s, pathogens, organic contaminants, etc.) (Agrafioti et al., 2013; Ahmad et al., 2014; Gunarathne et al., 2019; Rybova et al., 2018). Waste and by-products originating from agroindustrial activities represent another category of residual materials with a quite elevated generation rate, especially in countries where agriculture and agro-industries represent important sectors of the economy (Fountoulakis et al., 2008). The wine and olive oil production and the rice processing industries are among the most profitable agroindustries, yet they generate considerable quantities of wastes and by-products. In EU-28 in 2019, the production of grapes for wine, olives for oil, and rice, reached 22,370, 10,255 and 2,841 thousand tonnes, respectively, with Greece accounting for 466, 935 and 222 thousand tonnes, respectively (EUROSTAT, 2020).

Lately, more and more attention has been focusing on the use of waste as resources for both energy and added-value materials, in the framework of a circular economy (Elkhalifa et al., 2019). In this context, waste biomass of not only municipal, but also of agroindustrial origin, could prove quite promising due to both composition and availability.

Converting waste into biochar through pyrolysis is considered a viable method for valorizing such residual resources (Gunarathne et al., 2019). The reason for the increasing interest in biochar comes from the fact that, apart from being an effective method for reducing health and environmental hazards associated with waste biomass, it can find various beneficial applications, including its use as an adsorbent for contaminant removal from water or wastewater, as an amendment for improving soil characteristics and for remediation of contaminated sites (Ahmad et al., 2014; Aller, 2016). This high versatility of biochar is attributed to its wide variety of properties, which depend not only on the pyrolysis conditions

being adopted, but also on the type of feedstock being used (Aller, 2016; Fryda et al., 2019; Rehrah et al., 2016).

Biochar characterization usually includes the investigation of several properties, with each one of them playing a different role in the potential biochar applications. For example, proximate and ultimate composition can give insights regarding biochar stability in soil. High fixed carbon contents, as well as high aromaticity and hydrophobicity have been associated with greater carbon stability and thus a greater ability of biochars to act as carbon sequestration agents (Ahmad et al., 2012; Tag et al., 2016). Such biochars are usually produced at higher temperatures and are more resistant to microbial degradation and mineralization. On the other hand, biochars that are produced at lower temperatures are more hydrophilic and can contribute to increasing soil water holding capacity (Rehrah et al., 2016; Zhao et al., 2017). Determining the electrical conductivity of biochars can reveal their effect on soil quality and fertility (Rehrah et al., 2016; Zhao et al., 2017), while biochars with a large amount of surface functional groups and a high cation exchange capacity can be used in soils for enhancing nutrient exchange sites and for preventing nutrient leaching (Tag et al., 2016; Zhao et al., 2017). Biochar pH can be very important for both agronomic and environmental applications. Since biochars are often moderately to highly alkaline, they can exert liming effects resulting in acid soil amelioration, immobilization of metals in contaminated soils and removal of them from aqueous media (Ahmad et al., 2014). The point of zero charge (pHPZC) is another very important characteristic in terms of contaminant removal from water and wastewater It represents the pH value at which the surface charge of biochar is zero. More specifically, when the pH of the solution is greater than pHPZC, the biochar is negatively charged and tends to attract cations, while when the pH of the solution is lower than pHPZC, the biochar is positively charged and tends to attract anions (Li et al., 2017; Tan et al., 2015). Moreover, while biochars produced at higher pyrolysis temperatures tend to be more effective for sorbing organic contaminants, as a result of their usually higher surface area, microporosity and hydrophobicity, those generated at lower temperatures are more prone to sorbing inorganic and polar contaminants through electrostatic interactions, precipitation/co-precipitation, as well as interaction with surface functional groups (Ahmad et al., 2014). All the above, highlight the importance of a comprehensive characterization, and of the use of such information to thoroughly evaluate biochars for their use in more than one types of applications at the same time. Such an approach will be helpful in directing research towards the most efficient, effective and profitable solutions. In the literature there is a limited number of studies (Ibn Ferjani et al., 2019; Oh et

al., 2012a; Pariyar et al., 2020; Stylianou et al., 2020; Taskin et al., 2019) referring to biochar characterization aiming at both agronomic and environmental uses.

The present study contributes to this regard, by characterizing and investigating biochars of different natures regarding their potential environmental and agronomic uses Six different waste biomass feedstocks, specifically three of municipal origin, namely two types of sewage sludge and the organic fraction of municipal solid waste, and three of agroindustrial origin, namely grape pomace, rice husks and exhausted olive pomace, were used to produce biochar through pyrolysis at two different temperatures, i.e. 400 and 600°C. The resulting carbonaceous materials were then characterized through a series of physical and chemical analyses, and used in germination assays, in order to reveal eventual beneficial, inhibitory or toxic features. The objective of this chapter is to ultimately be able to assess, on the basis of the obtained results, the potential uses of each biochar for either agronomic or environmental purposes.

Nomenclature

CEC cation exchange capacity

EC electrical conductivity

EOP exhausted olive pomace

FC fixed carbon

FT-IR Fourier Transform Infrared spectra

GP grape pomace

OF organic fraction

OFMSW organic fraction of municipal solid waste

pHPZC point of zero charge

PTMs potentially toxic metal(loid)s

SS sewage sludge

SSC sewage sludge from Chania

SSP sewage sludge from Psyttalia

RH rice husks

VM volatile matter

3.2 Materials and methods

3.2.1 Waste biomass feedstocks

Six types of biomass were used as feedstocks for biochar production, namely two types of digested sewage sludge (SS), the organic fraction of municipal solid waste (OFMSW), grape pomace (GP), rice husks (RH) and exhausted olive pomace (EOP). The first SS sample (SSC) was obtained from the Municipal Wastewater Treatment Plant of Chania, Crete, Greece and consisted of anaerobically digested SS that had been mechanically dewatered. The second SS sample (SSP) was obtained from the Psyttalia Wastewater Treatment Plant, Athens, Greece and consisted of anaerobically digested SS that had been dewatered through drying. OFMSW originated from the Inter-municipal Enterprise of Solid Waste Management (DEDISA) of Chania. GP was obtained from a local winery in Chania, while RH originated from a rice mill in northern Greece. Finally, EOP was obtained from the local food industry Mills of Crete.

Prior to pyrolysis the six materials were subjected to a preparation procedure, which differed slightly depending on the material. More specifically, SSC was initially oven dried at 60 ± 5°C for 3 days and then ground to a particle size lower than 500 μm, while for SSP the procedure included only the grinding step, since the material was already dry when received. In the case of OFMSW, the sample was initially manually screened, aiming at removing any unwanted materials (e.g. inert, plastic, metallic and/or hazardous materials) and at leaving only putrescibles and (tissue) paper. Afterwards, the sample was oven dried at 60 ± 5°C for 3 days, further screened for unwanted materials that may have remained after the first screening, and finally ground to a particle size lower than 500 μm. GP was prepared through oven drying and grinding, as earlier mentioned, while RH and EOP were received as agro-industrial productsand were not further processed. The grinding procedures were carried out using either a food processor or a universal cutting mill (Pulverisette 19, Fritsch). After the above mentioned preparation procedures, all biomass feedstocks were stored in closed containers until further use.

3.2.2 Biochar preparation

The pyrolysis process was carried out in a muffle furnace (Linn High Therm) at two different temperatures, 400°C and 600°C, with a heating rate of 3°C/min and a residence period (at the target temperature) of 1 h. These two pyrolysis temperatures were chosen on the basis that

below 300°C pyrolysis of biomass may be incomplete, while above 700°C the amount of carbon left on char is minimum. Inert conditions were ensured by purging nitrogen in the furnace interior with a flow rate of 200 L/h. After cooling, the resulting materials were subjected to a washing procedure with the purpose of removing excess ash and eventual organic substances that may have been produced during pyrolysis. This procedure was adopted as a step in the production process aiming at limiting potential toxic effects of the biochars in future environmental and agronomic applications. In brief, the samples were mixed with deionized water at a solid/liquid ratio of 1/15 g/mL and agitated on an orbital shaking table at 200 rpm for 1 h. The solid and liquid fractions were then separated through vacuum filtration and the solid fractions were finally rinsed with deionized water and oven dried. The final products were homogenized using a mortar and ultimately stored in closed containers until use. Twelve types of biochar were obtained through the above-mentioned procedure, which are presented in Table 3.1.

Table 3.1: Biochar codification

Biomass feedstock	Pyrolysis Temperature (°C)	Codification
SSC	400	SSC400
	600	SSC600
SSP	400	SSP400
	600	SSP600
OFMSW	400	OFMSW400
	600	OFMSW600
GP	400	GP400
	600	GP600
RH	400	RH400
	600	RH600
EOP	400	EOP400
	600	EOP600

3.2.3 Characterization and analytical methods

The biochar materials were characterized regarding certain basic properties, aiming at evaluating their potential use in agronomic and environmental applications. These include proximate (ash, volatile matter (VM), fixed carbon (FC)) and ultimate (CHNS%) composition, contents in mineral elements and major oxides, pH, electrical conductivity (EC), point of zero charge (pHPZC), cation exchange capacity (CEC), zeta potential, bulk density, specific surface area, as well as determination of surface functional groups. The pyrolysis yields were calculated as well, by taking into consideration the initial mass of feedstock and the final mass of carbonaceous material obtained at the end of pyrolysis. Moreover, all biochars were used in germination assays, with Lepidium sativum as a test plant. Waste biomass feedstocks were also characterized, albeit focusing on proximate and ultimate analyses, pH and EC determination, as well as compositional analysis regarding mineral elements.

Proximate and ultimate analyses

Proximate analysis of biochars was carried out on the basis of ASTM method D1762-84, while for biomass feedstocks APHA (American Public Health Association) method 2540G and ASTM method E897-88 were used. Ultimate analysis was determined by flash combustion at 1,020°C using a EuroVector EA300 series elemental analyzer.

pH, EC, pHPZC, CEC, zeta potential

pH and EC were measured in the slurry obtained after agitating the materials with the respective liquid media. In the case of biochars, the materials were agitated both in deionized water (for pH and EC) and in KCl (1N) (only for pH), with a solid/liquid ratio of 1/20 g/mL for 1.5 h (Rajkovich et al., 2012). For the biomass agitation took place in deionized water with a solid/liquid ratio of 1/10 g/mL for 24 h. In order to determine the pHPZC of the different biochars, the pH 'drift' method was adopted, as reported by Uchimiya et al. (2011a). On the other hand, CEC was determined according to EPA method 9081 using sodium acetate and ammonium acetate (EPA, 1986). Zeta potential was measured following the methodology reported by Yao et al. (2011). The measurements were conducted by using a Zetasizer Nano-ZS (Malvern Instruments).

Bulk density and specific surface area

Bulk density was determined according to the method reported by Ahmedna et al. (1997), while the specific surface area of carbonaceous materials was determined using a Nicolet 380 (Thermo), after degassing all samples at 200°C.

Mineral elements and major oxides contents

Mineral element contents of the produced carbonaceous materials and their precursors were determined via Inductively Coupled Plasma Mass Spectrometry (ICP-MS) (CX 7500, Agilent) after sample acid digestion with HNO3. On the other hand, major oxides contents were determined via Energy Dispersive X-ray fluorescence (XRF) (S2 Ranger, Bruker) after fusion (Claisse Fluxer M4) of ignited (1,050ºC) biochar samples (ash samples) with Li-tetraborate.

Surface functional groups

The presence of surface functional groups on the biochars was evaluated by recording the materials' FT-IR spectra with a Fourier transform infrared spectrometer (Perkin Elmer Spectrum 1000) using the KBr pellet technique (sample: KBr = 1:100).

Germination assays

Germination assays were conducted in order to assess the eventual phytotoxic effect of the investigated biochars on Lepidium sativum seed germination and early seedling growth in terms of root elongation. In order to conduct the assays, the twelve biochars were mixed at a 1% rate, on dry basis, with PhytotoxkitTM (MicroBioTests Inc.) reference soil (85% sand, 10%

kaolin and 5% peat, according to the supplier). The amendment rate value (1%) was selected as a representative intermediate value that would provide an indication of the potential effects, either positive or negative, that the investigated biochars may have on higher plants. Briefly, equal quantities of each soil-biochar mixture were placed in circular Petri dishes (90 mm diameter) and wetted with a quantity of deionized water equivalent to 80% of the water holding capacity of the soil (Mumme et al., 2018). The same procedure was also followed using the reference soil with no amendments (Control assay). Afterwards, a piece of filter paper, which was also wetted to 80% of its water holding capacity, was placed inside each dish, on top of the soil mixtures and 10 seeds of Lepidium sativum were arranged in line on the filter paper, at a distance of at least 1 cm from the edge of the dish. Finally, both test (soil-biochar mixtures) and control dishes were covered with their lids and placed inside an incubation chamber set at 25°C at a 50-60° angle. After 3 d, digital images of the dishes were acquired and root lengths were determined through image analysis, using the ImageJ software. All assays were conducted in triplicates.

In order to evaluate the results, two parameters, i.e. the Germination Index (GI) and the Root Growth Inhibition (RGI), were calculated, according to literature (Nieto et al., 2016; Oleszczuk and Hollert, 2011):

$$GI=G\cdot(RLt/RLc) \quad (1)$$

$$RGI=(RLc-RLt)/RLc \quad (2)$$

where G is the percentage of seeds germinated in the test assays (germination rate), RLt is the mean root length of the seeds germinated in the test assays, and RLc is the mean root length of the seeds germinated in the control assays.

3.3 Results and discussion

3.3.1 Yield and proximate analysis

As shown in Figure 3.1 the pyrolysis yield was negatively correlated with the increase in pyrolysis temperature. In fact, while the yield obtained at 400°C ranged between 30.4 and 54.9%, the yield obtained at 600°C varied from 26.3 to 46.2%. Moreover, when comparing different feedstocks, higher yields and thus higher biochar quantities were obtained from the two sewage sludge types, SSC and SSP, followed by OFMSW, RH and GP. The lowest yields were associated with EOP pyrolysis.

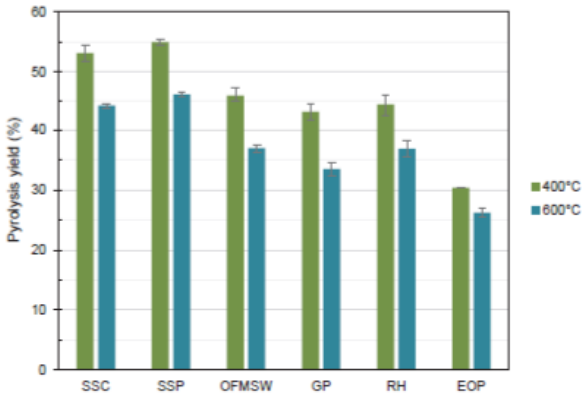

Figure 3.1: Pyrolysis yields for the six feedstocks at two temperatures (error bars represent standard deviations)

Proximate analysis (Figure 3.2) showed that the carbonaceous materials produced at 400°C contained less ash and more volatile matter, as compared to those produced at 600°C. As far as the FC contents are concerned, the results depended on the material origin. For biochars obtained from feedstocks of municipal origin, FC appeared to be decreasing as a function of pyrolysis temperature, while the opposite was observed for biochars obtained from feedstocks of agroindustrial origin.

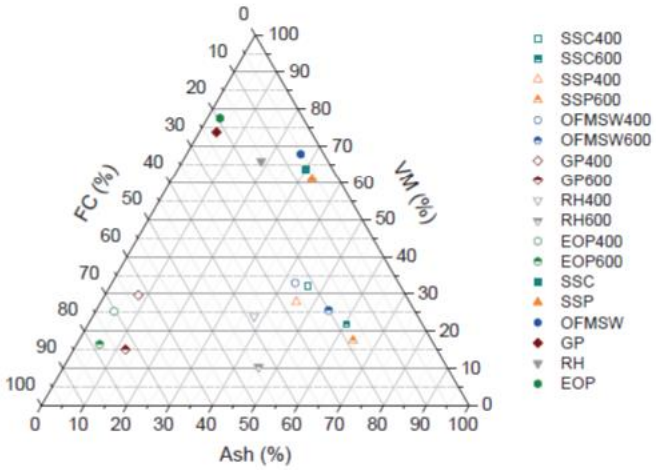

Figure 3.2: Proximate analysis of feedstocks and biochars

The decrease in pyrolysis yield with increasing temperature has been associated with decomposition of organic matter, as well as with dehydration of hydroxyl groups (Rehrah et al., 2016; Stefaniuk and Oleszczuk, 2015). This phenomenon was corroborated by the analogous reduction in VM contents (Zhao et al., 2017), which in turn resulted in an increase in the concentration of inorganic matter (Suliman et al., 2016; Tag et al., 2016; Zhao et al., 2017) and thus, in increased ash content. As far as FC is concerned, the trends observed in the present study, i.e. both increasing and decreasing trends as a function of temperature, has also been reported by other authors (Ahmad et al., 2012; Ahmad et al., 2014; Gómez et al., 2016; Hossain et al., 2011; Jin et al., 2014; Pellera and Gidarakos, 2015; Rajkovich et al., 2012; Suliman et al., 2016; Taherymoosavi et al., 2017; Zhao et al., 2017), and they may be associated with the ash content of the investigated materials. In fact, Enders et al. (2012) noticed that for materials with ash content above 20%, FC decreased as a function of pyrolysis temperature, while the opposite happens for materials with ash contents below 20%. These authors attributed this phenomenon to interactions between organic and inorganic constituents of the pyrolyzed materials during thermal treatment (Enders et al., 2012).

As far as the influence of feedstock type is concerned, the ash and VM contents of the six feedstocks exerted a significant effect both on the pyrolysis yield and on the proximate composition of the resulting biochars. In fact, pyrolyzing the material with the highest ash content, i.e. SSP, yielded not only a higher amount of biochar, but also higher-ash-containing materials. Such a relation between yield and ash content was highlighted also in previous studies (Song and Guo, 2012; Suliman et al., 2016).

3.3.2 Ultimate analysis

Ultimate analysis results (Table 3.2) demonstrated that feedstock origin played an important role in biochar composition. This was particularly evident when observing the biochar C content. Indeed, while biochars of municipal origin were characterized by C content ranging from 25.9 to 39.5%, for biochars of agroindustrial origin a much higher range of values was noticed, from 42.2 to 93.7%. H and N contents also presented differences in their range of values for different materials, with biochars of agroindustrial origin being characterized by generally lower values. As far as the influence of pyrolysis temperature is concerned, higher temperatures seemed to be generally associated with lower H and N contents, while in the case of C, reduced and increased values were observed for materials of municipal and agroindustrial origin, respectively.

Table 3.2: Ultimate analysis of feedstocks and biochars, on a dry basis

Element	Municipal feedstocks									Biochars												
	SSC			SSP			OFMSW			SSC400			SSC600			SSP400			SSP600			OFMSW400			OFMSW600		
C (%)	35.8	±	0.0	36.4	±	0.5	37.3	±	0.3	29.3	±	0.8	27.5	±	0.3	27.3	±	0.2	25.9	±	0.4	39.5	±	1.8	30.3	±	0.8
H (%)	11.9	±	0.0	12.4	±	0.3	9.33	±	0.25	3.01	±	0.99	1.88	±	0.03	2.77	±	0.18	0.56	±	0.09	2.06	±	0.02	0.75	±	0.03
N (%)	4.84	±	0.38	4.71	±	0.10	1.49	±	0.06	3.64	±	0.14	2.57	±	0.11	3.07	±	0.11	2.23	±	0.22	1.57	±	0.08	1.13	±	0.05
S (%)	< DL			< DL			< DL			< DL			< DL			< DL			< DL			< DL			< 0.4		
O * (%)	17.4	±	0.4	13.8	±	0.3	25.2	±	0.4	17.8	±	1.4	7.65	±	0.38	21.1	±	0.4	7.15	±	0.32	14.0	±	1.8	13.0	±	0.9
H:C	3.98	±	0.01	2.50	±	0.01	3.01	±	0.08	1.24	±	0.40	0.82	±	0.02	1.22	±	0.08	0.26	±	0.05	0.63	±	0.03	0.30	±	0.00
O:C	0.36	±	0.01	0.22	±	0.00	0.51	±	0.01	0.46	±	0.05	0.21	±	0.01	0.58	±	0.01	0.21	±	0.01	0.27	±	0.05	0.32	±	0.03
(O+N):C	0.48	±	0.00	0.39	±	0.01	0.54	±	0.01	0.56	±	0.05	0.29	±	0.01	0.68	±	0.01	0.28	±	0.01	0.30	±	0.05	0.35	±	0.03
Element	Agroindustrial feedstocks									Biochars												
	GP			RH			EOP			GP400			GP600			RH400			RH600			EOP400			EOP600		
C (%)	48.1	±	0.7	40.0	±	0.6	47.3	±	0.2	69.1	±	5.3	83.9	±	1.3	42.2	±	1.2	43.4	±	1.8	83.2	±	0.9	93.7	±	0.4
H (%)	9.23	±	0.56	8.62	±	0.13	9.84	±	0.06	5.34	±	0.08	2.17	±	0.19	2.05	±	0.10	1.19	±	0.02	1.84	±	0.90	1.32	±	0.13
N (%)	2.53	±	0.20	0.54	±	0.06	1.00	±	0.19	2.82	±	0.57	0.71	±	0.12	0.38	±	0.02	0.27	±	0.03	0.02	±	0.00	< DL		
S (%)	< DL			< DL			< DL			< DL			< DL			< DL			< DL			< DL			< DL		
O * (%)	36.2	±	0.6	32.5	±	0.5	38.9	±	0.3	14.9	±	4.8	1.10	±	1.06	17.6	±	1.3	9.54	±	1.78	10.6	±	1.0	<0.1		
H:C	2.30	±	0.16	2.59	±	0.06	2.50	±	0.01	0.93	±	0.06	0.31	±	0.03	0.58	±	0.02	0.33	±	0.02	0.27	±	0.13	0.17	±	0.02
O:C	0.56	±	0.01	0.61	±	0.02	0.62	±	0.01	0.16	±	0.06	0.01	±	0.01	0.31	±	0.03	0.17	±	0.04	0.10	±	0.01	0.00	±	0.00
(O+N):C	0.61	±	0.01	0.62	±	0.02	0.64	±	0.01	0.20	±	0.07	0.02	±	0.01	0.32	±	0.03	0.17	±	0.04	0.10	±	0.01	<0.01		

*DL: Detection Limit , * determined by difference , values are expressed as average ± standard deviation*

The decrease in H and O contents with increasing pyrolysis temperature is quite common in the literature and is usually attributed to breakage of weak bonds in the biochar structure (Al-Wabel et al., 2013; Rehrah et al., 2016). As far as the C content is concerned, the most commonly observed behavior is its increase as a function of temperature (Colantoni et al.,

2016; Gómez et al., 2016; Ibn Ferjani et al., 2019; Tag et al., 2016) and it is usually an indication of an intensified carbonization (Rehrah et al., 2016). On the other hand, C loss has also been reported (Cao and Harris, 2010; Kah et al., 2016; Lu et al., 2013). This phenomenon can most likely be associated with the composition of the biomass feedstocks being used, and particularly with their relatively high ash content, as was also concluded by Kah et al. (2016).

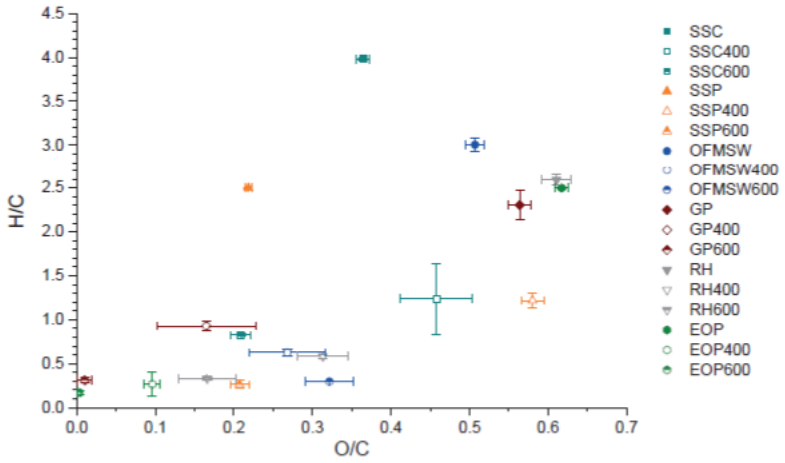

Figure 3.3: van Krevelen diagram (error bars represent standard deviation)

The ratios H:C and O:C are often used in order to determine the degree of aromaticity and polarity of biochars, respectively, with lower H:C ratios characterizing more aromatic materials and lower O:C ratios characterizing less hydrophilic materials (Ahmad et al., 2012; Rehrah et al., 2016). As it is observed in the Van Krevelen diagram (Figure 3.3), in this study both ratios decreased with increasing pyrolysis temperature, a behavior that has previously been associated with the occurrence of dehydration reactions during pyrolysis, as well as with a higher degree of carbonization for the obtained materials (Rehrah et al., 2016; Tag et al., 2016; Zhao et al., 2017). The highest H:C and O:C values were observed for biochars produced from the two sewage sludge feedstocks, i.e. SSC and SSP, at 400°C. Such elevated values may be attributed to the existence of residual organic material in the biochar (Ahmad et al., 2012; Rehrah et al., 2016). Moreover, the lower H:C values of biochars produced at 600°C suggest higher aromaticity, thus higher recalcitrance for these materials, while higher O:C values of biochars produced at 400°C indicate lower hydrophobicity, which could result in a higher water retention ability (Rehrah et al., 2016). Apart from the two abovementioned ratios, (O+N):C is also used as a polarity index (Ahmad et al., 2012; Oh et al., 2012a). This ratio presented a

generally decreasing trend with pyrolysis temperature (Table 2.2), indicating a progressive loss of polar surface functional groups (Ahmad et al., 2012).

3.3.3 pH, EC, pH_{PZC}, CEC, zeta potential

Pyrolysis resulted in materials with higher pH values (Table 3.4) compared with their respective precursors (Table 3.3), while biochar pH also increased with increasing production temperature. This behavior may be attributed to phenomena occurring during pyrolysis, such as the progressive loss of acidic functional groups from the materials surface (Mukherjee et al., 2011; Stefaniuk and Oleszczuk, 2015), as well as the separation of alkali salts from the materials organic matrices (Al-Wabel et al., 2013). It has also been previously associated with the increase in ash content of the biochars during pyrolysis (Rehrah et al., 2016; Tag et al., 2016). According to the obtained data all tested carbonaceous materials can be characterized as alkaline, with biochars of agro-industrial origin generally showing higher values, with the exception of RH400, which not only was associated with the lowest pH values among all materials, but it was also characterized as acidic.

Table 3.3: pH and EC of feedstocks

Properties	Municipal feedstocks									Agroindustrial feedstocks								
	SSC			SSP			OFMSW			GP			RH			EOP		
pH	7.09	±	0.03	7.10	±	0.08	6.11	±	0.04	3.82	±	0.06	5.91	±	0.02	5.50	±	0.23
EC (mS/cm)	2.00	±	0.01	2.18	±	0.06	7.95	±	0.12	2.53	±	0.02	0.79	±	0.01	2.01	±	0.04

Table 3.4: Chemical and physical properties of biochars

Properties	Biochars of municipal origin																	
	SSC400			SSC600			SSP400			SSP600			OFMSW400			OFMSW600		
Chemical properties																		
pH (DW)	7.53	±	0.04	7.45	±	0.04	7.94	±	0.05	8.63	±	0.06	8.50	±	0.06	9.76	±	0.04
pH (KCl)	7.40	±	0.05	7.43	±	0.02	7.27	±	0.01	8.05	±	0.01	8.38	±	0.03	9.50	±	0.04
pH_{PZC}	7.14	±	0.05	7.20	±	0.05	7.11	±	0.05	7.41	±	0.05	8.30	±	0.05	9.47	±	0.05
EC (μS/cm)	429	±	7	326	±	12	333	±	9	199	±	2	1785	±	80	871	±	7
CEC (meq/kg)	176	±	1	126	±	2	371	±	2	180	±	2	388	±	17	257	±	10
Zeta potential (mV)	-9.84	±	1.24	-11.5	±	1.8	-10.2	±	2.8	-11.9	±	1.7	-9.97	±	1.93	-13.8	±	2.9
Physical properties																		
Specific surface area (m^2/g)	2.87	±	0.03	23.8	±	3.4	14.4	±	0.1	52.5	±	5.9	8.03	±	0.82	101	±	4
Bulk density (kg/m^3)	711	±	12	945	±	11	652	±	9	751	±	3	400	±	2	464	±	0
Properties	**Biochars of agroindustrial origin**																	
	GP400			**GP600**			**RH400**			**RH600**			**EOP400***			**EOP600***		
Chemical properties																		
pH (DW)	9.05	±	0.04	9.93	±	0.22	6.49	±	0.06	9.23	±	0.03	9.52	±	0.16	10.05	±	0.04
pH (KCl)	7.76	±	0.04	9.23	±	0.10	4.44	±	0.03	7.36	±	0.06	8.02	±	0.27	9.03	±	0.06
pH_{PZC}	7.45	±	0.05	8.14	±	0.05	6.33	±	0.05	7.72	±	0.05	7.32	±	0.05	7.75	±	0.05
EC (μS/cm)	422.7	±	26.2	468.0	±	55.7	179.6	±	3.2	190.5	±	3.7	267.3	±	7.8	341.3	±	7.4
CEC (meq/kg)	196	±	28	134	±	3	494	±	25	212	±	2	203	±	4	119	±	2
Zeta potential (mV)	-20.4	±	1.3	-19.3	±	1.7	-12.2	±	0.4	-13.4	±	1.1	-11.2	±	1.5	-15.7	±	2.7
Physical properties																		
Specific surface area (m^2/g)	1.29	±	0.05	21.8	±	5.4	59.4	±	2.3	215	±	7	6.85	±	2.76	128	±	7
Bulk density (kg/m^3)	515	±	22	516	±	12	303	±	27	312	±	11	357	±	23	365	±	29

** these materials were analysed in particle form in all cases except specific surface area analysis (materials ground in mortar), values are expressed as average ± standard deviation*

In terms of pHPZC, the results were consistent with pH data, with values being lower compared with the respective pH values. The differences were more significant for biochars of agro-industrial origin. On the contrary, CEC of the tested materials decreased with increasing production temperature. CEC presented relatively high values ranging from 119 to 494 meq/kg. This behaviour for both parameters was a consequence of the intensified removal of surface functional groups at higher pyrolysis temperatures (Inguanzo et al., 2002; Lu et al., 2013; Suliman et al., 2016; Tag et al., 2016; Zhao et al., 2017).

In the case of EC, its variation as a function of pyrolysis temperature followed a different behavior for materials of different origin (Table 3.4). Specifically, for biochars of municipal origin a decrease was observed, while for those of agroindustrial origin the values were found to increase. Most studies refer to a positive correlation between EC, pH and ash contents (Rehrah et al., 2016; Song and Guo, 2012), which in turn comes as a result of volatile material loss (Stefaniuk and Oleszczuk, 2015); however an opposite behavior has also been observed in previous studies (Hossain et al., 2011; Luo et al., 2014; Manolikaki et al., 2016; Oh et al., 2012a). In addition, biochar EC values were lower compared with those of their respective precursors (Table 2.3).

EC is often used to estimate salinity and as an index for evaluating the quality of fertilizers. More specifically, if a biochar is characterized by high salinity, it is usually not recommended for soil applications, due to potential harmful effects on plants, while very low salinity is also undesirable (Tag et al., 2016). According to a classification reported by Belyaeva et al. (2012), materials with EC values (determined with a 1:5 soil:water ratio) between 500 and 1500 μS/cm are considered moderately saline, those in the range 1500-2000 μS/cm, extremely saline, while those above 2000 μS/cm, too saline for most plants. Assuming that the dilution factor between the above mentioned ratio and the one used in the present study (1:20) applies for EC values (Singh et al., 2017), most biochars might be characterized as moderately saline, whereas SSC400, GP400 and GP600 as extremely saline, and OFMSW400 and OFMSW600 as too saline for most plants.

As far as zeta potential is concerned, negative values for all biochars revealed the negative surface charge of the materials (Yargicoglu et al., 2015), while the increasing electronegativity with increasing pyrolysis temperature is in agreement with previous results (Mukherjee et al., 2011).

3.3.4 Specific Surface Area and bulk density

In terms of physical characteristics (Table 3.4), specific surface area and bulk density, a positive effect of pyrolysis temperature on these two parameters was observed. Increased surface area for biochars produced at 600°C is in agreement with the findings of other authors (Cao and Harris, 2010; Randolph et al., 2017) and is most likely a result of the progressive decomposition of organic matter and the more intense formation of micropores and channels within the structure of the biochars (Ahmad et al., 2012; Zhao et al., 2017). However, in the present study, the differences between lower- and higher-temperature biochars were very pronounced, or in other words, the specific surface areas of all materials produced at 400°C were comparatively quite low. Such a phenomenon has been previously reported in the literature and has been associated with partial blockage of pores by condensed volatile materials (tars), inorganic compounds (ash), and/or other amorphous decomposition products (Rehrah et al., 2014).

As far as bulk density is concerned, this parameter is often determined for biochar materials, especially when they are intended for soil applications, since it affects soil quality, particularly

in terms of porosity and compaction (Rehrah et al., 2016). In this study there was a positive relation between bulk density and pyrolysis temperature, in agreement with Rajkovich et al. (2012) and Rehrah et al. (2016).

3.3.5 Mineral elements content

Table 3.5 presents the results regarding the mineral elements content of the twelve biochars, obtained after acid digestion. Generally, biochars of municipal origin were richer in mineral elements compared with biochars of agroindustrial origin, with total concentrations ranging at levels of approximately 47-91 g/kg and 3.4-20 g/kg, respectively. For the former biochars, the most abundant element was Ca, with particularly elevated concentrations ranging from 32 g/kg (SSC400) to 82 g/kg (OFMSW600). Among other elements found also at relatively elevated concentrations, in the region around 1-10 (±2) g/kg, were, for SS-derived biochars Fe, Mg and Al, plus K and Na for SSP400 and SSP600, and for OF-derived biochars Mg, K, Na, Fe and Al. All the other tested elements, including potentially toxic metal(loid)s (PTMs), were found in concentrations not exceeding 0.8 g/kg (or even 0.2 g/kg in certain cases). Nevertheless, to this regard, the fact that in SS-derived biochars there was a more pronounced presence of Zn, Pb, Cu, Mn and Cr, compared with OF-derived biochars, is noteworthy. As far as agroindustrial biochars are concerned, the elements with the two highest concentrations were Ca and K, with the former being the most abundant for GP-derived biochars (max. ~11.6 g/kg), and the latter for RH- and EOP-derived biochars (max. ~4.6 g/kg). Intermediate concentrations, with values around 0.1-1.2 (±0.02) g/kg depending on the material, were measured for elements such as Mg, Fe, Mn, Al and Na. Finally, in this case, all elements found in lesser quantities reached values below 0.1 g/kg. It is worth mentioning that the orders of magnitude, as well as rank orders in each case, varied depending on the biochar feedstock.

Table 3.5: Mineral element content (mg/kg) of feedstocks and biochars, on a dry basis

Element	Municipal feedstocks			Biochars					
	SSC	SSP	OFMSW	SSC400	SSC600	SSP400	SSP600	OFMSW400	OFMSW600
B	7.27 ± 0.09	6.91 ± 0.12	9.23 ± 0.43	9.17 ± 1.47	8.30 ± 0.33	8.82 ± 0.02	8.24 ± 0.87	11.9 ± 0.4	15.7 ± 1.7
Na	274 ± 28	722 ± 9	1931 ± 8	314 ± 50	340 ± 8	700 ± 8	890 ± 102	1044 ± 61	1236 ± 9
Mg	1165 ± 8	2521 ± 15	1222 ± 84	1773 ± 284	1930 ± 62	3838 ± 7	4423 ± 505	1949 ± 59	2496 ± 8
Al	689 ± 8	4503 ± 65	395 ± 38	1070 ± 181	1593 ± 54	7293 ± 116	8074 ± 844	869 ± 14	1996 ± 35
K	212 ± 7	641 ± 6	3999 ± 123	314 ± 54	348 ± 10	992 ± 8	1181 ± 128	1788 ± 130	1890 ± 14
Ca	20637 ± 360	31035 ± 523	38679 ± 4658	32123 ± 5619	36036 ± 1205	51945 ± 411	55461 ± 6504	65207 ± 2162	81895 ± 793
Cr	12.1 ± 0.0	156 ± 2	5.34 ± 0.80	18.9 ± 3.1	16.3 ± 0.4	237 ± 5	191 ± 19	6.72 ± 0.35	9.13 ± 0.25
Mn	65.6 ± 0.1	55.9 ± 1.8	42.6 ± 10.7	109 ± 16	129 ± 3	102 ± 1	107 ± 11	85.9 ± 11.2	94.0 ± 4.2
Fe	9987 ± 153	2282 ± 8	716 ± 42	10462 ± 1404	10521 ± 396	2862 ± 82	3027 ± 175	905 ± 31	1213 ± 133
Co	0.52 ± 0.00	1.02 ± 0.01	0.40 ± 0.04	<1.37	<1.37	<1.37	<1.36	<1.36	<1.37
Ni	7.38 ± 0.15	22.4 ± 0.0	13.5 ± 15.0	16.4 ± 2.4	10.1 ± 0.2	34.1 ± 0.7	27.7 ± 3.5	5.29 ± 0.53	9.05 ± 0.14
Cu	87.1 ± 12.5	195 ± 7	30.0 ± 3.0	94.5 ± 8.9	102 ± 2	225 ± 2	205 ± 17	35.1 ± 0.3	59.7 ± 35.5
Zn	283 ± 0	379 ± 10	71.1 ± 3.7	515 ± 61	546 ± 21	705 ± 2	688 ± 63	127 ± 4	125 ± 0
As	1.18 ± 0.01	2.16 ± 0.04	0.20 ± 0.06	1.17 ± 0.11	1.06 ± 0.02	1.87 ± 0.03	1.68 ± 0.11	0.39 ± 0.01	0.54 ± 0.04
Se	<0.33	<0.32	<0.33	0.50 ± 0.22	<0.33	<0.33	<0.33	<0.33	<0.33
Mo	5.07 ± 0.08	3.73 ± 0.04	0.91 ± 0.06	6.97 ± 0.76	6.81 ± 0.13	4.92 ± 0.04	4.69 ± 0.44	0.89 ± 0.32	1.45 ± 0.06
Cd	0.28 ± 0.03	0.46 ± 0.09	<0.030	0.57 ± 0.06	0.58 ± 0.06	0.89 ± 0.03	0.94 ± 0.06	0.059 ± 0.005	0.060 ± 0.004
Hg	1.69 ± 0.05	1.45 ± 0.02	0.32 ± 0.00	0.35 ± 0.07	0.32 ± 0.08	0.44 ± 0.04	0.65 ± 0.14	0.34 ± 0.02	0.30 ± 0.01
Pb	55.9 ± 0.3	74.3 ± 1.7	23.3 ± 6.4	104 ± 13	110 ± 1	148 ± 1	148 ± 16	37.0 ± 3.0	40.4 ± 1.1

Element	Agroindustrial feedstocks			Biochars					
	GP	RH	EOP	GP400	GP600	RH400	RH600	EOP400	EOP600
B	21.6 ± 0.1	2.29 ± 0.15	3.98 ± 0.08	35.2 ± 1.7	10.1 ± 0.3	2.69 ± 0.04	2.34 ± 0.12	6.83 ± 0.12	1.44 ± 0.07
Na	52.5 ± 24.1	54.3 ± 10.9	170 ± 55	49.9 ± 0.5	32.1 ± 6.8	82.0 ± 40.8	60.1 ± 4.6	196 ± 5	88.6 ± 1.1
Mg	589 ± 20	302 ± 77	104 ± 0	1296 ± 71	522 ± 22	470 ± 5	277 ± 20	199 ± 3	42.1 ± 1.3
Al	<0.059	151 ± 118	<0.059	37.4 ± 4.9	36.7 ± 4.0	100 ± 20	128 ± 14	14.3 ± 12.5	4.47 ± 1.26
K	3721 ± 130	1199 ± 47	2935 ± 248	6899 ± 255	2472 ± 72	2074 ± 83	2136 ± 86	4616 ± 68	1908 ± 123
Ca	5407 ± 195	<471	<311	11551 ± 189	8780 ± 339	833 ± 265	520 ± 97	2469 ± 438	636 ± 98
Cr	1.19 ± 1.01	2.88 ± 2.99	0.33 ± 0.05	4.43 ± 5.16	0.38 ± 0.02	1.16 ± 0.36	0.88 ± 0.09	0.33 ± 0.06	0.26 ± 0.00
Mn	7.62 ± 0.16	176 ± 105	4.56 ± 1.91	18.2 ± 0.5	7.22 ± 0.21	202 ± 12	161 ± 8	4.51 ± 0.18	1.69 ± 0.18
Fe	78.4 ± 13.0	61.7 ± 49.7	48.3 ± 27.5	144 ± 22	56.3 ± 6.7	43.5 ± 1.4	73.3 ± 12.5	55.4 ± 17.3	29.5 ± 11.4
Co	<0.22	<0.21	<0.21	<1.36	<1.37	<1.36	<1.37	<1.37	<1.37
Ni	0.24 ± 0.14	0.46 ± 0.49	<0.12	0.57 ± 0.10	0.30 ± 0.17	0.56 ± 0.19	2.10 ± 0.45	1.07 ± 0.86	<0.082
Cu	30.3 ± 1.2	32.4 ± 40.0	26.6 ± 33.2	41.2 ± 0.9	7.77 ± 1.12	4.52 ± 0.03	4.60 ± 0.16	4.81 ± 0.12	1.66 ± 0.13
Zn	14.9 ± 2.1	19.1 ± 7.0	5.86 ± 1.50	32.4 ± 4.3	12.7 ± 3.6	30.8 ± 7.6	23.5 ± 1.7	7.19 ± 2.35	3.36 ± 0.18
As	<0.040	0.12 ± 0.03	<0.040	<0.017	<0.017	0.22 ± 0.01	0.10 ± 0.01	<0.017	<0.017
Se	<0.33	<0.33	<0.32	<0.33	<0.33	<0.33	<0.33	<0.33	<0.33
Mo	0.39 ± 0.09	1.19 ± 1.25	0.20 ± 0.01	0.20 ± 0.01	0.31 ± 0.05	0.21 ± 0.09	0.30 ± 0.02	0.19 ± 0.02	0.22 ± 0.01
Cd	<0.029	<0.029	<0.029	<0.075	<0.068	<0.029	<0.030	<0.030	<0.030
Hg	0.37 ± 0.00	0.35 ± 0.06	0.38 ± 0.08	0.56 ± 0.02	0.55 ± 0.03	0.91 ± 0.04	0.64 ± 0.00	0.49 ± 0.02	0.53 ± 0.00
Pb	0.65 ± 0.40	1.51 ± 1.86	<0.002	1.08 ± 0.08	0.51 ± 0.20	0.63 ± 0.26	0.56 ± 0.16	0.31 ± 0.26	0.13 ± 0.04

values are expressed as average ± standard deviation

Regarding the mineral elements detected in more significant amounts, i.e. Ca, Fe, Al, Mg, K, Mn and Na, pyrolysis resulted in increase in their concentrations (Table 2.5), while further increase in pyrolysis temperature led to mostly increased and mostly decreased concentrations for municipal and agroindustrial biochars, respectively. The results of the present study agree, in general, with similar findings reported elsewhere (Al-Wabel et al., 2013; Cao and Harris, 2010; Hossain et al., 2011; Jin et al., 2014; Lu et al., 2013; Rehrah et al., 2016; Shen et al., 2017; Song and Guo, 2012; Zhao et al., 2017). Regarding PTMs, their values were in general terms comparable to those in the literature (Domene et al., 2015; Jin et al., 2014; Kah et al.,

2016; Pituello et al., 2015), while they did not exceed the limit values set by the Council Directive 86/278/EEC on the use of sludge in agriculture (EC, 2009). As far as the effect of pyrolysis temperature on these elements is concerned, their behaviour was characterized by high variability, with both increasing and decreasing trends being noticed. This is most likely due to the ability of certain elements to volatilize at high temperatures (Hossain et al., 2011; Li and Jiang, 2017; Luo et al., 2014; Pituello et al., 2015; Zhao et al., 2017).

3.3.6 Surface functional groups

The presence of surface functional groups on biocharswas evaluated through the FT-IR spectra illustrated in Figure 3.4. At first glance, it is evident that there is a high degree of pattern similarity between the spectra of the two sewage sludge-derived biochars, as well as between those of GP- and EOP- derived biochars. Moreover, the spectra of the OFMSW-derived biochars, although presenting bands at similar wavenumbers as the SS- derived biochars, differ in terms of band intensity.

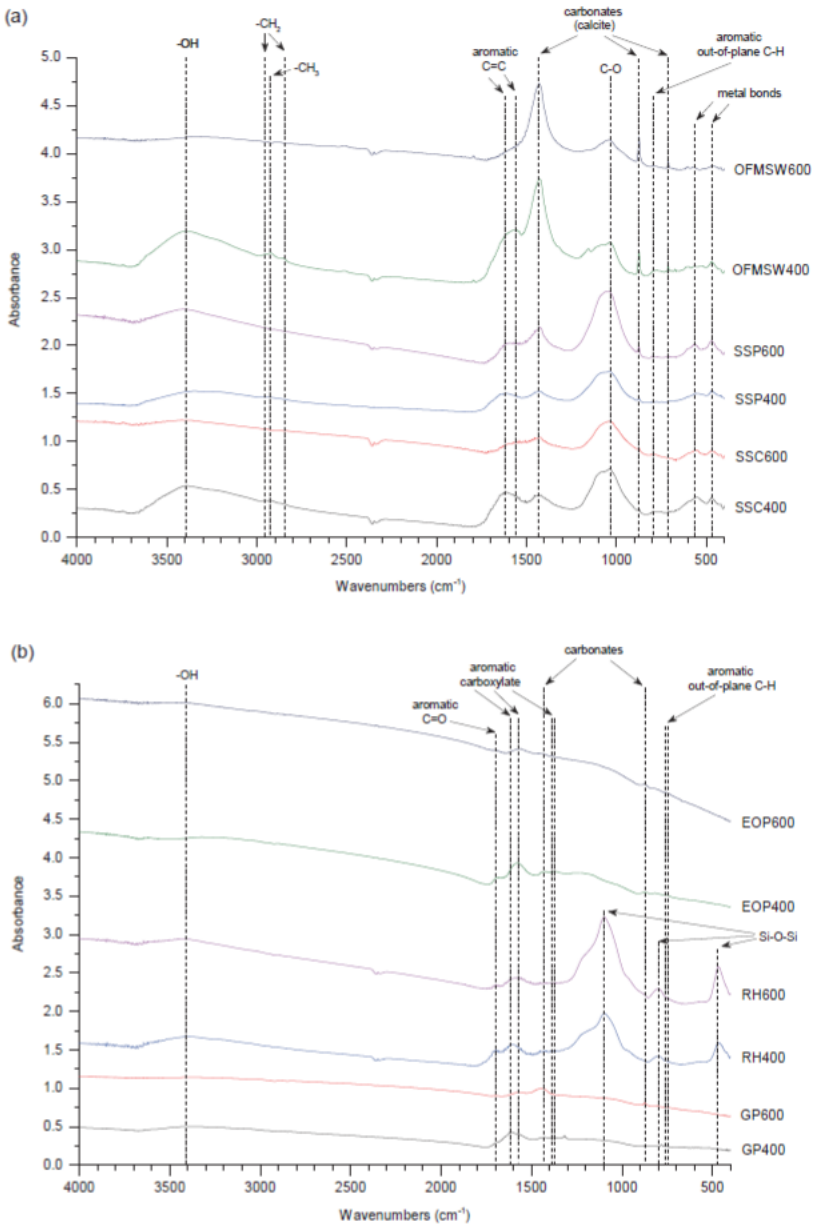

Figure 3.4: FT-IR spectra of (a) municipal and (b) agro-industrial biochars

In more detail, biochars of both municipal and agroindustrial origin, all presented distinct bands with highest points in the range 3418-3350 cm^{-1} and 3442-3328 cm^{-1}, as well as 1616-1558 cm^{-1} and 1614-1574 cm^{-1}, respectively. The former broad bands indicate the presence of hydrogen bonds and may be assigned to O-H stretching (Coates, 2000). As far as the latter bands are concerned, they are usually associated with the presence of aromatic compounds (Coates, 2000) and may be assigned to C=C stretching (Chen et al., 2008) and/or to carboxylate, which is especially likely in the cases of GP400 and EOP400, for which weak peaks at 1384 and 1372 cm^{-1}, respectively, were also observed (Coates, 2000). Moreover, all biochars, except those

derived from RH, presented peaks around 1434 and 874 cm^{-1}, which may be assigned to carbonates (Coates, 2000). Specifically in the case of biochars of municipal origin, these peaks combined with weak peaks at 712 cm^{-1}, are consistent with the possible presence of calcite, whose typical peaks are found around 1433, 874 and 713 cm^{-1} (Jimoh et al., 2017; Nasir et al., 2019). In addition to the above mentioned bands which were common to all biochars, some others were common only among certain materials. Indeed, weak bands with highest points between 2954 and 2864 cm^{-1}, as well as medium to strong peaks between 1046 and 1034 cm^{-1}, were observed only for biochars of municipal origin. The former bands indicate the presence of aliphatic groups, with specific assignments to –CH3 and –CH2 symmetric and asymmetric stretching (Ahmad et al., 2012; Coates, 2000; Hossain et al., 2011), while the latter peaks are most likely attributed to C-O stretching (Zhao et al., 2017). Similarly, weak bands in the range 1698-1694 cm^{-1} appeared only in the spectra of biochars of agro-industrial origin and could be assigned to C=O groups (Gai et al., 2014; Tran et al., 2016), possibly associated with the presence of carboxylic acids on these materials (Coates, 2000). In turn, both RH-derived biochars also presented a characteristic set of peaks, at 1096, 800 and 468 cm^{-1}, which may be assigned to Si-O-Si groups (Wang et al., 2018). Finally, weak bands around 750, 780 and 800 cm^{-1}, and below 600 cm^{-1}, could probably be associated with aromatic out-of-plane C-H bending (Coates, 2000), and the presence of metal bonds (Hossain et al., 2011), respectively. FT-IR spectra patterns and bands similar to those of the present study have also been observed in previous studies investigating materials of similar origins (Chen et al., 2014; Lu et al., 2013; Mitchell et al., 2018; Yi et al., 2016; Taherymoosavi et al., 2017; Trakal et al., 2017; Zhang et al., 2018).

As far as the influence of pyrolysis temperature is concerned, it was noticed that the increase to 600°C resulted in a general intensity reduction for O-H bands around ~3000 cm^{-1}, as well as for aromatic bands around ~1600 cm^{-1}. On the other hand, the peaks attributed to carbonates were preserved, with slight intensity variations. Moreover, while –CH3 and –CH2 bands, present on municipal biochars produced at 400°C, were completely eliminated with the increase in temperature, such an effect was not noticed for C-O peaks being observed for the same materials, with them being preserved. At the same time, while there was no significant change in the carboxylic acid bands of agro-industrial biochars, the increase in temperature most likely caused a reduction in carboxylate groups on the same materials, manifested by the elimination of peaks around ~1380 cm^{-1}. Finally, the bands being observed below 800 cm^{-1} were maintained only for municipal biochars produced at 600°C.

3.3.7 Germination assays

According to the results, none of the biochars had a negative effect on Lepidium sativum germination, since in all assays a 100% germination rate was noted (data not shown). As far as root growth is concerned, according to a scale reported by Nieto et al. (2016), phytotoxicity is indicated when GI values are below 80%, while values above 100% are an indication of phytostimulatory effects. Consequently, none of the examined biochars could be considered as phytotoxic at a 1% amendment rate, since GI values were all above 80% (Figure 3.5). Moreover, six biochars, specifically SSC600, SSP600, GP400, GP600, EOP400 and EOP600 could be considered as phytostimulant under the examined conditions, as a result of their corresponding GIs being greater than 100%. Nevertheless, some degree of inhibition, manifested by positive RGI values (Figure 3.5), was noted for the remaining six biochars, specifically SSC400, SSP400, OFMSW400, OFMSW600, RH400 and RH600.

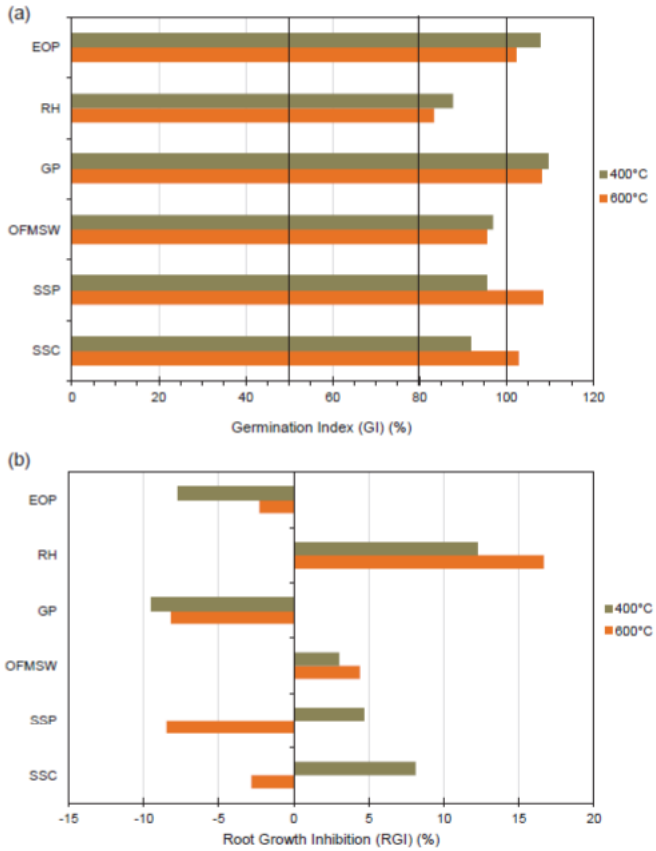

Figure 3.5: (a) Germination Index (GI) (%) and (b) Root Growth Inhibition (RGI) (%) obtained from germination assays with biochar amendment rate 1%

In the literature, root growth inhibition has been mainly associated with the effect that the addition of biochar can exert on the soil solution salinity, by inducing osmotic stress (Buss et al., 2016; Intani et al., 2018; Mumme et al., 2018). This was most likely the reason for the inhibition noticed in the present study for the four biochars of municipal origin, even if this negative effect was quite moderate. Although EC values corresponding to these biochars could suggest such an effect, in reality they could only partially predict the outcome. More specifically, if only EC was considered, the municipal biochars OFMSW400, OFMSW600 and SSC400 would be more likely to cause some inhibition, as mentioned earlier. Nevertheless, SSP400 also showed similar results, although its EC was not equally elevated. Therefore, EC values should not be used as the sole indicator for salinity levels. Such a conclusion was also drawn in a previous study (Buss et al., 2016). What indeed contributed to the increased salinity was most probably the elevated mineral load of the biochars in question (Table 2.5), especially in terms of PTMs. In fact, the elevated presence of such elements, including PTMs, in more soluble form has been previously associated with osmotic stress (Rucińska- Sobkowiak, 2016). Interestingly, OFMSW-derived biochars appeared to cause a lower degree of inhibition compared with the other materials. This could be attributed to the counterbalancing between their high EC and their low cumulative PTMs content, high pH and high macro-nutrient (Ca, K, Na, Mg) content. Indeed, it has been previously reported that at low amendment rates biochars with high pH and K concentrations could have a positive effect on root growth (Buss et al., 2016). Moreover, although SSC600 and SSP600 were also characterized by quite elevated PTMs loads, they showed no inhibiting effects. This could be related to their production temperature, since it has been shown that the bioavailability of PTMs is reduced for biochars produced at higher pyrolysis temperatures (Zeng et al., 2018).

As far as biochars of agroindustrial origin are concerned, the only materials that appeared to cause some inhibition were the two RH-derived biochars, which in fact were those ultimately being associated with the highest RGI values among all tested biochars. These results are not consistent with EC data, since GP400 and GP600, which presented higher EC values than RH400 and RH600, did not cause inhibition, but instead they exerted a phytostimulant effect on Lepidium sativum seeds, as did EOP400 and EOP600. The positive effect of GP- and EOP-derived biochars may most likely be attributed to their pH and macro-nutrient contents (Buss et al., 2016), as well as probably to their comparatively lower PTMs content. On the other hand, the inhibition caused by RH400 and RH600 may be mainly related to the quite pronounced

SiO_2 content of these biochars (Table 3.6), considering that SiO_2 has been reported to eventually have toxic effects on root elongation at elevated concentrations (Lee et al., 2010).

It is worth mentioning that some authors have linked root growth inhibition with the presence of organic water-soluble potentially toxic elements (e.g. PAHs, phenolic compounds, etc.) on biochars (Buss and Mašek, 2014; Gell et al., 2011; Intani et al., 2018). In the present study it was unlikely that such a phenomenon took place, since all biochars were washed before being used in germination assays and this procedure would have removed toxic or inhibitory water-soluble substances (Intani et al., 2018).

3.3.8 Major oxides content

XRF results presented in Table 6 refer only to selected biochars, chosen on the basis of the other characterization analyses and germination assays. Specifically, the selected materials were biochars of municipal origin and RH-derived biochars. According to the data, CaO was present in all biochars derived from SS and OFMSW, which is consistent with the FT-IR spectra regarding the presence of calcite in biochars before ignition (Leontakianakos et al., 2015), especially in the case of OFMSW400 and OFMSW600. Other oxides being detected in considerable amounts in municipal biochars include Fe_2O_3, SiO_2, P_2O_5 and Al_2O_3, while lower percentages of metal oxides in these materials are consistent with the considerations regarding metal bonds made in §2.3.6. Similarly, the results obtained for RH400 and RH600 confirmed the highly significant presence of SiO2 in these materials, again corroborating the FT-IR analysis.

Table 3.6: Major oxides content (%) in ash samples of selected biochars, on a dry basis

	SSC400	SSC600	SSP400	SSP600	OFMSW400	OFMSW600	RH400	RH600
Al_2O_3	2.37	3.66	9.35	10.8	1.85	5.02	0.79	0.78
CaO	21.6	27.7	28.9	29.3	48.7	47.1	0.73	0.89
Cr_2O_3	1.18	0.41	0.80	0.56	0.48	0.14	0.002	0.007
CuO	0.09	0.08	0.13	0.12	<0.005	<0.005	<0.005	<0.005
Fe_2O_3	42.5	28.5	14.2	10.7	8.98	4.59	1.17	1.21
K_2O	0.75	1.04	1.84	2.14	2.01	3.20	0.06	0.20
MgO	0.80	<0.005	2.90	2.90	2.00	3.67	0.84	0.82
MnO	0.43	0.15	0.15	0.11	0.17	0.11	0.15	0.17
Na_2O	<0.005	<0.005	<0.005	2.10	<0.005	2.55	0.78	0.54
NiO	0.73	0.14	0.25	0.15	0.21	0.06	0.02	0.02
P_2O_5	11.4	15.0	16.0	16.0	2.57	2.48	0.13	0.24
PbO	<0.005	<0.005	0.25	<0.005	<0.005	<0.005	<0.005	<0.005
SiO_2	15.4	20.7	22.5	22.8	23.3	25.3	89.2	97.1
SO_3	0.50	<0.005	0.28	0.22	7.27	5.40	<0.005	<0.005
TiO_2	0.90	1.13	1.13	1.12	0.63	0.85	<0.005	<0.005
ZnO	0.28	0.24	0.38	0.38	0.11	0.12	<0.005	<0.005

3.4 Conclusion

The present chapter focused on the characterization of twelve biochars derived from six types of biomass and produced at two temperatures, aiming at evaluating their potential use in agronomic and environmental applications. Both pyrolysis temperature and feedstock type appeared to have a significant effect on biochar characteristics, with the data implying various potential applications for the examined materials.

In terms of agronomic application, based on the characterization results, biochars generated at 400°C may be more able to improve soil characteristics, as well as enhance nutrient and water retention, compared to higher-temperature materials, due to their lower bulk density, as well as higher CEC and hydrophilicity, respectively. On the other hand, biochars obtained at 600°C could offer greater carbon stability due to their higher aromaticity, and thus be more suitable for carbon sequestration. Moreover, almost all biochars of agroindustrial origin, as well as some biochars of municipal origin may be good candidates for ameliorating acid soils, as a result of their high pH values. Although the germination assays showed no phytotoxic effects of the investigated biochars on Lepidium sativum seeds, under the examined conditions and at a soil amendment rate of 1%, prior to real-case use of these materials at rates >1%, a thorough assessment of their potential inhibitory or toxic effects should be performed in relation to the specific application for which they are intended (type of soil, type of plant, etc.). Attention should be given on the biochars' salinity and mineral contents, especially in terms of bioavailability.

As far as environmental applications are concerned, higher CEC as well as the stronger presence of surface functional groups in biochars produced at 400°C, suggest that these materials may be more suitable for metal retention in both soil and aqueous media compared with those produced at 600°C. Moreover, the presence of functional groups coupled with the higher polarity of the low temperature biochars is an indication of a potentially better performance with polar organic contaminants. On the contrary, biochars produced at 600°C, being characterized by higher specific surface area and higher hydrophobicity, may be more effective in remediating contamination by non-polar organic compounds. Furthermore, pH values suggest that several of the studied biochars could be effectively used to induce metal precipitation, while pHPZC values reveal a potential affinity of OFMSW400, OFMSW600 and GP600 also for anionic contaminants.

4. Experimental cycle 2. Production and characterization of graphene oxide-engineered biochars and application for organic micro-pollutant adsorption from aqueous solutions

ABSTRACT

In this chapter, conventional and Graphene Oxide-engineered biochars were produced and thoroughly characterized, in order to investigate their potential as adsorptive materials. Two types of biomass, Rice Husks (RH) and Sewage Sludge (SS), two Graphene Oxide (GO) doses, 0.1% and 1%, and two pyrolysis temperatures, 400°C and 600°C were investigated. The produced biochars were characterized in physicochemical terms and the effect of biomass, GO functionalization and pyrolysis temperature on biochar properties was studied. The produced samples were then applied as adsorbents for the removal of six organic micro-pollutants from water and treated secondary wastewater. Results showed that the main factors affecting biochar structure was biomass type and pyrolysis temperature, while GO functionalization caused significant changes on biochar surface by increasing the available C- and O- based functional groups. Biochars produced at 600°C showed higher C content and Specific Surface Area, presenting more stable graphitic structure, compared to biochars produced at 400°C. Micro-pollutant adsorption rates were in the range of 39.9%-98.3% and 9.4%-97.5% in table water and 28.3%-97.5% and 0.0%-97.5% in treated municipal wastewater, for the Rice Husk and Sewage Sludge biochars respectively. The best biochars, in terms of structural properties and adsorption efficiency were the GO-functionalized biochars, produced from Rice Husks at 600°C, while the most difficult pollutant to remove was 2.4-Dichlorophenol.

4.1 Introduction

Biochar is a carbonaceous solid product that can be produced by biomass pyrolysis or other carbonization processes (Ahmad et al., 2014; Zhao et al., 2021). One of the largest areas of biochar application concerns its environmental use as an adsorbent. High C content, large surface area and porosity, abundance of surface functional groups and other favorable physicochemical properties make biochar a candidate for organic or inorganic pollutant adsorption material from water or soil (Ahmed et al., 2016; Rajapaksha et al., 2016; Liu et al.,

2015). These properties are directly affected primarily by biomass type and pyrolysis temperature and secondarily by pyrolysis residence time and heat rate (Li et al., 2017). Moreover, these properties can be further tuned in by adopting several modification techniques, like acid or base treatment (Wang et al., 2019; Sizmur et al., 2017), or by incorporating in the biochar matrix materials with specific properties, such as carbon nanostructures (graphene, graphene oxide, CNTs) (Tan et al., 2016; Liu et al., 2016), metal oxides (Li et al., 2018), or magnetic materials (Wang et al., 2019), in order to serve targeted applications and needs.

One of these nanomaterials is Graphene Oxide (GO), which is a 2-D graphene sheet that can be produced by using various chemical methods to oxidize graphite (Dimiev & Tour, 2014). GO exhibits high surface chemical reactivity, by the existence of various C- and O- based functional groups and has good thermal and mechanical properties, due to its highly porous nature (De Marchi et al., 2018). The combination of GO with biochar can provide thermally stable products with greater properties and sorptive ability than the conventional biochars, even if used in small quantities (Zhang et al., 2012). For example, when GO is implemented into biochar, it improves biochar surface functional groups (Abdul et al., 2017), the specific surface area and pore volume (Ghaffar & Younis, 2014) and its adsorption ability, mostly for the removal of organic contaminants (Huang et al., 2017, Moyo et al., 2020).

Recently, organic contaminants, like pharmaceuticals, pesticides, hormones, personal care products and illicit drugs have been increasingly being found both in the influent and effluent of WWTPs, as well as in surface waters. Despite the fact that these compounds are being found in relatively small concentrations, the potential damage they can provoke to the recipient environment (surface water and its living organisms) could be great and of unknown scale (Rathi & Kumar, 2021). As a result, organic pollutants are being continuously monitored and studied, both for their occurrence and for the techniques available to treat them efficiently. Moreover, the potentially most dangerous and complicated organic pollutants are being monitored and included in the list of ‘Contaminants of Emerging Concern’, which is being updated and enriched on a yearly basis, due to its importance (Richardson & Kimura 2019; Palansooriya et al., 2019).

The use of waste biomass as feedstock for biochar production, combined with a relatively small dose of GO could lead to a sustainable, cost-effective and enhanced adsorptive material that could compete with other adsorptive materials and could be successfully applied as tertiary treatment for wastewater in WWTPs, in order adsorb difficult to conventionally remove

pollutants, such as ECs (Inyang & Dickenson, 2015; Qiu et al., 2022a). This application of biochar is favorable due to its sorptive abilities that are attributed to its porous nature, high surface area, carbonaceous structure and abundance of surface functional groups that play an active role concerning cost-effective organic or inorganic pollutant adsorption from water and wastewater (Jin et al., 2022). One of biochar main benefits is its ability to effectively remove these pollutants from wastewater even in low initial concentrations, like in realistic conditions (Qiu et al., 2021a; Liu et al., 2023).

As a result, the goal of this chapter was to produce GO functionalized biochars, using two waste biomasses, Rice Husks (RH), which is a carbon rich agronomic waste and Sewage Sludge (SS), which represents a difficult-to-manage, waste-originated biomass, at two pyrolytic temperatures (400°C and 600°C) and two GO doses (0.1% and 1%), in order to thoroughly characterize them and test them as sorptive materials for the adsorption of six organic micro-pollutants of emerging concern from water and wastewater samples. The novelty of this study concerns the extended physicochemical and structural characterization of GO-doped biochar nano-composites, combined with the realistic environmental application of the produced materials as adsorbents for EC removal from water and wastewater, in close-to-realistic initial pollutant concentrations, where usually in literature higher pollutant concentrations are being studied in order to provide easier and clearer trends concerning pollutant adsorption.

Nomenclature

ADT: Androsterone

GO: Graphene Oxide

BPA: Bisphenol A

E1: Estrone

EE2: 17α-Ethinylestradiol

NOR: 19-Norethindrone

RH: Rice Husks

RH400: Biochar from Rice Husks, produced at 400°C

RH600: Biochar from Rice Husks, produced at 600°C

RH_GO0.1_400: Biochar from Rice Husks, with 0.1% GO suspension, produced at 400°C

RH_GO0.1_600: Biochar from Rice Husks, with 0.1% GO suspension, produced at 600°C

RH_GO1_400: Biochar from Rice Husks, with 1% GO suspension, produced at 400°C

RH_GO1_600: Biochar from Rice Husks, with 1% GO suspension, produced at 600°C

SEM: Scanning Electron Microscope

SPME: Solid Phase Micro-Extraction

SS: Sewage Sludge

SS400: Biochar from Sewage Sludge, produced at 400°C

SS 600: Biochar from Sewage Sludge, produced at 600°C

SS _GO0.1_400: Biochar from Sewage Sludge, with 0.1% GO suspension, produced at 400°C

SS _GO0.1_600: Biochar from Sewage Sludge, with 0.1% GO suspension, produced at 600°C

SS_GO1_400: Biochar from Sewage Sludge, with 1% GO suspension, produced at 400°C

SS_GO1_600: Biochar from Sewage Sludge, with 1% GO suspension, produced at 600°C

WWTP: Wastewater Treatment Plant

2-4D: 2, 4-Dichlorophenol

4.2 Materials and Methods

4.2.1 Reagents

The reagents used in this work are described in the following list:

Androsterone 97,7%, Sigma Aldrich, CAS Number: 53-41-8.

Bisphenol A 99,5%, Dr Ehrenstorfer, CAS Number: 80-05-7.

Estrone 99,3%, Sigma Aldrich, CAS Number: 53-16-7.

Graphite powder, BAYCARBON Inc., Product SP-1.

Hydrochloric Acid, Sigma Aldrich, CAS Number: 7647-01-0.

Hydrogen Peroxide, Chem-Lab, CAS Number: 7722-84-1.

Nitric Acid, Sigma Aldrich, CAS Number: 7697-37-2.

19-Norethindrone 99.6%, Sigma Aldrich, CAS Number: 68-22-4.

Orthophosphoric Acid, Scharlau, CAS Number: 7664-38-2.

Potassium Bromide, Fluka, CAS Number: 7758-02-3.

Potassium Permanganate, Merck, CAS Number: 7722-64-7.

Sulfuric Acid, Sigma Aldrich, CAS Number: 7664-93-9.

Vanadium Pentoxide, Merck, CAS Number: 1314-62-1.

17α-Ethinylestradiol 99,5%, Dr Ehrenstorfer, CAS Number: 57-63-6.

2,4-Dichlorophenol 99,7%, Supelco, CAS Number: 120-83-2.

4.2.2 Graphene oxide production

GO was produced by adopting a modified Hummers method (Hummers & Offeman, 1958). Briefly, 12g of graphite powder were added into a conical flask, along with 1440mL of H_2SO_4 and 160mL of H_2PO_4. The mix was stirred overnight at 300rpm. Next, the flask was placed in an ice-bath, until the temperature dropped to 0±2°C. Then, 72g of $KMnO_4$ were gradually added for oxidation to take place. After approximately 4 to 5 hours, the temperature rose to 20±2°C and 250mL of H_2O_2 were added to neutralize excess $KMnO_4$. The mix was centrifuged to retrieve the oxidized graphite, washed with 3.6% HCl and centrifuged again after 1d. The next step was the exfoliation process, where the sample was daily centrifuged and washed with 1L of ultrapure water for approximately 12 days, until the sample's pH value was higher than 3.0. When the exfoliation process was completed, the produced GO was freeze-dried and stored in a dark airtight-sealed plastic container.

4.2.3 Biochar production

Two biomass types were used as feedstock for biochar production: a. Anaerobically digested dewatered secondary sewage sludge (SS), collected from the Psyttalia Wastewater Treatment Plant, located in Athens, Greece. b. Rice husks (RH), collected from a rice mill in northern Greece. After being received, the samples were oven-dried at 90°C for 48h and then pulverized to a particle diameter <0.5mm. After the pre-treatment procedure was completed, the samples were placed in a dark environment, stored in airtight plastic containers.

Untreated biochar samples were produced using air-tight sealed crucibles in a muffle furnace (Linn High Therm), at two pyrolysis temperatures, i.e. 400°C and 600°C. Pyrolysis conditions were achieved by supplying 99% pure Nitrogen gas at a 200L h^{-1} rate and using a heat rate of 6ºC min^{-1}. Concerning the engineered GO biochar production, the dip-coating (Inyang et al., 2014) procedure was adopted. First, GO suspensions were prepared by adding 0.4g GO in 400mL double-distilled, de-ionized water (0.1% GO w/v) and 4g GO in 400mL double-distilled, de-ionized water (1% GO w/v). Next, the water samples were ultra-sonicated at 25KHz for 1h, in order to create GO suspensions. After this step, 40g biomass was added to the suspensions and then homogenized at 800rpm, using a mechanical stirrer. Samples were, finally, oven-dried at 80°C for 48h and then were pyrolyzed for biochar production, in the same fashion as described above for the untreated samples. Based on the created suspensions, the produced functionalized biochars were comprised of two GO doses i.e. 1%(w/w) and 10%(w/w). After pyrolysis, all biochar samples were washed for impurities removal, using de-ionized water, oven-dried and stored in dark airtight plastic containers, until further use.

4.2.4 Biochar and GO characterization

A series of physicochemical analyses were performed in order to characterize the produced biochar samples. Biochar yield was calculated as the ratio of biochar to dry feedstock used for its production. Bulk density was determined using the analogue VDLUFA-Method A 13.2.1 (EBC, 2012). Specific surface area was determined by using a NOVA 2200, Thermo Scientific Surfer gas sorption analyzer (samples were de-gasified at 200°C), by applying the BET (Brunauer-Emmet-Teller) method. Ash content was determined by dry combustion in a muffle furnace at 750ºC for 6h (Rajkovic et al., 2012). C, N, H and S content was determined using a

CHNS-O EA 3000 (EuroVector) elemental analyzer. O content was calculated as described in Eq.(A1), while Volatile Solids (VS) content was calculated as described in Eq.(A2).

Eq. (A1). $O\ [\%] = 100\% - Ash\ [\%] - C\ [\%] - N\ [\%] - H\ [\%] - S\ [\%]$

Eq. (A2). $VS\ [\%] = 100\% - Ash\ [\%]$

pH and electrical conductivity (EC) values were determined using a multi-meter Crison Instruments (micropH 2202), after shaking biochar with de-ionized water, in a 1:20 ratio, for 90min (Rajkovic et al., 2012). The Point of Zero Charge (PZC) of the biochars was determined by applying the pH-drift method (Uchimiya et al., 2011b). Biochar surface functional groups were determined by FT-IR analysis, using a Perkin Elmer Spectrum 1000, FT-IR spectrometer. Finally, metal composition of the biomass and biochar samples was determined using an ICP-MS analyzer, after acid-digestion with nitric acid. All the analyses were performed in triplicate, while standard errors ranged between 0.1% and 5% for all measurements.

Additionally, five samples, i.e. GO, RH_600, RH_GO1_600, SS_600 and SS_GO1_600 were selected to perform further analysis (XPS and Raman). The surface analysis measurements were performed in a UHV chamber (P~5×10^{-10} mbar) equipped with a SPECS Phoibos 100-1D-DLD hemispherical electron analyzer and a non-monochromatized dual-anode Mg/Al x-ray source for XPS. The XP Spectra were recorded with MgKa at 1253.6 eV photon energy, combined with an analyzer pass energy of 15 eV, giving a Full Width at Half Maximum (FWHM) of 0.85 eV for Ag3d5/2 line. The analyzed area was of 1cm diameter. The atomic ratios were calculated from the intensity (peak area) of the XPS peaks, weighed with the corresponding relative sensitivity factors (RSF) derived from the Scofield cross-section, taking into account the electron transport properties of the matrix. For spectra collection and treatment, including fitting, the commercial software SpecsLab Prodigy (by Specs GmbH, Berlin) was used. The peaks were fitted using a mix of Gauss-Lorentzian peak functions, after a Shirley type background removal. The samples were in powder form and pressed onto In rod. *Micro-Raman measurements* were obtained using the T-64000 model of Jobin Yvon (ISA-Horiba group) in the backscattering configuration. The excitation wavelength (514.5 nm) was provided by a DPSS laser (Cobolt Fandango TMISO laser). The laser power on the sample was 2 mW and was focused on the samples by a 50x microscope objective. The scattered beam passed through an appropriate edge filter (for the removal of the strong elastically scattered photons) and directed into the slit of the monochromator in the single spectrograph configuration. Dispersion and detection of the Raman photons were done by a 600 grooves/mm

grating and a two-dimensional charge–coupled device (CCD) detector (operating at 140 K), respectively.

Finally, Scanning Electron Microscope (SEM) analysis was performed (Zeiss SUPRA 35VP-FEG, operating conditions 5–20 kV) on the above-mentioned samples, i.e. GO, RH_600, RH_GO1_600, SS_600 and SS_GO1_600, along with samples RH400, RH_GO1_400, SS400 and SS_GO1_400, in order to obtain a better view on the micro-structure of the samples and to investigate whether GO was successfully integrated in the final functionalized biochar samples.

4.2.5 Organic micro-pollutant adsorption experiments

Six organic micro-pollutants were selected for the conduction of the adsorption experiments; two phenols, 2-4D and BPA, two estrogens E1 and EE2, and two androgens, ADT and NOR. These compounds have been identified as Emerging Contaminants (ECs) and are being found in WWTP effluents, in concentrations of ng L^{-1} to μg L^{-1} (Palansooriya et al., 2019; Gogoi et al., 2018). Thus, the following initial concentrations were selected to produce the polluted mix: 2-4D and BPA: 20-40μg L^{-1}, E1 and EE2: 40-60μg L^{-1}, ADT and NOR: 70-90μg L^{-1}. The mentioned pollutants were spiked into 500mL of table water, creating the initial polluted mix. Fresh pollutant mix was synthesized daily, in order to avoid photolytic/photocatalytic processes, which combined with the analytical methods adopted resulted to this initial pollutant concentration range. The adsorption experiments took place in light-protected conical flasks, at 22±1°C, in duplicate repetition. 50mL of the aqueous polluted sample and 0.15g of biochar (equal to a dose of $3g \cdot L^{-1}$) were added in the flasks. Three adsorption residence times were investigated for each sample type, 10min, 30min and 60min. After the adsorption experiments, samples were filtered with 0.45μm PVDF Whatman filters. Additionally, four samples, i.e. RH600, RH_GO1_600, SS600 and SS-GO1_600 were selected to investigate their adsorptive behavior in a more realistic initial polluted mix, where the under investigation pollutants were spiked into 500mL of secondary wastewater sample (before the chlorination stage), acquired from the Municipal Water & Sewerage Company of Chania (DEYAX). Information about the characteristics of both table water and wastewater samples are presented in Table S1 (Supplementary Material).

4.2.6 Analytical methods for pollutant determination

The samples from the adsorption experiments were analyzed using Solid Phase Micro-Extraction followed by GC-MS analysis, according to a modified method developed by Antoniou et al., (2009). 10mL of sample was inserted into an amber vial (15mL, Supelco), which was airtight closed by means of a PTFE-silicone septum, along with 1.5g NaCl. Sample pH was adjusted into the range of 2.5-3. The samples were vortexed for 1min and then placed into a water-bath at 60°C and 530rpm for 1h, while an SPME Fiber Assembly 85μm Polyacrylate Fused Silica 24 GA, Supelco was inserted through the septum into the vial. After 1h, the fiber was removed from the vial and injected into a Shimatzu GCMS-QP5050A (Gas chromatograph Mass Spectrometer), where desorption took place for 10min at 290°C and the analysis followed.

4.3 Results and Discussion

4.3.1 Biochar physicochemical characterization

Table 4.1 contains the results regarding biochar characterization, in terms of physicochemical properties. More specifically, it includes information about biochar yield, pH, electrical conductivity, point of zero charge, ash content and volatile matter, specific surface area and bulk density. The results showed that there were three main parameters that affected biochar properties: pyrolysis temperature, feedstock type and functionalization with GO. Biochar yield was in the range of 38.3-48.5% for the RH biochars, while for SS biochars biochar yield was slightly higher, ranging between 45.8% and 55.7%. Biochar yield was mainly affected by pyrolysis temperature, where biochars produced at 600°C recorded lower yields than those produced at 400°C by 10-11%, and secondarily by feedstock type, where SS biochars recorded 7-8% higher yields than RH biochars. It is well known that in higher temperatures, biochar yield decreases due to the increased loss of biomass volatile content, leading to elevated biochar inorganic content and to better organized C structures (Liu et al., 2015).

Table 4.1: Biochar physicochemical characterization. Values are means (triplicate repetition) ± standard deviation

Sample ID	Yield (%)	pH	pH_{PZC}	EC ($\mu S \cdot cm^{-1}$)	Ash (%)	VS (%)	S_{BET} ($m^2 \cdot g^{-1}$)	Bulk Density ($Kg \cdot m^{-3}$)
RH_400	44.3±1.8	6.5±0.1	6.3	179.6±3.2	37.8±0.3	62.2±0.4	59.4±2.3	303±19
RH_600	38.4±1.4	9.2±0.0	7.2	190.5±3.7	45.6±0.0	54.4±0.1	214.9±7.1	312±8
RH_GO0.1_400	47±1.1	5.8±0.1	5.7	110.5±2.6	40.8±1.3	59.2±1.6	47.5±2.5	277±3
RH_GO0.1_600	39.6±0.7	8.5±0.0	6.8	136.6±5.8	45.9±1.0	54.1±1.2	234.2±4.3	284±8
RH_GO1_400	48.5±0.7	4.6±0.1	4.4	123.8±5.0	34.3±0.2	65.7±0.3	86.2±0.9	197±1
RH_GO1_600	38.3±0.6	6.7±0.0	5.6	101.7±2.8	42.4±0.5	57.6±0.6	211.8±5.9	203±3
SS_400	54.9±0.4	7.9±0.0	7.1	333.3±5.0	45.7±0.5	54.3±0.6	14.3±0.1	722±8
SS_600	46.2±0.4	8.6±0.1	7.4	199.3±2.1	64.1±1.8	35.9±2.2	52.5±5.9	751±2
SS_GO0.1_400	55.7±1.3	6.9±0.0	7.2	407.7±5.7	54.7±0.4	45.3±0.5	21.0±0.6	642±2
SS_GO0.1_600	45.8±0.5	7.8±0.1	7.7	226.7±3.5	71.1±0.7	28.9±1.0	69.3±1.2	683±9
SS_GO1_400	54.3±0.1	6.8±0.0	6.9	592.7±2.1	53.2±3.2	46.8±4.5	18.8±1.1	562±14
SS_GO1_600	45.9±0.3	7.9±0.0	7.5	326.3±4.2	60.4±0.4	39.6±0.5	55.2±2.6	530±5

pH values were in the range of 4.6-9.2 for the RH biochars and 6.8-8.6 for the SS biochars. Samples produced at the lower pyrolysis temperature showed slightly acidic to neutral pH values, while for the higher temperature, pH values were neutral to slightly alkaline. Biochar pH was affected mostly by pyrolysis temperature and by the functionalization process. Specifically, as mentioned above, higher pyrolysis temperature led to more alkaline pH values by 0.3-2.7 units, which is consistent to the findings of our previous work (Regkouzas & Diamadopoulos, 2019). On the other hand, GO functionalization decreased RH biochar pH values by 0.7 to 2.5 units and SS biochar pH values by 0.9 to 1.1 units, which is attributed to the acidic pH of GO. Concerning the pH_{PZC} analysis, RH biochars indicated acidic to mostly neutral pH_{PZC} values, ranging between 4.4 and 7.2, while for the SS biochars pH_{PZC} values were within a higher range of 6.9-7.7. In most samples, pH_{PZC} values were lower than their respective pH values, while GO functionalization led to the decrease of pH_{PZC} values by 0.4-1.9 for the RH samples, while no significant change was observed for the SS biochars. Additionally, the higher pyrolysis temperature also led to higher pH_{PZC} values in the range of 0.3-1.2 for all samples, which has also been found in the past by other researchers (Uchimiya et al., 2011b; Oh et al., 2012b). Furthermore, EC values ranged from 101.7μS cm^{-1} to 190.5μS

cm^{-1} for the RH biochars and from 199.3μS cm^{-1} to 592.7μS cm^{-1} for the SS biochars. The highest EC value was found in the SS_GO1_400 sample (i.e. 592.7μS cm^{-1}), while the RH_GO1_600 sample recorded the lowest value (i.e. 101.7μS cm^{-1}). Biomass type was the parameter that defined the most significant differences in the EC values. Specifically, the SS biochars recorded 70-80% higher values than the respective RH biochars. Moreover, GO functionalization and higher pyrolysis temperature caused decreased EC values for the RH samples, while the opposite trend was observed for the SS samples, where these two parameters increased biochar EC.

Ash content was in the range of 34.3%-45.9% for the RH biochars, while elevated values were found in the SS biochars, ranging between 45.7% and 71.1%. The exactly opposite results were observed for the VS values, which is normal since the ash content is directly connected to VM content through Eq. (A2). Specifically, VM content was in the range of 54.1%-65.7% for the RH biochars and 28.9%-54.3% for the SS biochars. Biochar ash content and VM were mainly affected by pyrolysis temperature and biomass type. Biochars produced at 600°C presented the highest ash and lowest VM contents, which is attributed to the carbonization process and the increase of biochar mineral content, when produced at higher temperatures (Zhang et al., 2020). Moreover, SS biochars recorded higher ash values, due to the higher inorganic content of SS biomass (Oh et al., 2016). Biochar bulk density and specific surface area (S_{BET}) were in the range of 197-312Kg m^{-3} and 47.5-234m^2 g^{-1} respectively for the RH biochars, while concerning the SS biochars, values were in the range of 530-751Kg m^{-3} and 14.3-69.3m^2 g^{-1} respectively. These results proved the physicochemical superiority of the RH biochars compared to the SS biochars. Biochar bulk density was mainly affected by biomass type, where RH biochars recorded lower values by more than 50%, and secondarily by pyrolysis temperature, where higher temperature resulted in slightly higher bulk density values. Higher temperatures result into more porous and with improved surface materials (Tripathi et al., 2016), which was reflected in the results of the specific surface area of our samples, where RH biochars, produced at 600°C, showed the highest S_{BET} values. Specifically, these samples had more than three times higher S_{BET} values, compared to the respective SS biochars. It should also be mentioned that GO-enriched biochars did not affect significantly biochar bulk density and S_{BET} values, which can be attributed to the small chosen GO doses (0.1% and 1%). S_{BET} is one of the main parameters that can be used to foresee the adsorption ability of biochars, where higher values provide more efficient adsorption potential (Ahmad et al., 2014). When compared to other biochar samples in literature (Abdul et al., 2017; Regkouzas & Diamadopoulos, 2019; Chu et

al., 2019), RH biochars presented good surface area values, but they could not reach the standards of activated carbons (Swat et al., 2017; Kong et al., 2019). This, however, does not mean that they will not be able to perform well as adsorptive materials.

Table 4.2: Biochar elemental composition. Values are means (triplicate repetition) ± standard deviation

Sample ID	C (%)	H (%)	N (%)	S (%)	O (%)	O/C	H/C
RH_400	38.1±0.3	1.8±0.1	0.5±0.0	BDL	21.8	0.43	0.57
RH_600	43.9±0.1	1.1±0.1	0.5±0.0	BDL	8.9	0.15	0.30
RH_GO0.1_400	41.5±2.1	1.9±0.1	0.5±0.0	0.1±0.0	15.2	0.27	0.55
RH_GO0.1_600	42.9±0.6	1.1±0.1	0.4±0.1	BDL	9.7	0.17	0.31
RH_GO1_400	45.4±0.2	1.5±0.0	0.6±0.0	0.4±0.0	17.8	0.29	0.40
RH_GO1_600	48.2±3.9	0.9±0.0	0.6±0.0	0.4±0.1	7.5	0.12	0.22
SS_400	30.9±1.6	2.1±0.0	3.8±0.0	0.9±0.0	16.6	0.40	0.82
SS_600	24.2±0.2	0.8±0.0	3.0±0.0	0.9±0.0	7	0.22	0.40
SS_GO0.1_400	26.9±1.3	1.8±0.0	3.7±0.1	1.2±0.1	11.7	0.33	0.80
SS_GO0.1_600	23.1±0.8	0.7±0.0	2.7±0.1	0.9±0.0	6.2	0.20	0.36
SS_GO1_400	30.8±0.3	1.8±0.0	3.7±0.0	1.5±0.1	11.7	0.28	0.70
SS_GO1_600	26.5±1.9	0.8±0.0	2.6±0.1	1.2±0.2	8.5	0.24	0.36

Table 4.2 contains the results of the elemental analysis that was performed on the biochar samples. The main element of interest, C, was in the range of 38.1%-48.2% for the RH biochars and 23.1%-30.9% for the SS biochars. RH biochars produced at 600°C had higher C content by up to13.2%, compared to those produced at 400°C, while the opposite trend was observed for the SS biochars, where samples produced at 400°C contained up to 21.7% more C than those produced at 600°C. The best biochar in terms of C content was RH_GO1_600. Generally, higher pyrolysis temperature is expected to provide biochars with higher C content, since better organized C layers are formed and biochars gain a more aromatic C nature (Rajapaksha et al., 2016). This was indeed confirmed by the RH biochars. The ambiguous results concerning the SS biochars, which have been previously observed by other researchers (Wang et al., 2019; Oh et al., 2012b; Kong et al., 2019; Jin et al., 2016), are attributed to the high ash content of sewage sludge, which affects the carbonization process, resulting in lower C content at higher pyrolysis temperatures (Fan et al., 2020). Additionally, GO functionalization slightly improved C content, but at very low percentages. Concerning the rest of the elements, H was found in small quantities in all samples (0.7%-2.1%), S was found at even smaller levels not exceeding 1.5%, while N was found in the range of 0.4%-0.6% for the RH biochars and 2.6%-3.8% for the SS biochars, which is attributed to the higher N content in the SS feedstock. Pyrolysis temperature

affected these elements in the same fashion as in the C measurements. Biochar O content was calculated as shown in Eq. (A1). RH biochars contained 7.5%-21.8% O, while SS biochars showed slightly lower values, ranging between 6.2% and 16.6%. Higher pyrolysis temperature provoked lower O contents for both RH and SS biochars by up to 59.2%. This was expected, since the main variable that affects Eq. (A1) is biochar ash (Zheng et al., 2019). Moreover, O/C and H/C ratios were calculated from the mean values of the elements shown in Table 2. RH biochar O/C and H/C contents were in the range of 0.12-0.43 and 0.22-0.57 respectively, while SS biochars scored 0.20-0.40 and 0.36-0.82 accordingly. Both parameters were found to be affected by higher pyrolysis temperature, where the ratios were reduced by 14.2%-51.2%. This is normal, since at higher temperatures, the organic part of biomass is more successfully converted into well-carbonized condensed carbon moieties of a more aromatic nature (Abdul et al., 2017; Chu et al., 2019). As an overall conclusion of the results presented above, pyrolysis temperature is the main parameter that affects the physicochemical nature of biochars.

4.3.2 Biochar metal composition

Results concerning the metal composition of biochars are presented in Table 4.3. SS biochars had a significantly larger metal content, which was expected, since sewage sludge is an anthropogenic waste, known to contain traces of metals in its structure. On the other hand, rice husks constitute an agronomic lignocellulotic waste, which is not expected to contain many metals, nor in large amounts. Specifically, K and Ca were the dominant metals in RH biochar structure, found in doses ranging from 1857mg kg^{-1} to 2214mg kg^{-1} and 520mg g^{-1}-1446 mg kg^{-1} respectively, followed by Mn, Mg and Al. The rest of the metals were found at much lower levels. SS biochars were significantly richer in terms of metal content, where Ca and Al were found in the highest quantity, ranging from 47081mg kg^{-1} to 64791mg kg^{-1} and 6911mg g^{-1}-9885 mg kg^{-1} respectively. Mg, Fe, K and Na were also found in significant quantity in the SS biochars. GO functionalization and pyrolysis temperature did not appear to affect biochar metal content. In some cases, higher pyrolysis temperature slightly raised the metal content of biochars, but not in a significant manner. Buss et al., (2016) stated that the effect of pyrolysis temperature on biochar metal content is strongly dependent on the physicochemical structure of the feedstock. It should also be highlighted that heavy metal (Zn, Cu, Ni, Cd, Pb, Hg, and Cr) values of all biochars did not exceed the limitations set by the European Union (Directive 86/278/EEC) for land application of sewage sludge. In addition to that, in our previous work it

was shown that conversion of sewage sludge to biochar could be an effective method for the valorization of this waste, since although these biochars were rich in metal content, their leaching potential was significantly limited (Regkouzas & Diamadopoulos, 2019). Other researchers also confirmed that conversion of biomass to biochar may increase the material's metal content, but significantly limits its leaching potential (Phoungthong et al., 2018; Mendez et al., 2012).

Table 4.3: Biochar metal composition. Values are means (triplicate repetition) ± standard deviation.

Metal	RH_400	RH_600	RH_GO0.1_400	RH_GO0.1_600	RH_GO1_400	RH_GO1_600	SS_400	SS_600	SS_GO0.1_400	SS_GO0.1_600	SS_GO1_400	SS_GO1_600
	mg metal · kg^{-1} sample											
B	2.7±0.1	2.3±0.1	3.3±0.4	3.5±0.8	4.8±0.0	5.8±0.2	8.8±0.0	8.2±0.9	15±5	11±0	10±0	10±1
Na	82±31	60±5	156±48	123±17	120±1	177±71	700±8	890±102	1186±323	1017±49	894±43	887±15
Mg	470±5	277±20	562±91	416±99	490±1	606±4	3838±7	4423±505	4947±723	5273±22	3811±129	4275±71
Al	100±20	128±14	110±13	145±21	145±3	151±5	7293±116	8074±844	8985±1328	9885±47	6911±141	7612±213
Si	BDL	BDL	BDL	BDL	BDL	BDL	BDL	BDL	BDL	BDL	BDL	BDL
K	2074±83	2136±86	2078±269	2109±259	2214±3.8	1857±75	992±8	1181±128	1390±342	1349±34	1081±49	1170±13
Ca	833±225	520±97	1371±243	1446±510	663±54	1027±9	51945±411	55461±6504	60027±7967	64791±206	47081±717	51976±1806
Cr	1.2±0.4	0.9±0.1	1.1±0.2	1.0±0.2	1.2±0.0	1.3±0.0	237±5	191±19	265±33	243±2	219±4	192±7
Mn	202±12	161±8	263±19	206±31	315±1	402±1	102±1	107±11	112±15	119±1	129±2	145±5
Fe	44±1	73±12	103±12	145±56	123±1	134±3	2862±82	3027±175	2710±409	2713±7	2200±5	2355±98
Co	BDL	BDL	BDL	BDL	BDL	BDL	0.4±0.0	0.4±0.2	0.7±0.2	0.8±0.1	0.4±0.0	0.5±0.0
Ni	0.6±0.2	2.1±0.5	0.5±0.1	1.8±0.2	0.9±0.1	1.9±0.1	34±1	28±4	41±7	34±1	33±1	29±1
Cu	4.5±0.0	4.6±0.2	21±1	36±4	15±1	17±1	225±2	205±17	225±22	227±1	188±1	194±7
Zn	31±8	24±2	84±4	86±3	124±0	151±5	705±2	688±63	827±92	858±1	704±9	717±15
As	0.2±0.0	0.1±0.0	0.3±0.0	0.2±0.0	0.3±0.0	0.3±0.0	1.9±0.0	1.7±0.1	2.1±0.2	1.9±0.0	1.8±0.0	1.7±0.0
Se	BDL	BDL	BDL	BDL	BDL	BDL	0.3±0.0	0.1±0.0	0.6±0.2	0.5±0.0	0.4±0.0	0.2±0.0
Mo	0.2±0.0	0.3±0.0	0.3±0.0	0.5±0.0	0.3±0.0	0.6±0.0	4.9±0.0	4.7±0.5	6.0±0.8	5.2±0.0	5.4±0.1	5.3±0.0
Cd	BDL	BDL	BDL	BDL	BDL	BDL	0.9±0.0	0.9±0.1	1.0±0.2	1.0±0.0	0.9±0.0	0.8±0.1
Hg	0.9±0.1	0.6±0.0	0.7±0.0	0.7±0.1	0.7±0.0	0.7±0.0	0.5±0.0	0.7±0.1	0.4±0.1	0.3±0.0	0.4±0.0	0.4±0.1
Pb	0.6±0.3	0.6±0.2	2.0±0.0	2.1±0.2	1.9±0.1	2.2±0.2	148±1	148±17	149±1	158±1	139±1	145±1

4.3.3 Biochar FTIR analysis

Figure 4.1 depicts the results of the FTIR analysis on the RH biochars. This analysis was performed to qualitatively determine biochar surface functional groups, which is valuable information, especially when biochar is studied as an adsorbent. RH biochars consisted of various functional groups, where C-O (1038 cm^{-1}), C=N and C=C (1599 cm^{-1}) were the dominant ones. Other functional groups that were found on RH biochar surface were C-H groups (887 cm^{-1}), Si-O-Si (1038 cm^{-1}) and Si-O (1100 cm^{-1}) groups, O-H (1544 cm^{-1}), as long as several –OH and amide groups in the region of 3440-3700 cm^{-1}. It should be noted that the biggest vibrations, especially for C-O and –OH groups, were observed for samples produced at 600°C, which confirms that higher pyrolysis temperatures provide better carbonization of biochar (Ahmed et al., 2016; Rajapaksha et al., 2016), as shown in the elemental analysis.

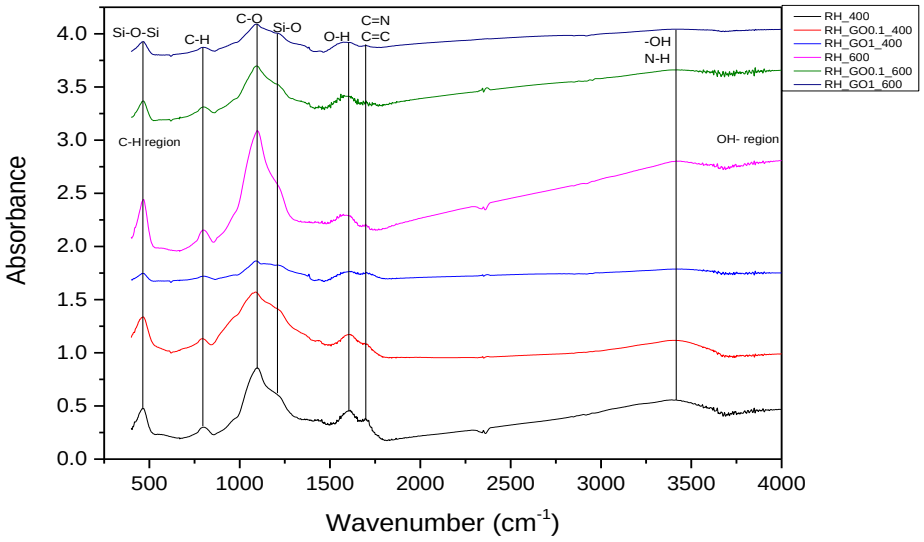

Figure 4.1: FTIR spectra of RH biochars

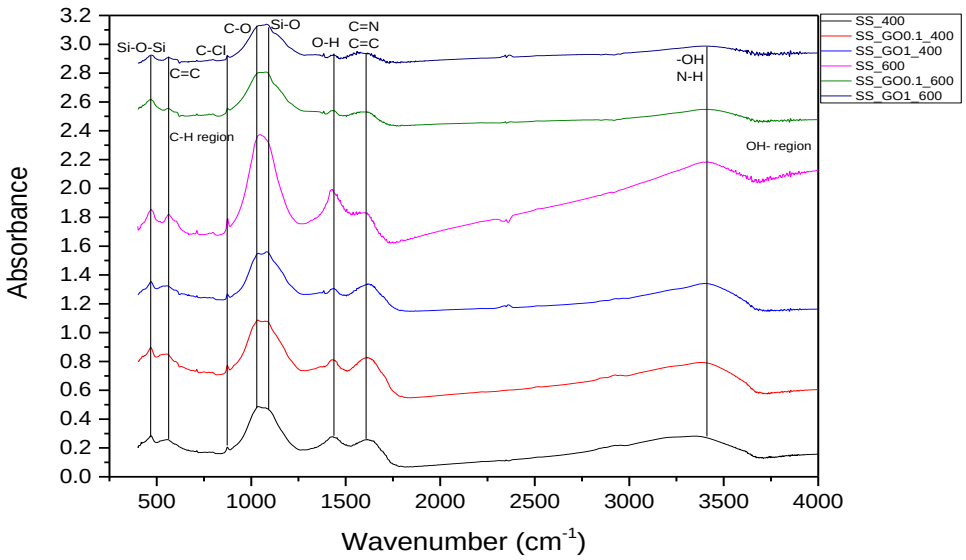

Figure 4.2: FTIR spectra of SS biochars

Similar functional groups were also found on SS biochar surface, as shown in Figure 4.2. C-O (1038 cm^{-1}), C=N (1599 cm^{-1}) and C=C (665 cm^{-1} and 1599 cm^{-1}) were the dominant groups in this case too, yet it can be observed that peaks at 1599 cm^{-1} were bigger compared to RH biochars. This is attributed to the N compounds in SS biochar, that provide stronger C=N functional groups. Although it is expected that SS biochars have more N-containing functional

groups (Fan et al., 2020; Hossain et al., 2011), due to its mineral composition, this was not clear in this work. Moreover, -OH and –O functional groups were also found in higher quantity, compared to RH biochar. Other functional groups that were observed on SS biochar surface were C-H groups (887 cm^{-1}), Si-O-Si (1038 cm^{-1}), C-Cl (800 cm^{-1}), Si-O (1100 cm^{-1}) and O-H (1544 cm^{-1}) groups.

4.3.4 Raman, XPS and SEM analyses on selected samples

In order to attain a spherical view over the graphitic structure of our samples, additional analyses, Raman and XPS, were performed on selected samples, i.e. GO, RH600, RH_GO1_600, SS600 and SS_GO1_600. Additionally, SEM analysis was performed at the before-stated samples, along with biochars produced at 400°C, i.e. RH400, RH_GO1_400, SS400 and SS_GO1_400.

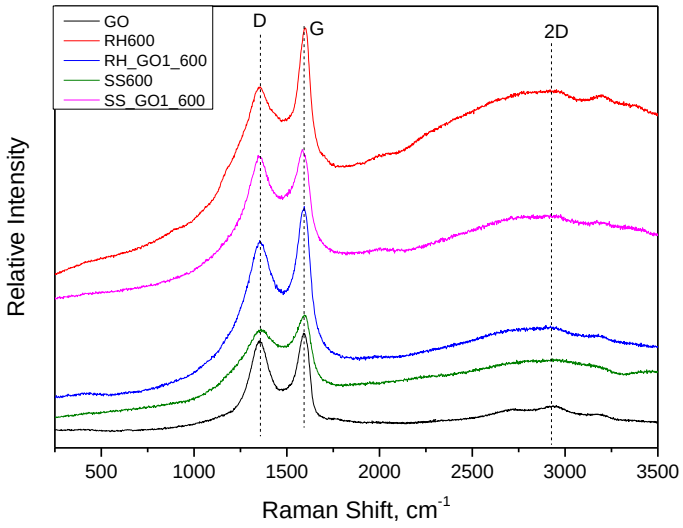

Figure 4.3: Raman spectra of selected samples.

The results of the Raman analysis are presented in Figure 4.3. Two dominant peaks were observed at 1359 cm^{-1} and 1594 cm^{-1} that correspond to the D band (sp^3 hybridized C) and to the G band (sp^2 hybridized C) (Abdul et al., 2017). Among the tested samples, important differences were observed for the D band and especially for the G band. Specifically, in RH biochars it was clear that the G band was stronger than the D band, implying different graphitic

structure, compared to the SS biochars. Moreover, reduced peak intensity was observed for both D and G bands in the SS biochars, compared to RH biochars, which was also expected, since SS biochars have almost half of the C content, as shown in the elemental analysis. GO functionalization did not seem to significantly affect the Raman spectra of biochars, making biomass type the main parameter that affects the graphitic nature of biochar in our experiment. Finally, a third peak was observed at 2925 cm^{-1}, corresponding to the 2D band (Zhang et al., 2018), which can provide information about the quantity of graphene sheet layers. The fact that in all samples small and narrow peaks were observed suggests that there may be stacked graphene/graphitic sheets in the samples' core.

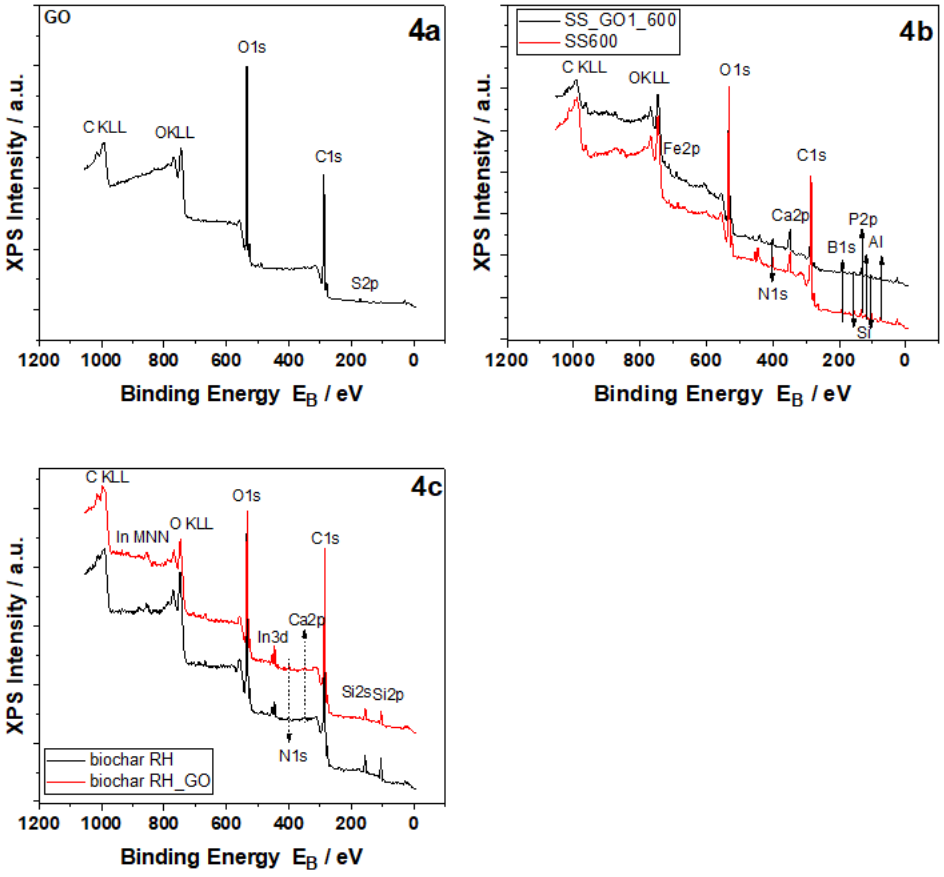

Figure 4.4: XPS survey scans of the investigated samples. 4a: Graphene Oxide (GO), 4b: SS biochars, 4c: RH biochars.

Figure 4.4 presents the XPS survey scans of the investigated samples. Figure 4a refers to the results of GO, where two main atoms (C and O) were detected, along with some small traces of S, which could be attributed to the use of H_2SO_4 during GO production. Quantification in

terms of atomic concentration is presented in Table 4.4. C was the main atom detected on GO surface at a percentage equal to 69.59%, while O was found at 30.41%. The absence of any other atoms was expected, since GO is a nano-scale carbonaceous structure, manufactured by graphite oxidation (Dimiev & Tour, 2014). Figure 4b depicts the survey scan of the SS biochars, where the presence of C, O, P, Al, Si, N, Ca, B and Fe atoms was detected on biochar surface (Melia et al., 2018). The presence of multiple atoms can be confirmed by the ICP-MS and elemental analysis, where these atoms were detected in the highest quantity. It also shows that these elements are located both in biochar core and surface, creating various functional groups. Table 3.5 contains the necessary information about the atomic concentration of these atoms on SS600 and SS_GO1_600 surface. C and O were the main atoms detected in both biochar samples, in percentages equal to 32.33% and 34.06% respectively for SS600, while SS_GO1_600 had more C (53.50%) and less O (24.40%), which makes the engineered biochar better in physicochemical terms, since it contains more C-based functional groups on its surface, making it stronger as an adsorptive material (Zhang et al., 2018; Melia et al., 2018). Other atoms found on the surface of SS biochars were Al (6.13% and 4.70%), B (10.16% and 4.82%), P (6.07% and 2.88%) and Ca (4.48% and 2.37%).

Table 4.4: % atomic concentration and relative atomic ratios on GO surface.

Peak	Eb [eV]	ASSIGNEMENTS	% ATOMIC C	RAR*
C1s	286.77	C-C	69.59 ± 0.02	1
`O1s	532.60	Mainly C-O	30.41 ± 0.02	0.44

*RAR: Relative Atomic Ratio

Table 4.5: % atomic concentration and relative atomic ratios on SS600 and SS_GO1_600 surface.

			SS600		SS GO1 600	
Peak	**Eb [eV]**	**ASSIGNEMENTS**	**% ATOMIC C**	**RAR***	**% ATOMIC C**	**RAR***
C1s	284.90	C-C	32.33 ± 0.10	1	53.50 ± 0.08	1
Ca2p	347.72	$Ca_3(PO_4)_2$	4.48 ± 0.02	0.14	2.37 ± 0.02	0.044
O1s	532.05	Mainly C-O	34.06 ± 0.08	1.05	24.40 ± 0.04	0.46
Al2p	74.77	Al_2O_3	6.13 ± 0.08	0.19	4.70 ± 0.05	0.089
Si2p	103.24	SiO_2	3.11 ± 0.05	0.10	3.34 ± 0.04	0.062
P2p	133.89	$Ca_3(PO_4)_2$, $CaHPO_4$	6.07 ± 0.04	0.19	2.88 ± 0.03	0.054
B1s	191.29	N.D.**	10.16 ± 0.13	0.31	4.82 ± 0.08	0.09
Fe2p3/2	~712	FeOOH, Fe_2O_3	0.31 ± 0.01	0.01	0.20 ± 0.00	0.004
N1s	400.41	N-C	3.36 ± 0.03	0.10	3.79 ± 0.02	0.071

*RAR: Relative Atomic Ratio, **N.D.: not determined

Figure 4c shows the survey scan of the RH biochars. Fewer atoms were detected in these samples, when compared to the SS biochars, which was attributed, as stated above, to the feedstock biomasses. C, Ca, O, Si and N atoms were detected in both biochars. The main atoms were C and O in this case too, presenting similar trends regarding the C/O ratio to the SS biochars. Specifically, RH600 had 34.77% C and 44.05% O, while RH_GO1_600 had 66.37% C and 23.57% O, as presented in Table 3.6. This suggests that regarding the RH biochars, GO functionalization led to even better engineered biochar in physicochemical terms, having almost 29% more C on their surface. The rest of the atoms were detected in smaller quantities, except Si, which was detected at 19.27% for RH600 and 8.87% for RH_GO1_600.

Table 4.6: % atomic concentration and relative atomic ratios on RH600 and RH_GO1_600 surface.

			RH600		RH_GO1_600	
Peak	**Eb [eV]**	**ASSIGNEMENTS**	**% ATOMIC C**	**RAR***	**% ATOMIC C**	**RAR***
C1s	285.16	C-C	34.77 ± 0.04	1	66.37 ± 0.05	1
Ca2p	349.15	$Ca_3(PO_4)_2$	0.13 ± 0.01	0.004	0.18 ± 0.01	0.003
O1s	534.31	Mainly C-O	44.05 ± 0.04	1.27	23.57 ± 0.03	0.36
Si2p	104.91	SiO_2	19.27 ± 0.05	0.55	8.87 ± 0.04	0.13
N1s	400.61	N-C	1.79 ± 0.04	0.051	1.03 ± 0.02	0.016

*RAR: Relative Atomic Ratio

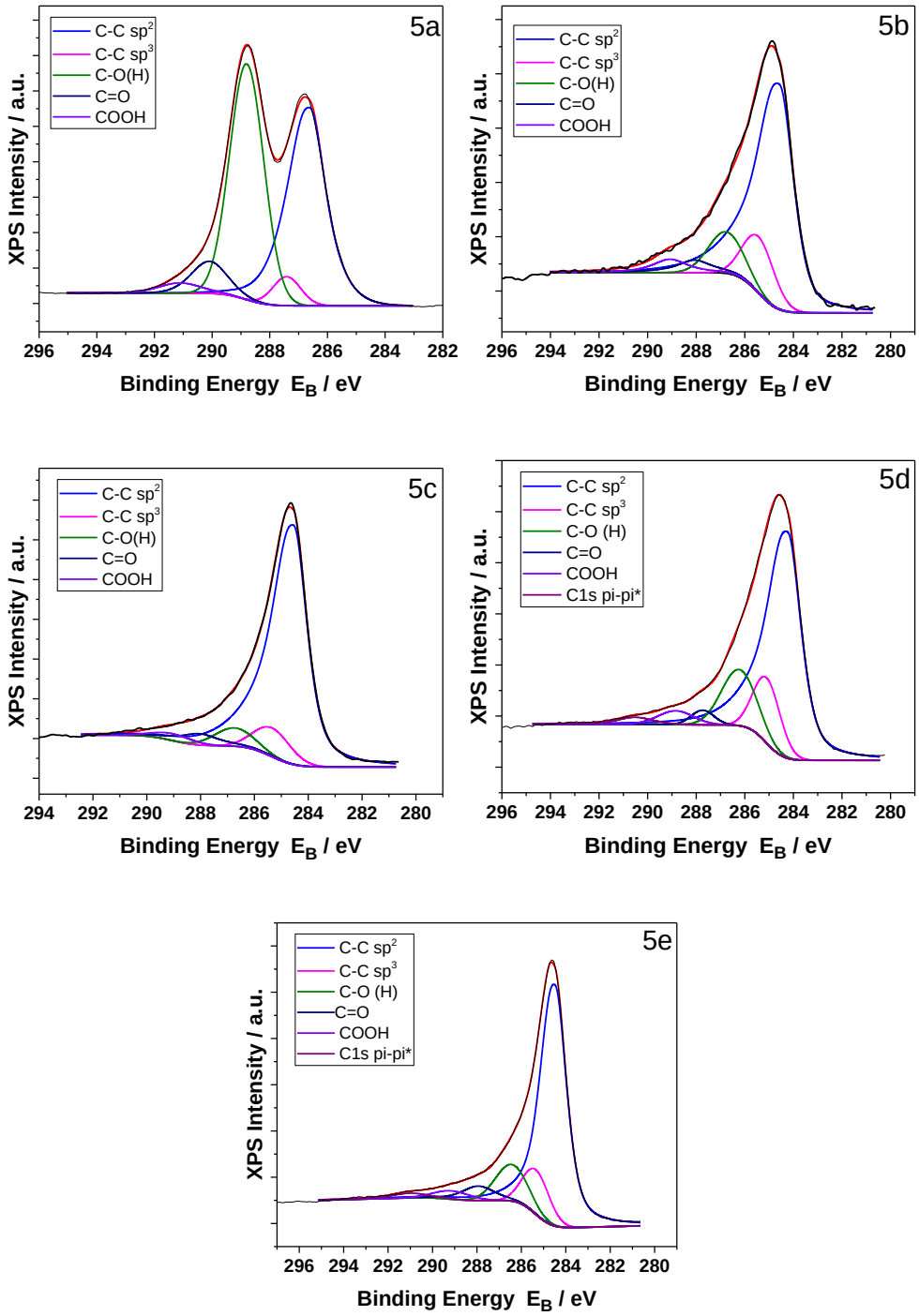

Figure 4.5: Deconvoluted C1s peaks of 5a: GO, 5b: SS600, 5c: SS_GO1_600, 5d: RH600, 5e: RH_GO1_600.

Table 4.7: % component concentrations of C1s peaks

SS600			
Peak	**Eb (eV)**	**% Component C**	**Assignement**
C1s	284.58	69.67 ± 1.90	C-C sp^2
C1s	285.43	11.78 ± 1.67	C-C sp^3
C1s	286.78	9.78 ± 0.66	C-O(H)
C1s	288.08	4.34 ± 0.59	C=O
C1s	289.08	4.42 ± 1.15	COOH
SS_GO1_600			
Peak	**Eb (eV)**	**% Component C**	**Assignement**
C1s	284.54	80.50 ± 1.29	C-C sp^2
C1s	285.34	7.77 ± 0.49	C-C sp^3
C1s	286.74	5.26 ± 0.85	C-O(H)
C1s	288.04	4.47 ± 1.14	C=O
C1s	289.04	1.99 ± 0.28	COOH
RH600			
Peak	**Eb (eV)**	**% Component C**	**Assignement**
C1s	284.24	66.68 ± 0.72	C-C sp^2
C1s	285.09	12.07 ± 0.18	C-C sp^3
C1s	286.24	13.58 ± 0.47	C-O(H)
C1s	287.74	2.30 ± 0.24	C=O
C1s	288.84	3.41 ± 0.84	COOH
C1s	290.52	1.97 ± 0.17	pi-pi*
RH_GO1_600			
Peak	**Eb (eV)**	**% Component C**	**Assignement**
C1s	284.49	69.58 ± 1.71	C-C sp^2
C1s	285.34	10.50 ± 0.51	C-C sp^3
C1s	286.44	10.51 ± 1.50	C-O(H)
C1s	287.94	4.95 ± 1.51	C=O
C1s	289.14	2.67 ± 0.62	COOH
C1s	291.02	1.79 ± 0.18	pi-pi*

Figure 4.5 contains the results regarding the deconvoluted C1s peaks of the samples under investigation, while Table 6 provides their quantification. Figure 5a concerns the GO sample, where the C1s peak shape is characteristic for GO samples. The C1s peak was deconvoluted into five components assigned to C-C with sp^2 configuration, C-C with sp^3 configuration, C-O(H), C=O and COOH bonds, as described in detail elsewhere (Sygellou et al., 2016). Figure 5b and 5c show the results that concerns biochars SS600 and SS_GO1_600 respectively. SS biochar C1s peaks were deconvoluted into the same five components, as the GO sample. Interesting information can be derived by the quantification of the different components, shown in Table 3.7, where the main components of SS biochars were C-C bonds with sp^2 configuration (69.67% and 80.50%), followed by C-C bonds with sp^3 configuration (11.78% and 7.77%), C-O (H) bonds (9.78% and 5.26%), C=O bonds (4.34% and 4.47%) and COOH bonds (4.42% and 1.99%). The main component that was affected by GO functionalization were the C-C

bonds with sp^2 configuration, where SS_GO1_600 had almost 11% more of this component than the non-functionalized SS600 sample, while the rest components concentration did not change significantly. Finally, Figure 5d and 5e show the results of biochars RH600 and RH_GO1_600. RH600 and RH_GO1_600 biochar C1s peaks deconvoluted into six components, i.e. C-C bonds with sp^2 configuration (66.68% and 69.58%), C-C bonds with sp^3 configuration (12.07% and 10.50%), C-O (H) bonds (13.58% and 10.51%), C=O bonds (2.30% and 4.95%), COOH bonds (3.41% and 2.67%) and pi-pi* bonds (1.97% and 1.79%). As in the SS biochars, GO functionalization only affected the main component (C-C bonds with sp^2 configuration), but in a smaller extent. Moreover, it is clear that in RH biochars, components are more evenly distributed, recording higher percentages in all components, compared to the SS biochars. This could mean that RH biochars would be better as adsorptive materials, due to their greater variety in C1s bonds on their surface.

The results of the XPS analysis are similar to other works in literature, such as Abdul et al., (2017), who produced GO-wood biochar nanocomposites at three temperatures (300°C, 500°C and 700°C). They observed similar functional groups to those in our samples, mostly C- and O- containing groups. They also found that GO biochars had higher content, compared to the untreated ones. Moreover, they found that at 500°C the percentage of C=O bonds increased by 27%-30%, but at 700°C it decreased by 29%-31%, compared to the samples produced at 300°C. Furthermore, Tang et al., (2015) produced GO coated wheat straw biochars at 600°C and observed a significant increase on the oxygen based functional groups of the engineered biochar. Finally, Ghaffar et al., (2014) used peanut shell biochars treated with GO at 300°C and 500°C. They observed a slightly different behavior, where GO treatment improved C-based functional groups, but higher temperature decreased them. Though, both GO treatment and pyrolysis temperature provided biochars that were significantly more effective adsorptive behavior for the removal of organics from water, compared to the untreated ones.

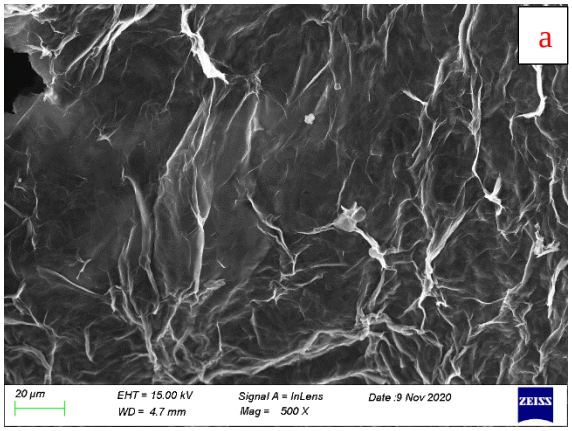
a
20 µm
EHT = 15.00 kV
WD = 4.7 mm
Signal A = InLens
Mag = 500 X
Date :9 Nov 2020
ZEISS

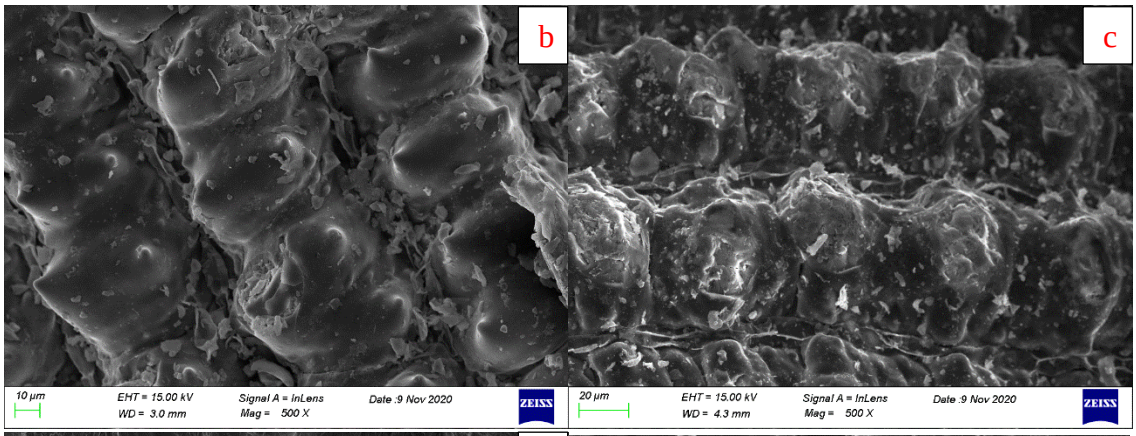
b
10 µm
EHT = 15.00 kV
WD = 3.0 mm
Signal A = InLens
Mag = 500 X
Date :9 Nov 2020
ZEISS
c
20 µm
EHT = 15.00 kV
WD = 4.3 mm
Signal A = InLens
Mag = 500 X
Date :9 Nov 2020
ZEISS

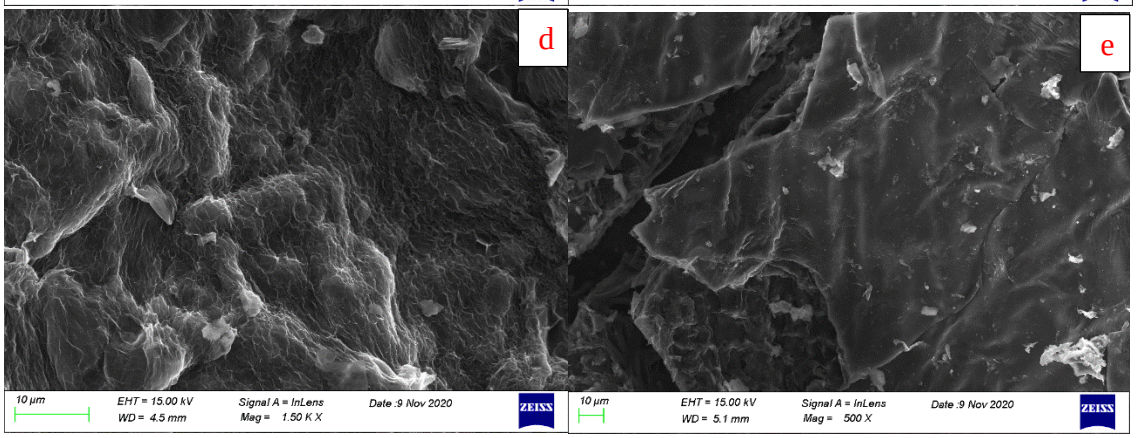
d
10 µm
EHT = 15.00 kV
WD = 4.5 mm
Signal A = InLens
Mag = 1.50 K X
Date :9 Nov 2020
ZEISS
e
10 µm
EHT = 15.00 kV
WD = 5.1 mm
Signal A = InLens
Mag = 500 X
Date :9 Nov 2020
ZEISS

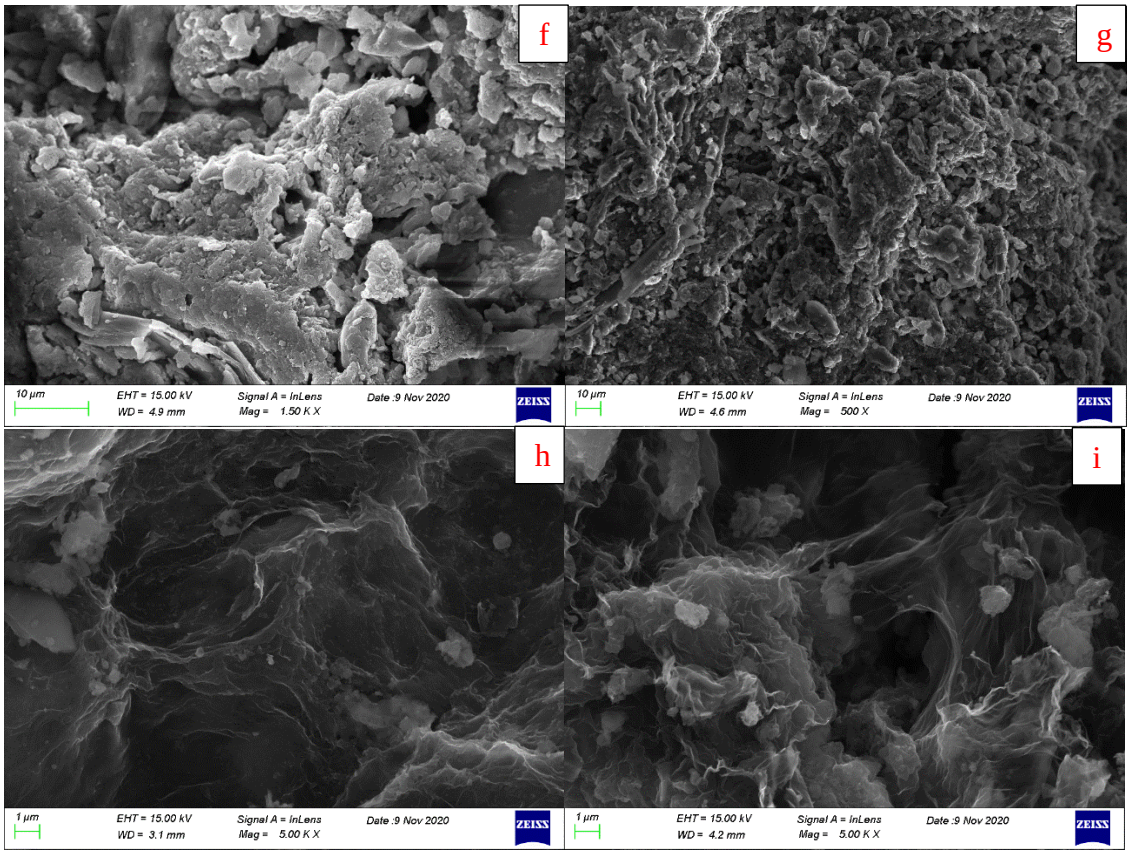

Figure 4.6: SEM analysis: a: GO, b: RH_400, c: RH600, d: RH_GO1_400, e: RH_GO1_600, f: SS_400, g: SS600, h: SS_GO1_400, i: SS_GO1_600.

SEM images of the investigated samples are depicted in Figure 4.6. Results showed that higher temperature (6b, 6f) led to more carbonized biochar, presenting a rougher and more porous surface (6c, 6g), which agrees to the results obtained from the physicochemical characterization of the samples. The main goal of this analysis though was to investigate the success of GO implementation to the biomass and consequently to the produced functionalized biochars. Functionalization was clearly a success, which can be witnessed in Figures 6d, 6e, 6h and 6i, where the net-like structure of GO (6a) got implemented on the pores of biochar surface, providing it with additional surface functional groups, as witnessed in the XPS analysis of the samples.

4.3.5 Organic micro-pollutant adsorption experiments

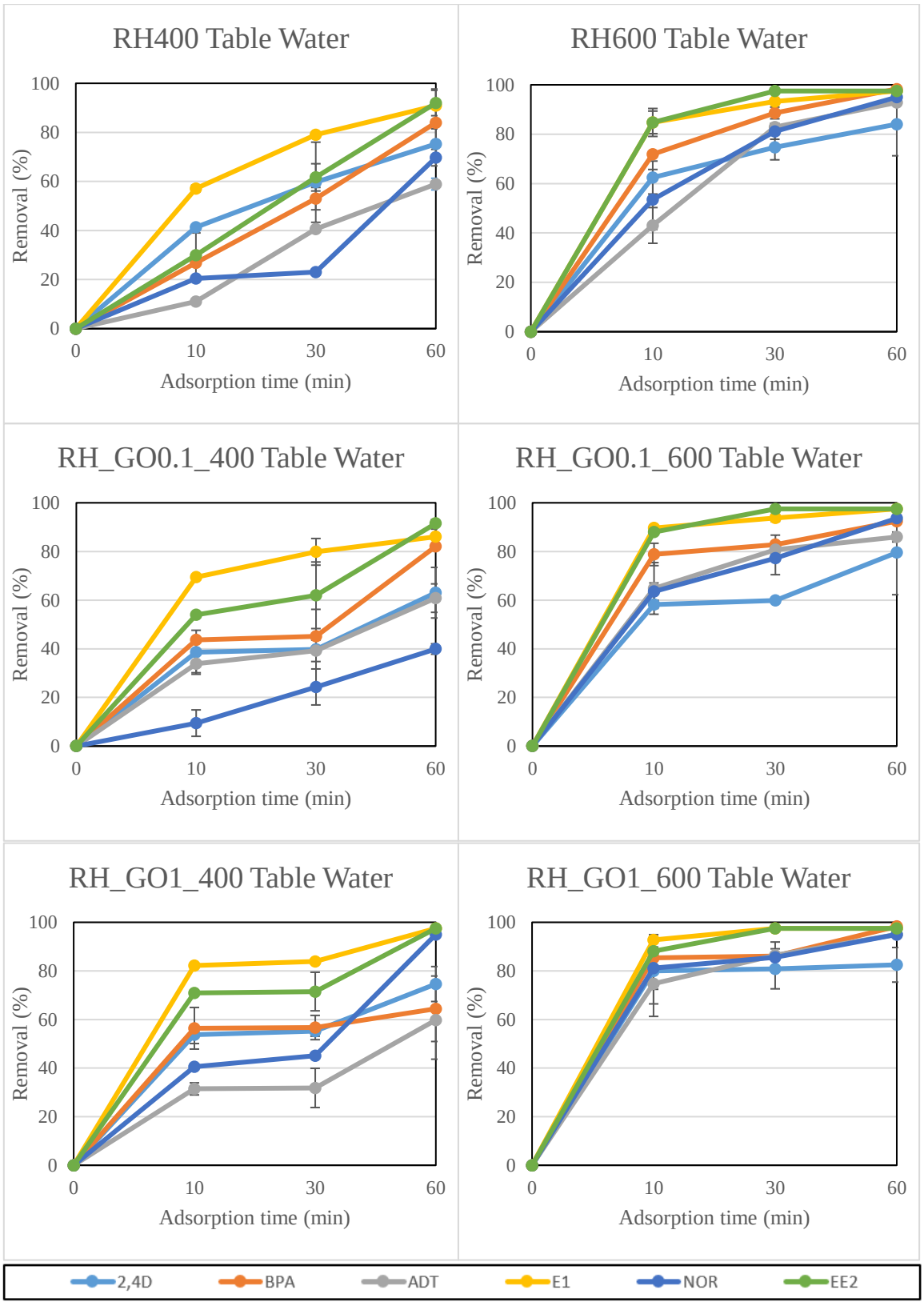

Figure 4.7: Organic micro-pollutant adsorption on RH biochars in table water. Error bars depict standard deviation of duplicate repetition.

Figure 4.7 depicts the results concerning the adsorption of six organic micro-pollutants on conventional and GO-engineered RH biochars, in table water. Organic micro-pollutant removal was in the range of 58,9%-92,0% for RH400, 84,1%-98,3% for RH600, 39,9%-91,5% for RH_GO0.1_400, 79,5%-97,5% for RH_GO0.1_600, 59,8%-97,5% for RH_GO1_400 and 82.5%-98,3% for RH_GO1_600, in 60min of adsorption time. These results indicate that biochars produced at 600°C were more efficient concerning the adsorption of the six organic micro-pollutants by achieving higher removal rates (79,5%-98,3%), compared to biochars produced at 400°C (39,9%-97,5%). This was expected and has been witnessed by several researchers before (Regkouzas & Diamadopoulos, 2019; Tang et al., 2015), since higher pyrolysis temperature results into more stable, porous and organized C-structures, making the final product a better adsorbent. Moreover, GO functionalization provided better results in terms of adsorption time. Specifically, GO-functionalized biochars produced at 600°C achieved >70% pollutant removal by the first 30min, while sample RH_GO1_600, which was the most effective of the biochars tested, achieved approximately >74.7% pollutant removal by the first 10min of adsorption time.

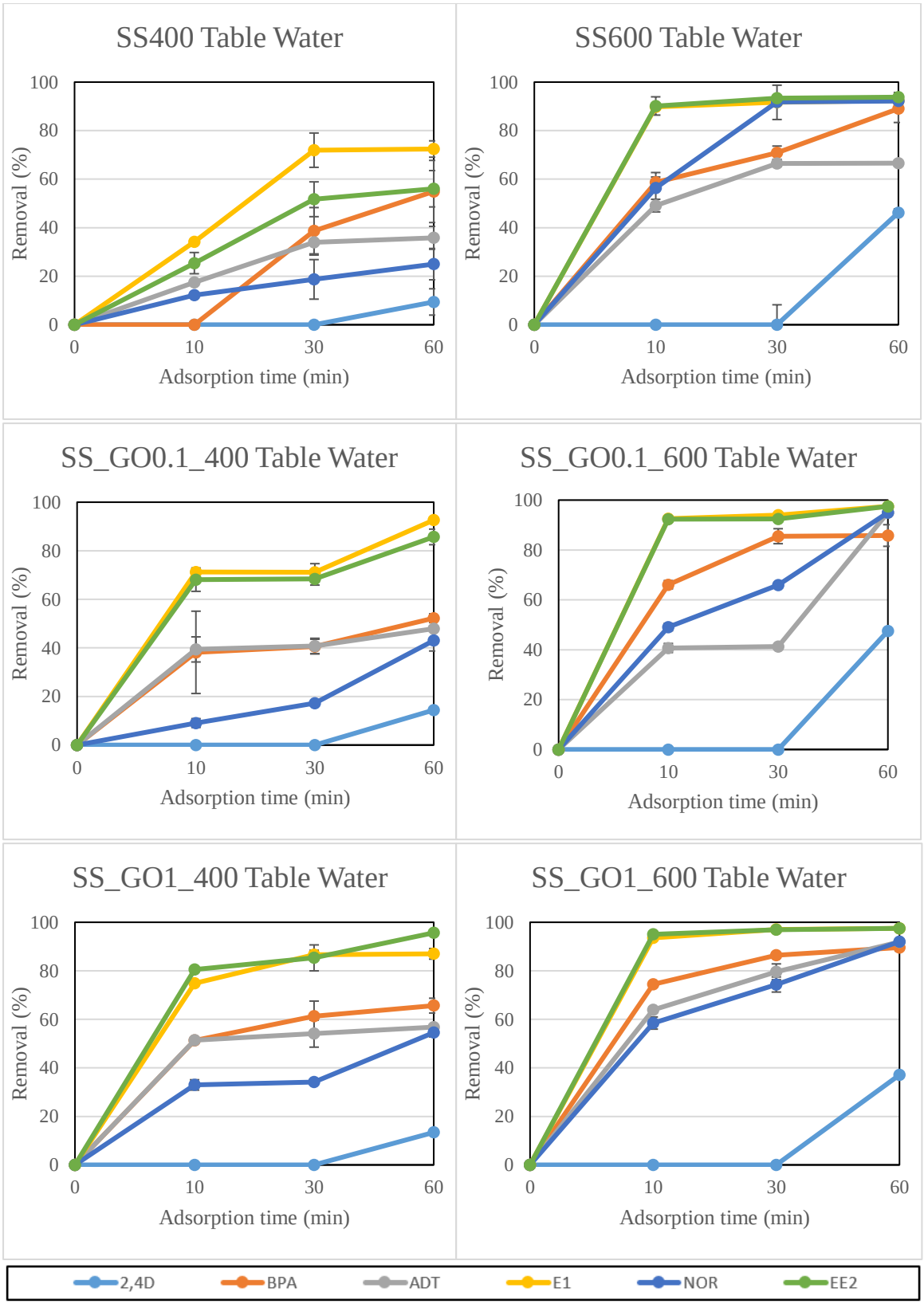

Figure 4.8: Organic micro-pollutant adsorption on SS biochars in table water. Error bars depict standard deviation of duplicate repetition.

Figure 4.8 depicts the results concerning the adsorption of the investigated organic micro-pollutants on conventional and GO-engineered SS biochars, in table water. Removal was in the range of 9,4%-72,4% for SS400, 46.2%-93,8% for SS600, 14,4%-92,6% for SS_GO0.1_400, 47,5%-97,5% for SS_GO0.1_600, 13,4%-95,7% for SS_GO1_400 and 37,1%-97,5% for SS_GO1_600, in 60min of adsorption time. The role of higher pyrolysis temperature for biochar production was even more highlighted by the SS biochar adsorption results, where samples produced at 600℃ showed higher adsorption rates (14.4%-97.5%) compared to those produced at 400℃ (9.4%-95.7%). Furthermore, GO functionalization was proved to be important for the SS samples too, where functionalized biochars could remove micro-pollutants faster and at higher rates compared to untreated biochars. Specifically, GO functionalized biochars at 600℃ achieved >40% pollutant removal by the first 10min of adsorption time for the majority of the investigated compounds. This was attributed to the additional and important surface C-based functional groups that GO provided to the integrated biochar samples, combined with its large surface area and porosity (Plaza et al., 2019). An important observation concerning the SS biochar adsorption results in table water was the significant difficulty concerning the removal of 2.4D. Removal rates for this compound were significantly low (9.4%-46.2%) and achieved only after 60min of adsorption time. These results were attributed to the higher pH_{PZC} values of SS biochars (6.9-7.7) compared to RH biochars (4.4-7.2), which made it more difficult for 2.4D to get adsorbed. 2.4D has a pk_a value of 7.89, which is close to the pH_{PZC} median values of SS biochars. In our previous work, we observed similar trends and concluded that adsorption of 2.4D is less efficient when solution pH values and biochar pH_{PZC} values are equal or higher than the pk_a value of the pollutant (Regkouzas & Diamadopoulos, 2019), leading to reduced adsorption efficiency and potential pore blockage (Xiong et al., 2021).

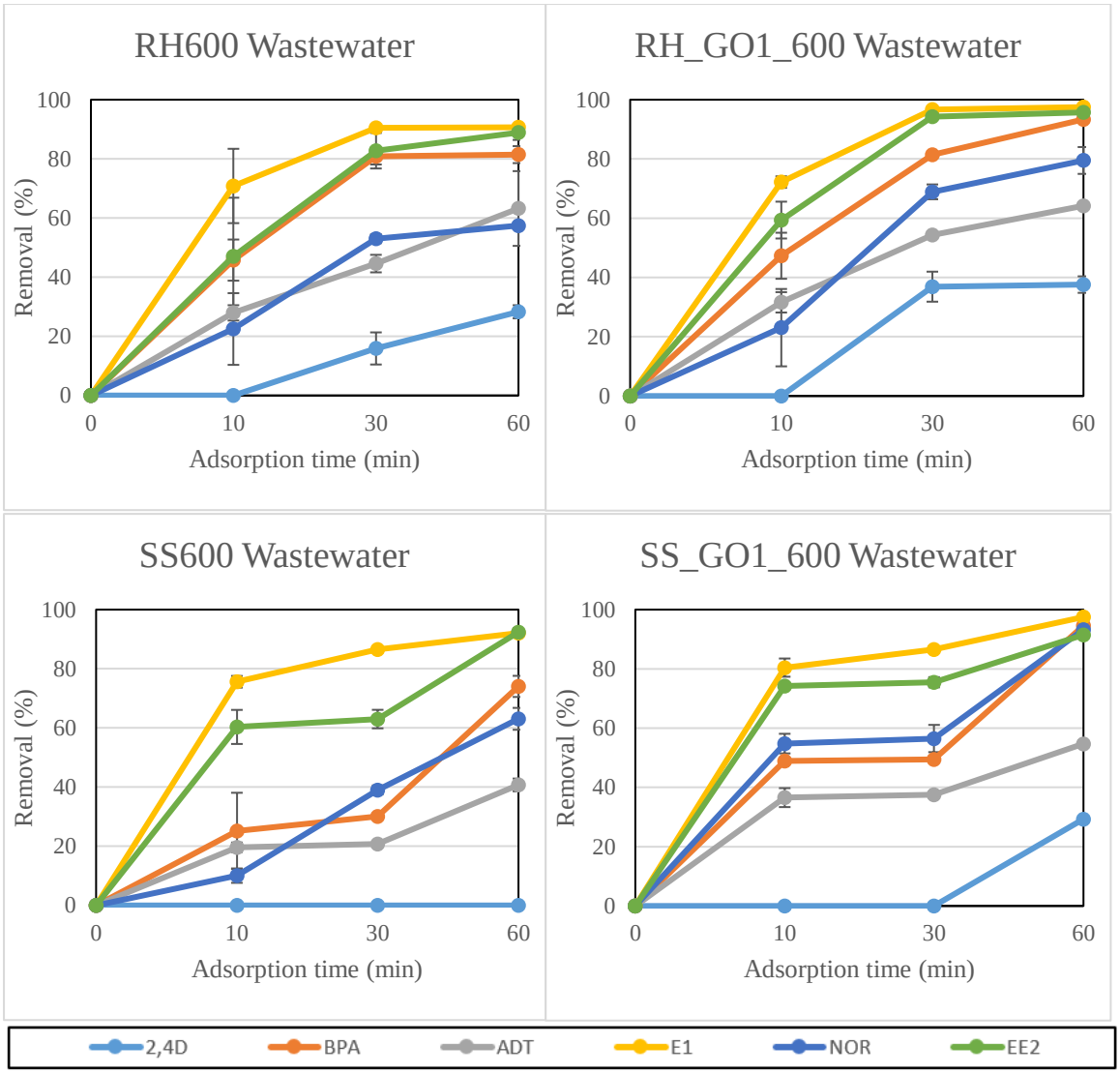

Figure 4.9: Organic micro-pollutant adsorption on RH and SS biochars in wastewater. Error bars depict standard deviation of duplicate repetition

Figure 4.9 contains the results regarding the micro-pollutant adsorption on selected RH and SS biochars in wastewater. Experiments were performed on untreated and 1% GO-functionalized biochars at 600°C. Pollutant removal was in the range of 28.3%-97.5% for RH biochars and 0%-97.5% for SS biochars. Adsorption efficiency was higher for RH biochars, which is consistent with the table water adsorption results. Moreover, GO-functionalized biochars were also more effective compared to the untreated ones, leading to slightly higher pollutant removal rates. The two estrogens, E1 and EE2 were removed at the highest rates (88.9%-97.5%), followed by NOR, BPA and ADT, while 2.4D was the hardest compound to adsorb in this case too. 2.4D removal rates ranged between 0% and 37.6% in 60min of adsorption time, where

SS600 completely failed to adsorb the compound, even after 60min of contact time. Apart from the parameters discussed in the SS biochar table water results, antagonistic interactions between the organic or inorganic compounds existing in the secondary effluent along with the investigated pollutants were probably another significant reason for the reduced adsorption rates of 2.4D (Kalderis et al., 2017). This phenomenon leads to biochar pore blockage and as a result, lower adsorption efficiency (Chen et al., 2021a). For the same reasons, micro-pollutant removal from treated municipal wastewater was lower compared to the table water adsorption results, which was also witnessed in our previous work (Regkouzas & Diamadopoulos, 2019).

The adsorption mechanisms that took place concerning both water and wastewater adsorption experiments were not thoroughly investigated, but some assumptions can be made based on the available data. The most likely involved mechanisms in the case of this study were pore-filling, which is strongly connected to biochar micro- and meso- porous nature formed in temperatures above 400°C and is described by high and fast pollutant removal rates (Regkouzas & Diamadopoulos, 2019), electrostatic interactions with ionic compounds or chemisorption, which created strong electrostatic interaction between biochar surface and the polar nature of the investigated pollutants (Abbas et al., 2018), along with hydrophobic reactions, which combine partitioning and hydrophobic attraction, which is attributed to the non-carbonized or partially carbonized fractions on biochar surface and play a significant role concerning hydrophobic compound adsorption (Ambaye et al., 2020).

Moreover, a significant matter that has been concerning biochar research community is exhausted biochar reuse. Biochars that have been previously used for adsorption purposes usually present lower adsorption efficiency when used in consecutive adsorption experiments, concerning either organic or inorganic pollutants, which creates the need for proper reuse strategies of the material (Gao et al., 2022). Agronomic application of exhausted biochar as soil amendment seems to be the most sustainable solution, as it can offer beneficial properties to the amending soil and cultivation, such as nutrient supplementation, carbon mitigation, increase of the water holding capacity, enhancement of soil microbial activity and several other properties (Mosa et al., 2018; Mosa et al., 2020). In order to assess EC loaded exhausted biochar, further experimental work is needed, but based on previous works, the majority of the adsorbed ECs would probably remain in non-leachable form in biochar structure without posing a threat to the applied soil (Mer et al., 2021). Other works have shown that exhausted biochar could also be reused in the building industry as cement additive, leading to a significant carbon footprint decrease of these materials (Legan et al., 2022; Danish et al., 2021).

4.4 Conclusion

The results of this chapter showed that the main parameter that affected biochar physicochemical structure and composition was biomass type, followed by pyrolysis temperature and GO functionalization. RH is an agronomic lignocellulotic biomass and biochars produced from it showed significantly more favorable properties than SS, which is an anthropogenic waste, containing various burdening compounds in its structure, such as high inorganic content, which works negatively for many of biochar properties. Moreover, higher pyrolysis temperature also improved biochar, by increasing the carbon content, S_{BET} and surface functional groups, thus presenting a more aromatic structure. The metal content of biochars was within the permissible limits set by the European Union and in combination with our previous work, it could be suggested that RH and SS biochar could be safely used for environmental applications. FTIR and XPS analyses showed an abundance and variety of elements and functional groups on biochar surface, where SS biochar showed greater elemental variety, but RH biochars showed better distributed C-based functional groups, which is very important for their use as adsorptive materials. This was confirmed by the organic micro-pollutant adsorption results, where RH biochars were better than SS biochars as adsorbents, achieving higher pollutant removal rates in less contact time. Based on the results of this work, we conclude that the best biochar produced was RH_GO1_600, where the abundance and variety of its C-based functional groups made it a successful adsorbent for organic micro-pollutants from water and treated municipal wastewater.

4.5 Supplementary material

Table S4.1: Table water and wastewater sample characterization

Table water		**Wastewater**	
pH	7.9	**pH**	7,8
EC	251μS cm^{-1}	**BOD**	6mg L^{-1}
Dry Residue	162mg L^{-1}	**COD**	13-15mg L^{-1}
Total Hardness	128 mg L^{-1} $CaCO_3$	**TOC**	5,3ppm
		TSS	7mg L^{-1}

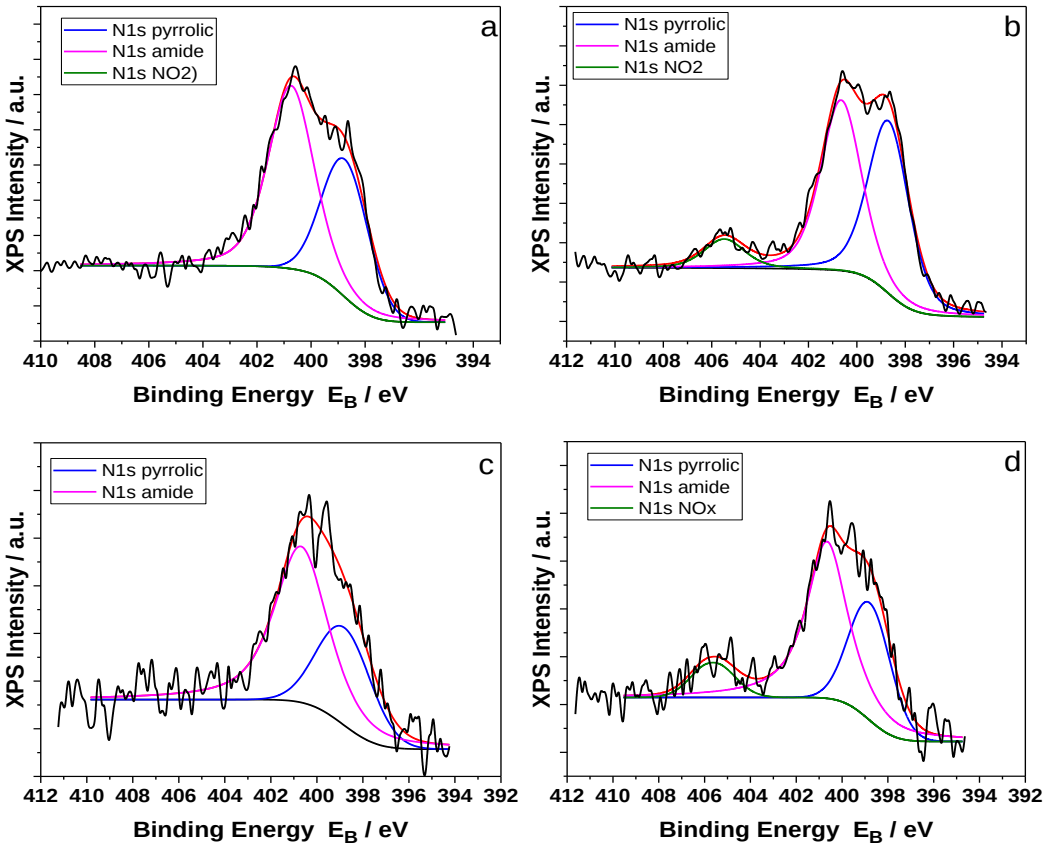

Figure S4.1: Deconvoluted N1s peaks of S1a: SS600, S1b: SS_GO1_600, S1c: RH600, S1d: RH_GO1_600.

Table S4.2: % component concentrations of N1s peaks.

SS600			
Peak	**Eb (eV)**	**% Component C**	**Assignement**
N1s	398.74	38.72 ± 1.95	Pyrrole (N-C)
N1s	400.74	61.28 ± 1.95	Amide (N-C=O)
N1s	405.61	0.00 ± 0.00	NO2 (C-NO2)
SS_GO1_600			
Peak	**Eb (eV)**	**% Component C**	**Assignement**
N1s	398.68	45.54 ± 2.51	Pyrrole (N-C)
N1s	400.65	46.53 ± 2.20	Amide (N-C=O)
N1s	405.48	7.93 ± 0.80	NO2 (C-NO2)
RH600			
Peak	**Eb (eV)**	**% Component C**	**Assignement**
N1s	398.80	32.23 ± 5.13	Pyrrole (N-C)
N1s	400.69	67.77 ± 5.13	Amide (N-C=O)
RH_GO1_600			
Peak	**Eb (eV)**	**% Component C**	**Assignement**
N1s	398.78	31.33 ± 3.70	Pyrrole (N-C)
N1s	400.66	59.10 ± 4.51	Amide (N-C=O)
N1s	405.59	9.57 ± 2.73	NO2 (C-NO2)

5. Experimental cycle 3. Emerging Micro-Contaminant adsorption from water and wastewater using CNT-doped biochar nanocomposites from rice husks and sewage sludge

ABSTRACT

In this chapter, two biomass feedstocks, rice husks (RH) and sewage sludge (SS), were used to produce carbon nanotube (CNT) doped biochar nanocomposites. The samples were produced by pyrolysis at 400℃ and 600℃, they were physico-chemically and structurally characterized and finally utilized as adsorbents to remove six micro-contaminants of emerging concern (EMCs) from water and treated municipal wastewater under near-realistic initial concentrations. RH biochar nanocomposites were more effective than SS biochar nanocomposites on the adsorption of EMCs, requiring lower adsorption times (5min as compared to 10min) to sufficiently remove (>80%) of the investigated pollutants. This was in agreement with the physicochemical analysis of biochar nanocomposites which showed a more developed porous structure for RH samples. The main mechanisms of adsorption were found to be π-π EDA interactions accompanied by pore-filling mechanisms, along with hydrophobic and electrostatic interactions, in a less dominant role. This study showed that RH and SS biochar nanocomposites can be effective in decontaminating water and wastewater from emerging pollutants.

Keywords: biochar nanocomposites, CNTs, emerging contaminants, wastewater treatment

5.1 Introduction

Water quality has been one of the subjects that concerned multiple fields of engineering during recent years. Anthropogenic activities, agriculture and industrial development are some of the main factors responsible for the pollution of surface waters with organic and inorganic contaminants, leading to various and not yet fully known consequences for the recipient organisms [Palansooriya et al., 2019]. Water contamination with organic pollutants, especially with those that have been characterized as Emerging Contaminants (ECs), is a serious environmental issue nowadays that needs to be efficiently addressed. The main characteristics of these contaminants are the low concentrations in which they are detected, along with the inability of conventional treatment techniques at Wastewater Treatment Plants (WWTPs) to remove them [Rathi et al., 2021]. Moreover, they are usually resistant to biodegradation, while they easily bioaccumulate in living organisms, increasing the risk for hormonal disfunction and genetic mutations [Sivaranjanee & Kumar, 2021]. As newly occurring emerging organic contaminants are being frequently detected in wastewater effluents and surface waters, environmental sciences have focused on the need to monitor them properly and find effective treatment techniques to ensure water and wastewater quality [Taheran et al., 2018].

In order to address the serious problem of water contamination, various techniques have emerged, such as advanced oxidation, photocatalysis, filtration and adsorption [Varsha et al., 2022]. Biochar is a low-cost carbonaceous adsorbent produced by biomass pyrolysis, representing a sustainable technology which reuses waste to produce new materials that can be further used for anti-pollution purposes, abiding to circular economy [Singh et al., 2022]. The final product is a porous and rich in organic C material, which presents various favorable physicochemical features that are mostly dependent on the biomass used as feedstock, along with the pyrolysis production conditions [Kumar et al., 2022]. The main fields of biochar application have been agriculture, where it can be used as soil amendment and environmental engineering, where it can be applied as an adsorbent for water or soil remediation [Zhou et al., 2021]. Biochar technology shares the same production processes with its main competitor, activated carbon (AC), except for the final activation part, usually performed using steam, which makes activated carbon more efficient as an adsorbent, though with a significantly higher cost [Kah et al., 2017].

As research has progressed and various data concerning biochar efficiency as an adsorbent have been published in literature, a new technology has emerged, called biochar

nanocomposites. This is the result of combining two scientific fields, pyrolysis and nanotechnology, which aim to the formation of advanced sorptive products. These innovative sorbents, biochar nanocomposites, are characterized by reduced pore size and the enhanced sorption ability due to their significantly improved physicochemical structure rendering them able to antagonize the efficiency of AC [Chausali et al., 2021]. Various nanomaterials have been tested as precursors for nanobiochar production, such as graphene, graphene oxide, CNTs, chitosan etc. [Liu et al., 2022]. Carbon Nanotubes (CNTs) are cylindrical graphene (nano) tubes that present several favorable properties, such as abundance in surface functional groups and micro-porosity, mechanical and electrical strength, large surface area, small diameter and mass density, along with high surface hydrophobicity [Roy et al., 2019]. The combination of low doses of a costly but highly effective nanomaterial, such as CNTs, with a low-cost sorptive material like biochar could lead to the formation of integrated adsorbents, capable to remove persistent contaminants from water and wastewater [Inyang et al., 2015].

The goal of this chapter was to develop CNT-doped biochar nanocomposites, using Rice Husks (RH) as an agricultural biomass and Sewage Sludge (SS) as an anthropogenically derived waste biomass, two CNT doses (1% and 10% w/w), at two pyrolytic temperatures (400°C and 600°C) and to thoroughly test them for the adsorption of six organic Emerging Micro-Contaminants (EMCs) from table water and treated secondary effluent, in real-realistic conditions .

5.2 Materials and methods

5.2.1 Biochar nanocomposite production

Two biomass types were selected for nanomaterial induction, towards biochar nanocomposite production using pyrolysis: a. Rice husks (RH), obtained from a rice mill in northern Greece. b. Secondary sewage sludge (SS), that has been anaerobically digested and dewatered, was obtained from the Psyttalia Wastewater Treatment Plant (Athens, Greece). After oven-drying the biomass samples at 90°C for 48h, they were pulverized to a particle size <0.5mm. Then, they were stored in airtight plastic containers in a dark environment to prevent oxidation and photolytic processes.

CNT grafting into the biomass was implemented by adopting the dip-coating procedure, as described in our previous work [Regkouzas et al., 2023]. In this work, -COOH functionalized graphitized multi-walled Carbon Nanotubes were used, with 99.99% purity and 28-48nm outside diameter (Nanografi S.A.). Briefly, CNTs were suspended in double de-ionized water

by adding either 0.4g CNTs or 4g CNTs in 400mL double de-ionized water (0.1% CNT w/v and 1% CNT w/v, respectively). The suspensions were then ultra-sonicated at 25KHz for 1h, in order to achieve complete dispersion of CNTs in the water. This step was followed by the addition of 40g biomass to each suspension and by homogenization by a mechanical stirrer at 800rpm, resulting to CNT-doped biomasses, i.e. 1% w/w and 10% w/w. After the homogenization stage, samples were oven-dried at 80°C for 48h and then placed in air-tight sealed crucibles for biochar production.

Biochar nanocomposite production took place by pyrolysis in a muffle furnace (Linn High Therm). Two pyrolysis temperatures were used, 400°C and 600°C, while the heating rate was set at 6ºC min^{-1}. During pyrolysis, 99% pure Nitrogen gas was supplied at a 200L h^{-1} rate to ensure anoxic conditions. Samples stayed in the pyrolysis chamber for 60min at the desirable temperatures to achieve total carbonization. After pyrolysis, all biochar nanocomposite samples were washed with de-ionized water to remove any impurities, oven-dried and finally stored in dark airtight plastic containers, until further use. Sample coding and description is presented in Table 5.1.

Table 5.1: Biochar nanocomposite codification and description

Code name	Description
RH_CNT1_400	Rice Husks biochar nanocomposite, CNT dose 1% w/w, at 400°C
RH_CNT10_400	Rice Husks biochar nanocomposite, CNT dose 10% w/w, at 400°C
RH_CNT1_600	Rice Husks biochar nanocomposite, CNT dose 1% w/w, at 600°C
RH_CNT10_600	Rice Husks biochar nanocomposite, CNT dose 10% w/w, at 600°C
SS_CNT1_400	Sewage Sludge biochar nanocomposite, CNT dose 1% w/w, at 400°C
SS_CNT10_400	Sewage Sludge biochar nanocomposite, CNT dose 10% w/w, at 400°C
SS_CNT1_600	Sewage Sludge biochar nanocomposite, CNT dose 1% w/w, at 600°C
SS_CNT10_600	Sewage Sludge biochar nanocomposite, CNT dose 10% w/w, at 600°C

5.2.2 Biochar nanocomposite characterization

The properties of the biochar nanocomposites were assessed by several physicochemical analyses. Ash content was determined by dry combustion in a muffle furnace at 750ºC for 6h. pH and Electrical Conductivity (EC) values were determined using a multi-meter Crison Instruments (micropH 2202), after shaking biochar with de-ionized water, in a 1:20 ratio, for 90min, while the Point of Zero Charge (PZC) of the samples was determined by applying the pH-drift method, as described in our previous work [Regkouzas et al., 2023]. Organic Carbon

(C_{ORG}) content was determined using the SSM-500A solid sample module of a Shimadzu Total Organic Carbon analyser. Specific surface area was determined in a NOVA 2200 Thermo Scientific Surfer gas sorption analyzer (samples were de-gasified at 200°C), by applying the BET (Brunauer-Emmet-Teller) method, while bulk density was determined using the analogue VDLUFA-Method A 13.2.1 [EBC, 2012]. All analyses were performed in triplicate repetition.

Investigation of biochar nanocomposite surface functional groups was achieved by performing X-ray Photoelectron Spectroscopy (XPS) analysis. The XPS measurements were performed in a UHV chamber (base pressure $P \sim 5 \times 10^{-10}$ mbar) equipped with a dual anode Mg/Al x-ray source and a SPECS Phoibos 100-1D-DLD hemispherical electron analyzer. The unmonochromatized MgKα line at 1253.6 eV and an analyzer pass energy of 15eV (giving a full width at half maximum (FWHM) of 0.85 eV for the $Ag3d_{5/2}$ peak) were used. The commercial software SpecsLab Prodigy (from Specs GmbH, Berlin) was used to collect and process the spectra including fitting. The XPS core level spectra were analysed using a fitting routine, that can decompose each spectrum into individual mixed Gaussian-Lorentzian peaks after a Shirley background subtraction. The samples were pressed on Indium foil and the analysed area was a spot of 3mm diameter.

5.2.3 Emerging Micro-Contaminant kinetic adsorption experiments

Six organic micro-pollutants that are identified as EMCs were chosen to study the adsorption kinetics: two phenols, 2.4-Dichlorophenol (2-4D) and Bisphenol A (BPA), two estrogens, Estrone (E1) and 17α-Ethinyl Estradiol (EE2), and two androgens, Androsterone (ADT) and 19-Norethindrone (NOR). These pollutants are being increasingly detected in WWTP effluents, at levels ranging from ng L^{-1} to μg L^{-1} [Richardson & Tennes, 2018]. In order to recreate close to realistic experimental conditions, the initial concentrations in the pollutant mix were in the low microgram per litre range: 2-4D and BPA: 20-40μg L^{-1}, E1 and EE2: 40-60μg L^{-1}, ADT and NOR: 70-90μg L^{-1}. The polluted mix was created by spiking the abovementioned pollutants into 500mL of table water and secondary effluent (prior to chlorination), obtained from the municipal wastewater treatment plant of Chania (DEYAX). Table S1 (Supplementary Material) provides information on the characteristics of both table water and wastewater samples. In order to prevent photolytic/photocatalytic processes and ensure experimental validity, the pollutant mix was synthesized daily.

Adsorption kinetic experiments were performed in duplicate using light-protected conical flasks, at 22±1°C. 50mL of the spiked pollutant sample along with 0.15g of biochar (equal to a dose of 3g L^{-1}) were added into the flasks. The adsorption residence times investigated were 5min, 10min and 30min, respectively. Adsorption pH was in the range of 7.5-8 for both water and wastewater experiments, which simulated what would naturally happen in real conditions without any modifications with the original water pH being 7.9, while wastewater pH was 7.8. When the required adsorption time was reached, the samples were filtered with 0.45μm PVDF Whatman filters to retrieve the aqueous phase. After this stage, analytical methods were applied for pollutant determination, as described in the next sub-chapter.

5.2.4 Analytical chemical method for EMCs determination

The samples from the adsorption experiments were analysed using Solid Phase Micro-Extraction followed by GC-MS analysis, according to a modified method developed by Antoniou et al., (2009) and integrated in our previous work [Regkouzas et al., 2023]. Specifically, 10mL of the polluted mix was inserted into an amber vial (15mL, Supelco), which was airtight closed by means of a PTFE-silicone septum, along with 1.5g NaCl to increase salinity. The sample pH was adjusted to 2.5-3. The samples were vortexed for 1min and then placed into a water-bath at 60°C and 530rpm for 1h, while an SPME Fiber Assembly 85μm Polyacrylate Fused Silica 24 GA, Supelco was inserted through the septum into the vial. After 1h, the fiber was removed from the vial and directly inserted into the injection port of a Shimatzu GCMS-QP5050A (Gas chromatograph Mass Spectrometer), where desorption took place for 10min at 290°C followed by the analysis. GC-MS detection limit for the investigated compounds was in the range of 1-3 μg L^{-1}.

5.2.5 Adsorption mechanisms determination

The investigation of the mechanisms involved in pollutant adsorption was achieved by performing X-ray Photoelectron Spectroscopy (XPS) analysis on biochar nanocomposite samples after the adsorption experiments, to investigate which surface functional groups of the adsorbents were involved in pollutant removal. Specifically, all biochar nanocomposites were retrieved after 10min of adsorption of the EMCs from wastewater, filtered to remove the aqueous part and oven-dried at 30°C for 1d. After that, XPS analysis was performed on all samples to investigate changes in the synthesis of biochar nanocomposite surface functional groups compared to the initial XPS analysis on raw biochar nanocomposites.

5.3 Results & discussion

5.3.1 Biochar nanocomposite characterization

Table 5.2 contains the results of the physicochemical characterization performed on RH and SS, CNT-doped biochar nanocomposites. Sample pH values were neutral to slightly alkaline, ranging from 5.5 to 8.2 for RH biochar nanocomposites and 6.9 to 7.9 for SS biochar nanocomposites. The main variable that affected sample pH values was pyrolysis temperature, where higher temperature resulted to higher pH values by 0.9 to 2.9 units. This confirms information found in literature supporting that biochar pH values are mostly affected by carbonization type and temperature, while at the same time biochar pH values provide insight on the carbonization degree of the samples [Weber & Quicker, 2018]. Similar trends were also observed for the pH_{PZC} analysis. Specifically, pH_{PZC} values were found in the range of 5.7-7.9 and 7.0-7.4 for the RH and SS biochar nanocomposites accordingly, where higher pyrolytic temperature provided higher pH_{PZC} values. This was attributed to the higher inorganic content of biochar nanocomposites, when pyrolyzed at higher temperatures, resulting to more positively charged adsorbents [Zhou et al., 2019]. Moreover, when pH_{PZC} is found to be higher than pH, it is suggested that the sample is positively charged, like in the case of biochar nanocomposites of this work produced at 400℃ [Essandoh et al., 2017]. On the other hand, biochar nanocomposites produced at 600℃ followed an opposite trend, being negatively charged. EC results suggest that biomass type was the main factor affecting this parameter, where SS biochar nanocomposites showed significantly higher EC values (296.3-596.7μS cm^{-1}) compared to RH biochar nanocomposites (146.4-178.77μS cm^{-1}), followed by pyrolysis temperature to a much lesser extent. This significant difference between the two biomasses was expected due to the higher inorganic content of SS that indicates high presence of soluble salts in its structure [Chen et al., 2021b].

Table 5.2: Physicochemical characterization of CNT-doped biochar nanocomposites

Sample ID	pH	pH_{PZC}	EC (μS cm^{-1})	Ash (%)	S_{BET} (m^2 g^{-1})	Bulk Density (Kg m^{-3})	C_{ORG} (%)
RH_CNT1_400	5.5 ± 0.1	5.9 ± 0.0	178.7 ± 5.8	33.4 ± 0.6	63.9 ± 2.5	265 ± 3	46.3 ± 1.2
RH_CNT1_600	8.4 ± 0.1	6.6 ± 0.1	157.8 ± 4.3	39.1 ± 0.5	253.6 ± 9.5	257 ± 12	48.8 ± 2.1
RH_CNT10_400	5.6 ± 0.1	5.7 ± 0.2	151.9 ± 3.4	28.7 ± 0.3	88.0 ± 3.3	216 ± 8	54.4 ± 0.8
RH_CNT10_600	8.2 ± 0.0	7.9 ± 0.0	146.4 ± 3.3	34.1 ± 0.3	261.8 ± 3.5	204 ± 4	58.1 ± 1.8
SS_CNT1_400	6.9 ± 0.1	7.1 ± 0.1	566.7 ± 10.4	51.8 ± 0.2	88.2 ± 1.7	549 ± 16	26.9 ± 1.3
SS_CNT1_600	7.9 ± 0.2	7.4 ± 0.0	296.3 ± 5.7	61.0 ± 0.4	48.2 ± 2.5	539 ± 13	25.9 ± 0.6
SS_CNT10_400	6.9 ± 0.0	7.0 ± 0.0	596.7 ± 3.6	44.9 ± 0.2	91.8 ± 0.8	482 ± 10	38.8 ± 1.2
SS_CNT10_600	7.6 ± 0.1	7.4 ± 0.0	380.3 ± 16.1	53.1 ± 0.2	53.2 ± 1.2	406 ± 12	37.9 ± 1.0

Biochar nanocomposite ash content was in the range of 28.7-39.1% for the RH samples and 44.9-61.0% for the SS samples. It is obvious that SS biochar nanocomposites have almost double ash content compared to RH biochar nanocomposites, which was expected because of SS high initial inorganic content, mostly in the form of metal oxides and hydroxides [Naqvi et al., 2018]. Additionally, an important factor that affects biochar ash content is pyrolysis temperature, which was obvious in this case too, where higher pyrolysis temperature led to higher ash content by 6-9.2%. This happened due to the extended decomposition of organic matter and volatile compounds that takes place in higher temperatures, leading to inorganic content increase [Pellera et al., 2021]. A similar trend was observed for bulk density results, where SS biochar nanocomposites (204-265kg m^{-3}) showed double values compared to the RH ones (406-549kg m^{-3}), except for the pyrolysis temperature which in this case, higher pyrolysis temperature resulted to lower bulk density values, due to the extended volatilization of organic compounds in biochar structure [Lin et al., 2023].

Organic C content and Specific Surface Area (SSA) are two parameters that provide valuable insight on biochar adsorptive ability and potential. Based on the C_{ORG} results, RH biochar nanocomposites were proven to be significantly more efficient, providing results in the range of 46.3-58.1%, while SS biochar nanocomposites were limited to a smaller range of 25.9-38.8%. The roles of pyrolysis temperature and CNT dose were obvious in this case, leading to higher C_{ORG} content with their increase in the case of RH samples, while on the case of SS samples an opposite trend was observed. In literature, higher temperatures usually lead to higher C content, as a result of intensified carbonization [Xie et al., 2022], like in the case of RH, but in the case of SS an opposite trend was observed both by this work and by other researchers, which was attributed to SS high inorganic content resulting to this effect

[Regkouzas & Diamadopoulos, 2019; Khan et al., 2023]. Results concerning sample Specific Surface Area (S_{BET}) showed that biomass type and pyrolysis temperature were the main variables that affected this parameter. S_{BET} results were in the range of 63.9-261.8$m^2 g^{-1}$ for RH samples and 48.2-91.8$m^2 g^{-1}$ for SS samples. RH biochar nanocomposites showed higher values at 600°C, while SS samples showed the highest values at 400°C, showing a similar trend for the C_{ORG} results. The best results were achieved by RH biochar nanocomposites at 600°C, where samples RH_CNT1_600 and RH_CNT10_600 scored 253.6m^2 g^{-1} and 261.8m^2 g^{-1} accordingly. These results were expected since lignocellulotic biomasses, such as RH, are known to score high SSA contents due to low inorganic content and high carbonization [Li et al., 2020], while waste-derived biomasses, such as SS, provide lower SSA results because of the existence of prohibiting factors, such as high inorganic content, lower porosity and higher bulk density [Ihsanullah et al., 2022; Rangabhashiyam et al., 2022].

Biochar nanocomposite surface composition is presented in Table 5.3, as a result of the XPS analysis. RH biochar nanocomposites were mostly comprised of C- containing surface functional groups (63.3-73.5%), where the higher CNT dose (10% w/w) presented the highest percentages, as expected because of the addition of the carbonaceous nanomaterial. Second in terms of quantity were the O- containing functional groups (18.6-26.1%) being mostly represented by C-O groups and presenting higher percentages in the lower pyrolysis temperature (400°C), followed by Si- containing functional groups (5.4-8.2%) and traces of N-containing functional groups (0.7-1.8%). The existence of Si- containing functional groups was previously witnessed by other studies concerning RH biochar, because Si is an element commonly found in this biomass, which consequently creates surface functional groups and silica structures that often play an active role in the adsorption of organic pollutants [Regkouzas et al., 2023; Severo et al., 2020; Wei et al., 2017].

SS biochar nanocomposites showed a wider variety concerning the elements found in their surface creating the relevant functional groups. C- containing functional groups were found in the range of 47.3-70.2%, being dominant in this case as well, but in relatively lower portion compared to RH biochar nanocomposites. Following, O- containing functional groups were second in quantity, found in the range of 16.6-27.6%. SS biochar nanocomposites with the higher CNT dose (10% w/w) presented more C- and less O- functional groups compared to the relevant ones with the smaller dose, which was also observed for the RH biochar nanocomposites. SS biochar nanocomposites showed a variety of surface functional groups in smaller portions, such as Ca- containing functional groups (1.4-2.8%), Al- containing

functional groups (2.1-4.8%), Si- containing functional groups (1.5-3.3%), P- containing functional groups (1.6-3.2%), B- containing functional groups (3.6-6.4%) and N- containing functional groups (3.2-4.4%). This wide variety of elements on SS biochar nanocomposite surface is strongly connected to the higher ash and mineral content of SS, due to its waste origin and nature [Singh et al., 2020].

Table 5.4 provides valuable information on the analysis of C- peaks retrieved from the XPS analysis to further understand the distribution of the relative functional groups. In general, similar trends were observed for RH and SS biochar nanocomposites concerning the distribution of C peaks, although SS biochar nanocomposites showed less C- containing groups in total (Table 3). RH biochar nanocomposite results showed that pyrolysis temperature played an important role in the distribution of sp^2 and sp^3 hybridized C-C bonds, where samples produced at 400℃ showed lower C=C (C-C sp^2) content (22.3% and 46.4% for CNT doses 1% and 10% w/w respectively) and higher C-C sp^3 content (46.3% and 25.9% for CNT doses 1% and 10% w/w respectively), while samples produced at 600℃ showed higher C=C (C-C sp^2) content (81.1% and 61.7% for CNT doses 1% and 10% w/w respectively) and lower C-C sp^3 content (1.4% and 22.5% for CNT doses 1% and 10% w/w respectively). This was attributed to the fact that biochar presents a more carbonized structure at higher pyrolysis temperatures, thus presenting more aromatic C=C bonds at these conditions [Li et al., 2018]. An important fraction of the C assignments were the C-O(H) bonds, found in the range of 7.3-20.3%, followed by C=O bonds in a smaller ratio of 1.7-6.3%, COOH bonds in the range of 2.0-4.5% and a small fragment of carbonates (1.2-2.0%).

Based on Table 5.4, SS biochar nanocomposites showed a different distribution of the C assignments compared to RH biochar nanocomposites. In this case, C=C (C-C sp^2) content of the samples was found in the range of 43.8-62.7%, while C-C sp^3 content was found in the range of 15.3-34.2%, being half the quantity compared to C=C content. It is obvious that SS biochar nanocomposites showed less C-C (sp^2 and sp^3) content compared to the RH ones, as well as an opposite trend concerning the distribution of these two groups. Moreover, SS biochar nanocomposites were rich in C-O(H) bonds, found in the range of 18.4-27.3% and 7.6-12.1% for samples produced at 400℃ and 600℃ accordingly. This was attributed to the semi-pyrolyzed fractions on biochar nanocomposite surface occurring in lower pyrolysis temperatures, along with the higher ash content found in SS [Janu et al., 2021]. The rest of C bonds were found in similar ranges compared to RH biochar nanocomposites, where C=O

bonds were in the range of 3.4-6.6%, COOH bonds in the range of 1.3-4.5% and a small portion of carbonates (1-1.9%).

Table 5.3: % surface atomic concentration of biochar nanocomposites, as derived from the XPS analysis

XPS Peak	Eb (eV)	Assignement	RH_CNT1_400	RH_CNT10_400	RH_CNT1_600	RH_CNT10_600	SS_CNT1_400	SS_CNT10_400	SS_CNT1_600	SS_CNT10_600
C1s	285.0± 0.1	**C-C**	63.3	73.5	71.1	71.6	52.7	70.2	47.3	64.8
Ca2p	347.7± 0.1	**Ca3(PO4)2**	0.2	BDL	BDL	BDL	2.5	1.4	2.8	1.6
O1s	532.1± 0.1	**Mainly C-O**	26.1	20.2	20.6	18.6	25	16.6	27.6	18.8
Al2p	74.8± 0.1	**Al2O3**	BDL	BDL	BDL	1.0	4.3	2.1	4.8	3.2
Si2p	103.2± 0.1	**SiO2**	8.2	5.4	7.6	7.1	3.1	1.5	3.3	1.9
P2p	133.9± 0.1	**Ca3(PO4)2, CaHPO4**	0.3	BDL	BDL	0.3	3.2	1.6	4	2.4
B1s	191.3± 0.1	**B-C-O**	BDL	BDL	BDL	0.7	5	3.4	6.4	4
Fe2p3/2	~712	**FeOOH, Fe2O3**	BDL	BDL	BDL	BDL	BDL	BDL	0.3	BDL
N1s	400.5± 0.1	**N-C**	1.8	0.9	0.7	0.7	4.4	3.2	3.8	3.2

*BDL: Below Detection Limit

Table 5.4: % component concentration of C1s XPS peaks of biochar nanocomposites, as derived from the XPS analysis

Eb (eV)	Assignement	RH_CNT1_400	RH_CNT10_400	RH_CNT1_600	RH_CNT10_600	SS_CNT1_400	SS_CNT10_400	SS_CNT1_600	SS_CNT10_600
284.4± 0.1	**C-C sp^2**	22.3	46.4	81.1	61.7	43.8	57.2	62.7	51.6
285.2± 0.1	**C-C sp^3**	46.3	25.9	1.4	22.5	17	15.3	16.9	34.2
286.2± 0.2	**C-O(H)**	20.3	18.1	7.3	10.9	27.3	18.4	12.1	7.6
287.5± 0.2	**C=O**	4.5	4.3	6.3	1.7	6.6	4.6	3.9	3.4
288.6± 0.2	**COOH**	4.5	3.5	2.3	2	4.3	2.9	3.1	1.3
~290	**carbonates**	2	1.9	1.5	1.2	1	1.6	1.3	1.9

5.3.2 Emerging Micro-Contaminant adsorption experiments

Results concerning EMC adsorption from water on RH biochar nanocomposites are presented in Figure 5.1. The charts represent pollutant removal over time, based on the initial pollutant concentrations described in the Materials & Methods section. Sample RH_CNT1_400 showed the slowest kinetics, being able though to remove >84.5% of the investigated pollutants after 30min of contact time, except for BPA, which was removed by just 73% after the same time. Regarding the three other biochar nanocomposites, adsorption of the investigated EMCs was almost instant, where all pollutants were removed by >81% after just 5min of contact time, resulting to removal rates up to 93.5% after the last investigated contact time of 30min. Since the last three samples showed similar and efficient adsorptive behaviour, the best sample was proven to be RH_CNT1_600, due to the low nanomaterial dose of 1% w/w, resulting to the most cost-efficient RH biochar nanocomposite. Compared to our previous work, where simple RH biochars and Graphene Oxide -doped biochar nanocomposites were tested on the same EMCs, samples of this work were significantly more efficient by 55min of adsorption time, since RH/Graphene Oxide biochar nanocomposites required 60min of contact time to achieve pollutant removals higher than 80% [Regkouzas et al., 2023].

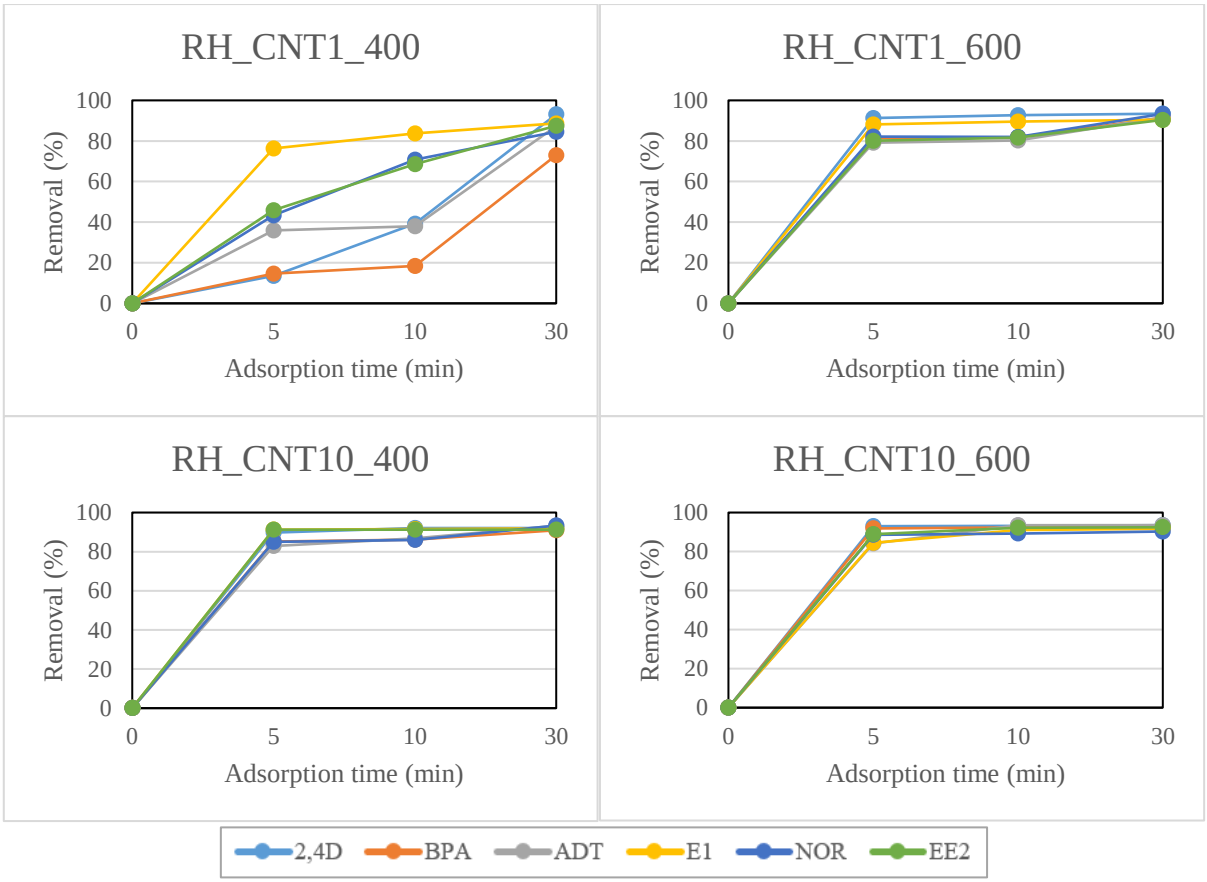

Figure 5.1: Emerging Micro-Contaminant adsorption from water on RH biochar nanocomposites

Figure 5.2 depicts the results concerning EMC adsorption from water on SS biochar nanocomposites. The least efficient sample was again the one produced at 400°C, at the low nanomaterial dose of 1% w/w (SS_CNT1_400), presenting the slowest kinetics during the first two investigated contact times of 5min and 10min. It was able though to sufficiently remove the investigated pollutants by 80.4-92.2% after 30min of contact time. A similar trend was observed for sample SS_CNT1_600 too, which was faster than SS_CNT1_400 but still needed 30min of contact time to achieve removal rates >79% for all pollutants. On the other hand, samples SS_CNT10_400 and SS_CNT10_600 were the most efficient SS biochar nanocomposites, achieving EMC removal rates >82% after 10min and 5min of contact time accordingly. Comparing Figures 1 and 2 it was clear that RH biochar nanocomposites were faster and more efficient compared to SS ones, in terms of EMC adsorption from water, but the existence of nanomaterials even in a small dose significantly improved the adsorption efficiency of the produced biochar nanocomposites, even for the SS originated ones, which are not so efficient in general, based on other works found in literature [Ji et al., 2022; Kończak & Huber, 2022].

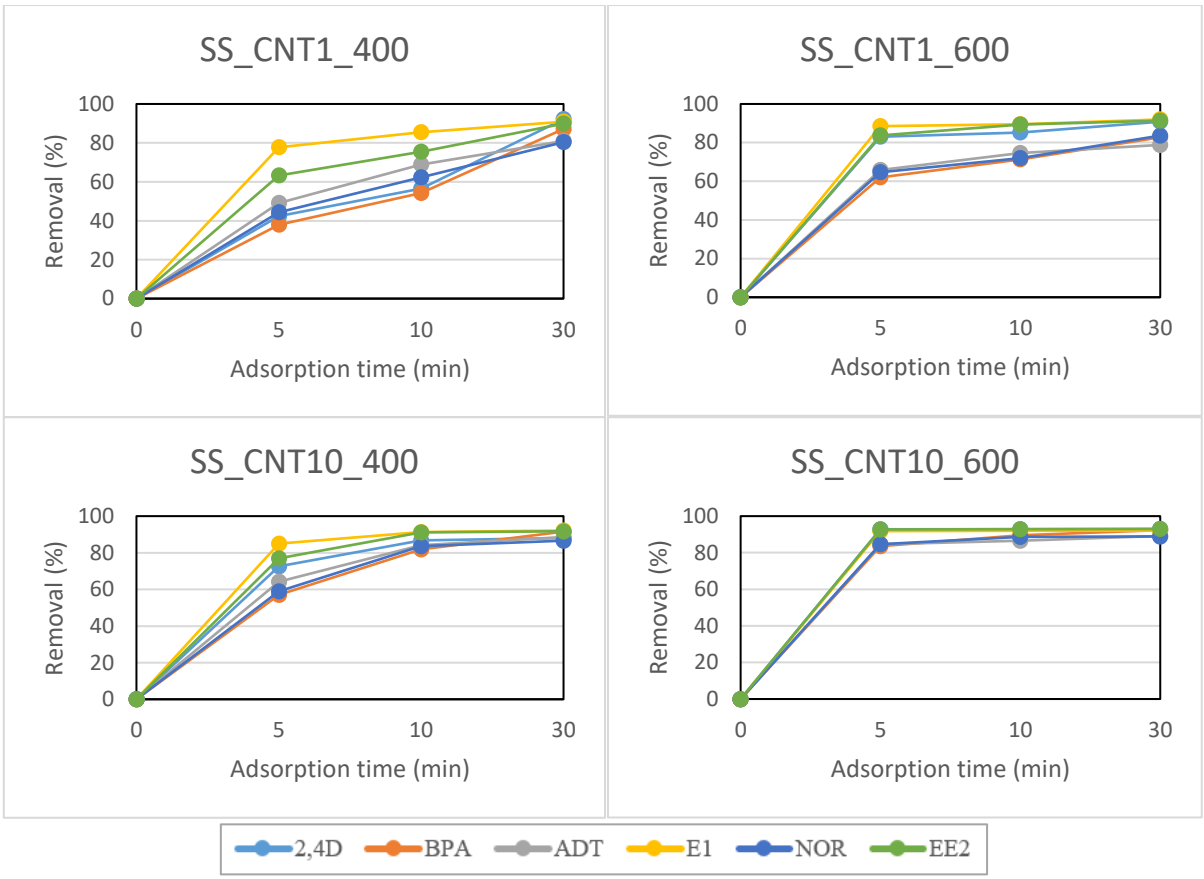

Figure 5.2: Emerging Micro-Contaminant adsorption from water on SS biochar nanocomposites

Figure 5.3 contains the results concerning EMC adsorption from wastewater on RH biochar nanocomposites. Biochar nanocomposites produced at 400°C needed the maximum contact time of 30min to sufficiently adsorb the investigated EMCs from wastewater by 78-96%. On the other hand, biochar nanocomposites produced at 600°C were able to remove faster the investigated pollutants, where RH_CNT1_600 achieved removal rates >84.1% after 10min of adsorption time and RH_CNT10_600, being the most efficient RH biochar nanocomposite by removing more than 82.7% of the pollutants after just 5min of contact time. Compared to the similar experiments performed on water (Figure 1), it was obvious that adsorption was a little slower in this case, which was normal due to the existence of other organic or inorganic compounds in wastewater, resulting to antagonistic pollutant adsorption on biochar nanocomposites [Cheng et al., 2021]. Despite the existence of this phenomenon though, the results of this work showed that the produced RH biochar nanocomposites were more efficient

than those of our previous works [Regkouzas & Diamadopoulos, 2019; Regkouzas et al., 2023], and in agreement with other studies [Ambaye et al., 2021; Qiu et al., 2022b].

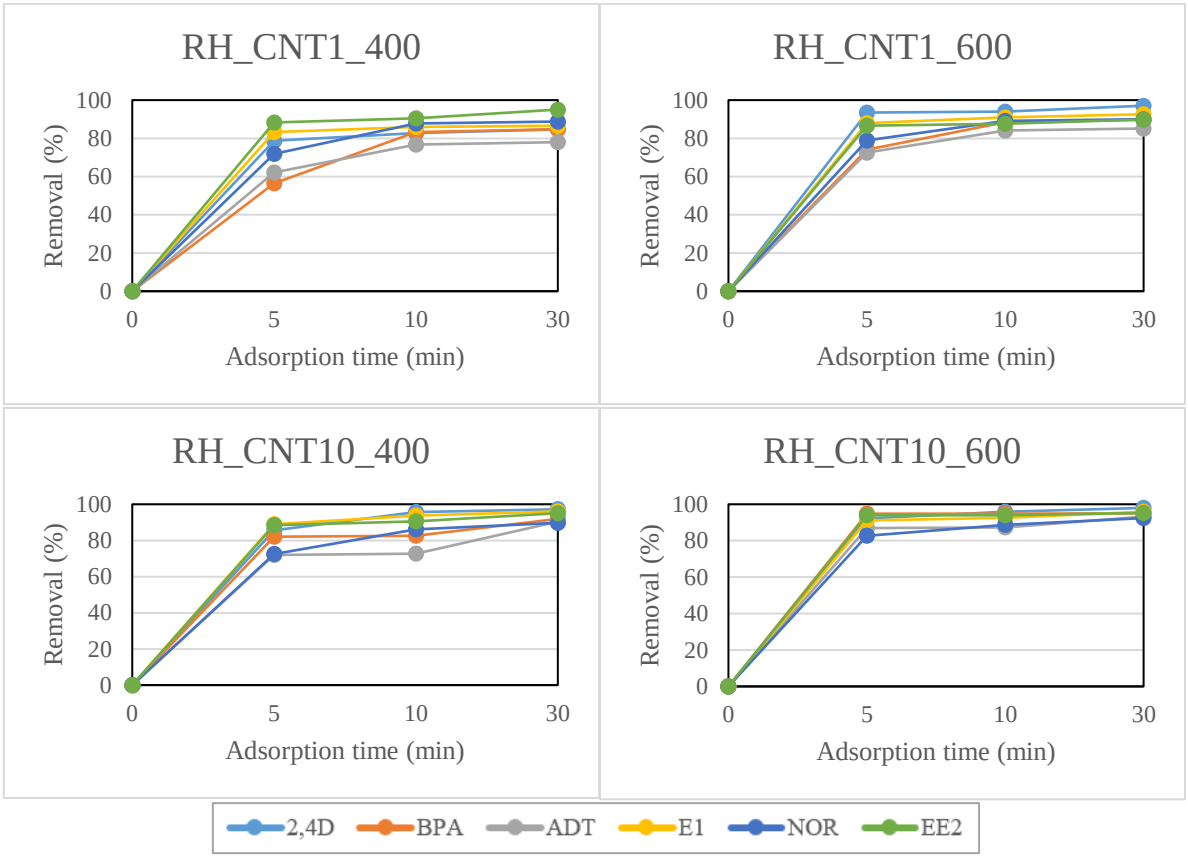

Figure 5.3: Emerging Micro-Contaminant adsorption from wastewater on RH biochar nanocomposites

Results on EMC adsorption from wastewater on SS biochar nanocomposites are presented in Figure 5.4. A similar behaviour to the RH samples was observed in this case too, where SS biochar nanocomposites produced at 400°C were less effective as adsorbents applied in wastewater, compared to those produced at 600°C. Specifically, sample SS_CNT1_400 removed the investigated pollutants by 71.9-87.3% after 30min of contact time, while sample SS_CNT10_400 achieved removal rates in the range of 81.4-93.6% after the same contact time. SS biochar nanocomposites produced at 600°C provided faster results on the adsorption of the investigated pollutants from wastewater, where SS_CNT1_600 achieved removal rates of 79.9-87.5% after 10min of contact time and SS_CNT10_600 adsorbed the investigated EMCs from wastewater by 80.8-94.2% after the first 5min of contact time, providing the best results among SS biochar nanocomposites and a viable realistic solution for tertiary wastewater treatment.

Results showed that CNTs are nanomaterials that have the potential to successfully enhance SS biochar, providing significantly better results compared to our previous work, where Graphene Oxide was chosen to create SS biochar nanocomposites, leading to removal rates of 29.3-95.1% after 60min of contact time [Regkouzas et al., 2023].

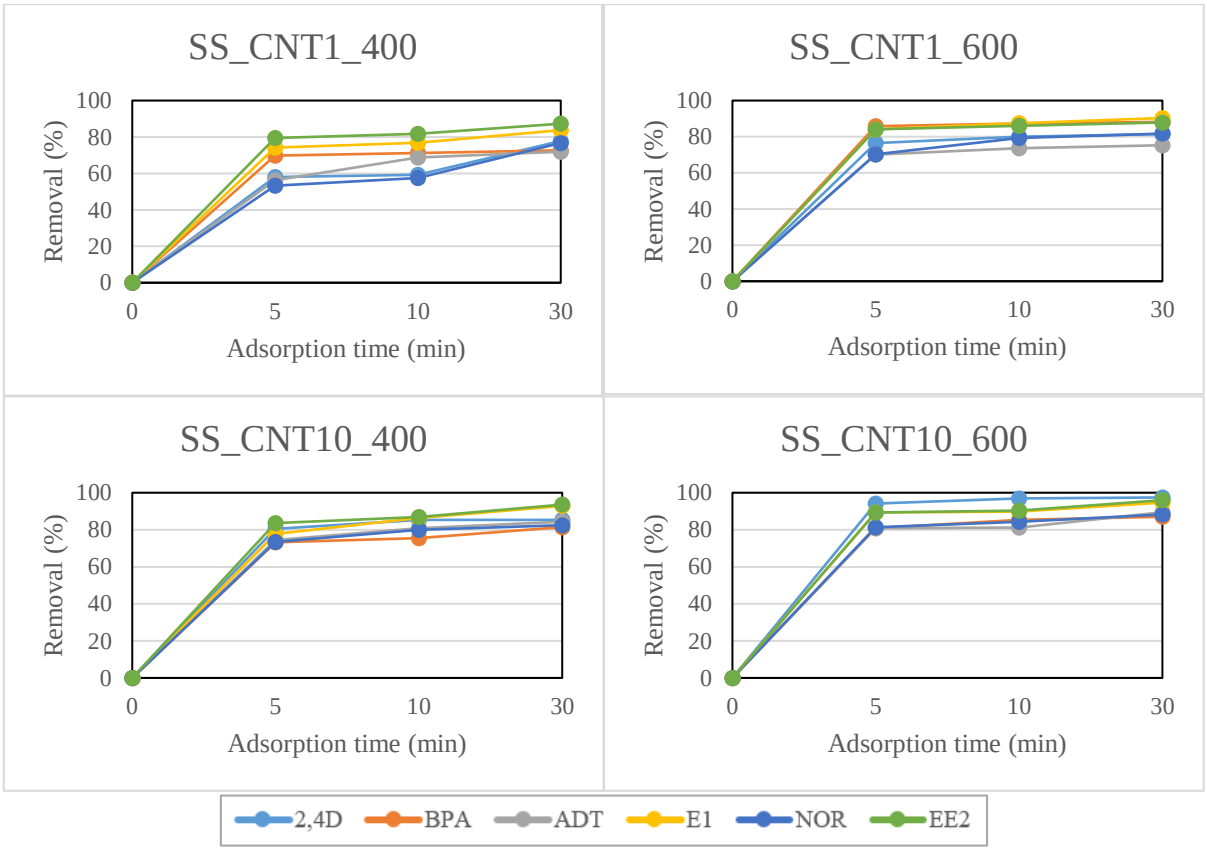

Figure 5.4: Emerging Micro-Contaminant adsorption from wastewater on SS biochar nanocomposites

3.3. Investigation of adsorption mechanisms

In order to obtain valuable information on the mechanisms involved in the adsorption of EMCs on biochar nanocomposites, XPS analysis was performed on all samples after 10min of adsorption time from wastewater, as a tool to observe changes on their surface as a result of the adsorption process. Table 5.5 contains the results concerning the new surface elemental composition of biochar nanocomposites. Surface elemental changes can be extracted by comparing Tables 5.3 and 5.5. RH biochar nanocomposites with the high CNT dose (10% w/w) presented a reduction in C- containing groups, while those with the smaller dose (1% w/w) along with all SS biochar nanocomposites presented a slight increase of these groups, after the

adsorption of EMCs. O- containing groups, mostly represented by C-O assignments, showed a significant (up to 17.1%) decrease for all RH and SS biochar nanocomposites after the adsorption, except for sample RH_CNT10_600, which presented a significant (33.2%) increase of O- containing groups and on the same time the highest C- containing groups decrease among the other samples. An interesting result concerns the significant reduction (11.1-44.0%) of Si-containing groups for SS biochar nanocomposites, which indicated the involvement of silicate structures of these samples on EMC adsorption. The rest of surface elemental groups presented slight increase in all biochar nanocomposite samples. These increases were a result of the adsorption of both the investigated EMCs and other naturally occurring compounds in wastewater, such as NOM and N- containing compounds that stayed on biochar nanocomposite surface after the adsorption incurring chemical oxidation [Fan et al., 2018].

Table 5.6 presents the results concerning the new surface C composition of biochar nanocomposites, which in combination with Table 4 can provide information on the changes concerning surface C composition and the relevant groups that were affected by EMC adsorption from wastewater. RH_CNT1_400 presented losses of C-C (14.9%), COOH (10.2%) and carbonate (52.5%) bonds, which combined to the results from Table 5 that showed 4.9% loss of O- containing groups, mainly represented by C-O bonds, indicates that adsorption of EMCs was achieved mostly by O- and in a lesser extent C- surface functional groups on biochar nanocomposite surface. RH_CNT10_400 showed greater involvement of C- surface functional groups by presenting losses of C=C (8.7%), C-C (26.3%), COOH (16.3%) and carbonate (47.3%) bonds, while on the same time, this sample presented the minimum O-containing group losses of 1%, indicating that C- functional groups were mainly involved in the adsorption of EMCs from wastewater. RH_CNT1_600 showed significantly higher O- surface functional group involvement in the adsorption of EMCS from wastewater by presenting the highest O-losses (14.2%) among RH biochar nanocomposites. C-containing groups presented losses of C=C (8.25), C=O (55.1%), COOH (71.7%) and carbonates (47.3%), confirming the strong involvement of O-containing bonds in the adsorption process. RH_CNT10_600 presented losses of C-C (31.9%), COOH (6.0%) and carbonate (37.5%) bonds, but simultaneously presented no losses in O- containing groups. This sample also presented the highest C-containing groups losses among RH biochar nanocomposites (Table 5), indicating that C-functional groups were dominant in the adsorption of EMCs from wastewater.

SS biochar nanocomposites showed a different behaviour from the relevant RH ones, by indicating the involvement of not just C- and O- functional groups on the adsorption of EMCs

from wastewater. Based on Tables 4 and 6, SS_CNT1_400 presented losses of C=C (8.2%), C-C (15.3%) and carbonate (10.0%) bonds, along with Si- containing group losses equal to 12.6%, indicating that silicate structures played an active role on EMC adsorption from wastewater, combined with C- functional groups. SS_CNT10_400 presented losses of C-C (37.5%) and C-O(H) (18.7%), but, at the same time, it presented the highest Si- containing group losses of 44.0%, along with 8.3% decrease in O- containing groups. This indicated that this sample used C-, O- and Si- functional groups for the adsorption of EMCs from wastewater. SS_CNT1_600 presented C=C (24.7%) and carbonates (61.5%) bond losses, along with O- (4.9%) and Si- (13.9%) containing group losses, presenting a similar behaviour to the previous sample. Finally, SS_CNT10_600 presented losses only for C-C bonds (69.0%) concerning the C- containing groups, but showed greater variety of other elemental groups involved in the adsorption process, such as O- (17.1%), Si- (11.1%), P- (16.3%) and B- (21.5%) containing groups.

Several mechanisms can be involved in the adsorption of organic pollutants as EMCs on biochar nanocomposites. These could be pore-filling mechanisms, hydrophobic attraction/repulsion, electrostatic interactions and π-π EDA interactions between the adsorbent and the pollutant, which are greatly affected by the nature of the pollutants along with the porous and surface properties of the adsorbent [Luo et al., 2022]. Pore filling mechanisms are strongly connected to the porous structure of the adsorbent, where higher surface area and micro- and meso- porous structure of the adsorbent favors the adsorption of organic pollutants by filling the available pores of the adsorbent [Tong et al., 2019]. This mechanism was involved in the adsorption of EMCs from wastewater mostly on RH biochar nanocomposites that presented >50% higher S_{BET} values compared to SS biochar nanocomposites, without being the dominant mechanism though, as would happen in adsorbents with significantly higher surface area and porous structure [Qiu et al., 2022b]. Hydrophobic interactions can also represent a dominant mechanism in the adsorption of organic compounds on biochar nanocomposites. Usually, higher pyrolysis temperatures and the semi-carbonized portion of biochar favor this mechanism to play an active role in the adsorption process [Regkouzas et al., 2023], which was confirmed especially for samples RH_CNT10_400, RH_CNT10_600 and SS_CNT10_600 that presented high C-C bond losses after 10min of EMCs adsorption from wastewater. The fact that the polluted mix used in this work contained six EMCs with various characteristics suggests that different mechanisms could work for different pollutants, such as 2.4D and BPA that are hydrophobic compounds and could be adsorbed on biochar

nanocomposites mainly through this mechanism [Wang & Zhang, 2020]. Another mechanism is the electrostatic interaction between pollutant and adsorbent, which is usually favored by pollutants with polar nature, such as androgens and estrogens [Barquilha & Braga, 2021]. Biochar nanocomposites may attract anionic compounds when their pH values are lower that their pH_{PZC} values [Oh & Seo, 2016], which was observed for all biochar nanocomposites produced at 400°C and cationic compounds in the opposite case ($pH > pH_{PZC}$), which was observed for all biochar nanocomposites produced at 600°C. The fact though that samples produced at 600°C were more efficient than those produced at 400°C concerning EMC adsorption from wastewater, but not in a significant manner, since all adsorbents of this work were extremely efficient, led to the conclusion that hydrophobic interactions did contribute to the adsorption as a mechanism, but not in a dominant manner. The last adsorption mechanism commonly found in organic pollutant adsorption is π-π electron donor-acceptor (EDA) interaction. O- containing functional groups, such as -COOH, -OH, C=O and C-O indirectly representing polar functional groups, can be found especially at lower pyrolytic temperatures and their loss suggests π-π EDA interaction between the pollutants and the adsorbent [Tran et al., 2020]. This was the main mechanism for the adsorption of EMCs from wastewater, especially on RH and secondly on SS biochar nanocomposites, which was expected due to the involvement of -COOH functionalized CNTs in the biochar nanocomposite matrix and was confirmed by the XPS results that showed the intense use of O- functional groups in the adsorption process.

Table 5.5: % surface atomic concentration of biochar nanocomposites after 10min of EMC adsorption from wastewater, as derived from the XPS analysis.

XPS Peak	Eb (eV)	Assignement	RH_CNT1_400	RH_CNT10_400	RH_CNT1_600	RH_CNT10_600	SS_CNT1_400	SS_CNT10_400	SS_CNT1_600	SS_CNT10_600
C1s	**285.0± 0.1**	**C-C**	64.9	72.0	74.5	63.1	52.4	72.1	48.0	68.9
Ca2p	**347.7± 0.1**	**Ca3(PO4)2**	BDL	BDL	BDL	BDL	2.5	1.43	2.9	1.7
O1s	**532.1± 0.1**	**Mainly C-O**	24.8	20.0	17.7	24.8	25.2	15.2	26.3	15.6
Al2p	**74.8± 0.1**	**Al2O3**	BDL	BDL	BDL	BDL	4.3	2.5	5.2	3.3
Si2p	**103.2± 0.1**	**SiO2**	8.2	6.8	7.1	10.8	2.7	0.8	2.8	1.7
P2p	**133.9± 0.1**	**Ca3(PO4)2, CaHPO4**	BDL	BDL	BDL	BDL	3.2	1.5	4.1	2.0
B1s	**191.3± 0.1**	**B-C-O**	BDL	BDL	BDL	BDL	5.0	2.9	6.6	3.1
Fe2p3/2	**~712**	**FeOOH, Fe2O3**	BDL	BDL	BDL	BDL	BDL	BDL	0.3	BDL
N1s	**400.5± 0.1**	**N-C**	2.1	1.3	0.7	1.3	4.4	3.5	3.9	3.4

Table 5.6: % component concentration of C1s XPS peaks biochar nanocomposites after 10min of EMC adsorption from wastewater, as derived from the XPS analysis.

Eb (eV)	Assignement	RH_CNT1_400	RH_CNT10_400	RH_CNT1_600	RH_CNT10_600	SS_CNT1_400	SS_CNT10_400	SS_CNT1_600	SS_CNT10_600
284.4± 0.1	**C-C sp^2**	24.7	42.4	74.5	63.8	40.2	61.6	47.2	63.4
285.2± 0.1	**C-C sp^3**	39.4	19.1	10.1	15.3	14.4	9.6	27.0	10.6
286.2± 0.2	**C-O(H)**	22.4	25.6	11.6	13.2	27.3	15.0	16.4	13.0
287.5± 0.2	**C=O**	8.4	9.3	2.8	5.0	12.1	7.7	5.5	8.3
288.6± 0.2	**COOH**	4.0	2.9	0.7	1.9	5.1	4.2	3.4	2.8
~290	**carbonates**	1.0	0.8	0.8	0.8	0.9	2.0	0.5	1.9

5.4 Conclusion

This chapter showed that CNT- doped biochar nanocomposites from two biomass feedstocks, RH and SS, can be effectively used as adsorbents for the removal of organic micro-pollutants from water and wastewater. Characterization of the samples showed that RH biochar nanocomposites presented better physicochemical structure than SS biochar nanocomposites, especially in terms of C content, specific surface area and surface functional groups. Sample RH_NT10_600 showed the best properties concerning adsorption potential, where C_{ORG} content was 58.1% and S_{BET} was 261.8m^2 g^{-1}. Biochar nanocomposites were comprised mostly of C- and O- containing surface functional groups, as the XPS analysis showed. Biochar nanocomposites were then used as adsorbents to remove six EMCs from water and wastewater, where pollutant removal was higher than at least 80% after 10min of contact time in most cases, with RH biochar nanocomposites proving their physicochemical superiority, by achieving >80% in just 5min of adsorption time, even from wastewater. The main mechanisms involved in the adsorption process were π-π EDA interactions accompanied by pore-filling mechanisms, along with hydrophobicity and electrostatic interactions to a lesser extent. The realistic conditions under which this experiment was conducted, with emphasis on the low initial pollutant concentrations that were chosen, leads to the conclusion that RH and SS biochar nanocomposites could be realistically and effectively used to provide tertiary treatment in water and wastewater treatment plants.

6. Overall discussion

As a result of the three experimental cycles that were described in the previous chapters, valuable information was extracted concerning RH and SS biochar and biochar nanocomposite physicochemical structure, along with their effectiveness as adsorbents for the removal of Emerging Micro-Contaminants (EMCs) from water and wastewater. In this chapter, the correlation of the three cycles will be discussed, emphasizing the ability of the produced materials to be used as effective adsorbents for tertiary water and wastewater treatment.

Towards that direction, the upcoming figures investigate the comparative adsorption efficiency of RH and SS biochar and biochar nanocomposites, after 10min of contact time with polluted water and wastewater. Figure 6.1 concerns the adsorption results for the investigated EMCs from water on RH biochar and biochar nanocomposites (1% w/w), produced at 600°C. The results showed that pollutants BPA, E1 and EE2 were adsorbed similarly by all samples, while for 2.4D, ADT and NOR the best results were achieved by RH_CNT1_600, which was 17-30% efficient compared to the other samples. It is worth mentioning that the same sample achieved removal >80% for all the investigated pollutants, after 10min of contact time. Sample RH_GO1_600 presented a similar behaviour to conventional sample RH600, being 4-20% more effective concerning pollutant adsorption, except for 2.4D, where efficiency was 4% lower compared to the conventional sample.

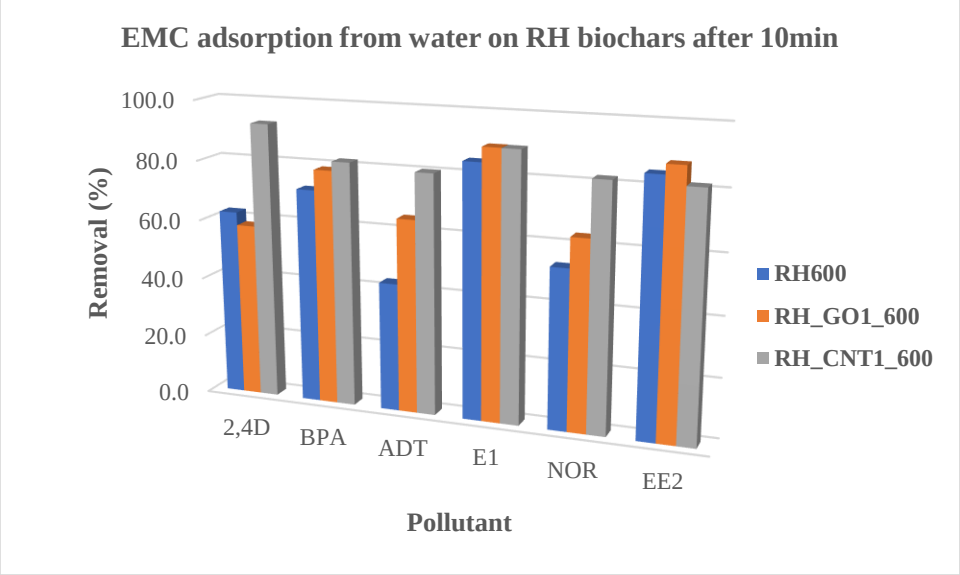

Figure 6.1: Emerging Micro-Contaminant adsorption from water on RH biochar and biochar nanocomposites (1% w/w), after 10min of contact time

Figure 6.2 contains the comparative results concerning the adsorption of EMCs from water on SS biochar and biochar nanocomposites. The two estrogens, E1 and EE2, were similarly removed (>87%) by all samples after 10min of contact time. Androgens ADT and NOR were most effectively removed (>72%) by SS_CNT1_600, followed by SS600 (>47%) and SS_GO1_600 (>40%). 2.4D could be adsorbed only by SS_CNT1_600 (82%), where the other samples were totally ineffective. Pollutant BPA was removed sufficiently by all samples (58-67%) with the CNT-doped sample being the most effective in this case as well. Based on Figures 6.1 and 6.2 that concern pollutant adsorption from water on RH and SS biochar and biochar nanocomposites, biochar functionalization with nanomaterials improved its adsorptive capacity, especially in the case of CNTs. CNT-doped biochar nanocomposites provided significantly better results on the adsorption of the investigated EMCs, even for difficult to adsorb pollutants, such as 2.4D. Moreover, RH feedstock provided better adsorbents compared to SS. RH biochars presented better physicochemical structures, as shown in the previous chapters, and at the same time they were more efficient concerning EMC adsorption from water.

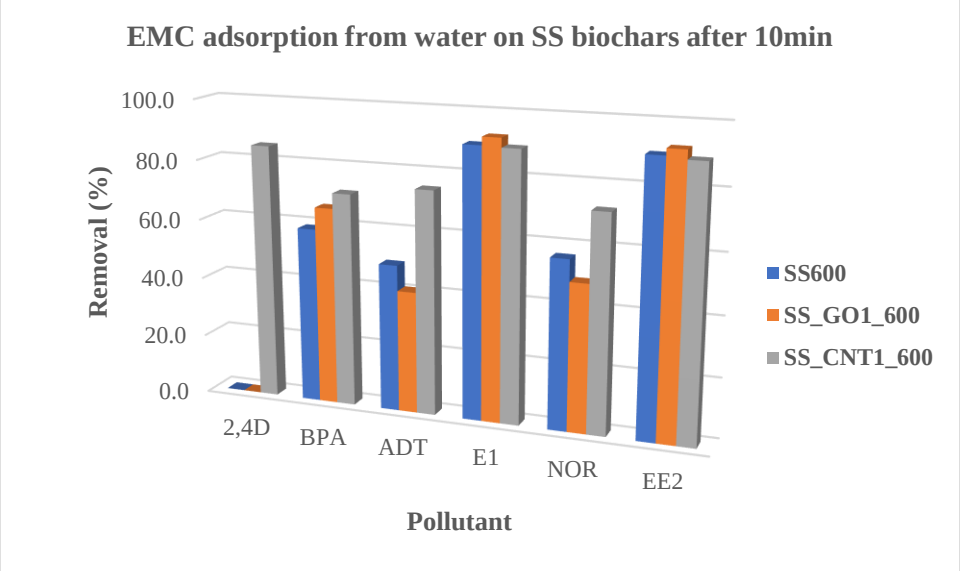

Figure 6.2: Emerging Micro-Contaminant adsorption from water on SS biochar and biochar nanocomposites (1% w/w), after 10min of contact time

Figure 6.3 presents the results of EMC adsorption from wastewater on RH biochar and biochar nanocomposites, after 10min of contact time. Differences were much clearer in the case of secondary wastewater effluent, where CNT-doped biochar nanocomposites were more

effective by 20-90%, compared to the other samples, removing all pollutants by 81% or higher, after 10min of contact time. The differences among the two CNT doses (1% and 10% w/w) were minimal, proving that even the lowest dose can provide the desirable results, therefore with lower cost. A similar behaviour was also observed for samples RH600 and RH_GO10_600 that provided insufficient removal rates for most pollutants. 2.4D could not be removed by the abovementioned samples, while androgens ADT and NOR were also removed at low percentages (28-30% and 20-21% respectively). BPA was also insufficiently removed (43-44%), while the two estrogens showed slightly better adsorption efficiency, 72-73% for E1 and 45-58% for EE2.

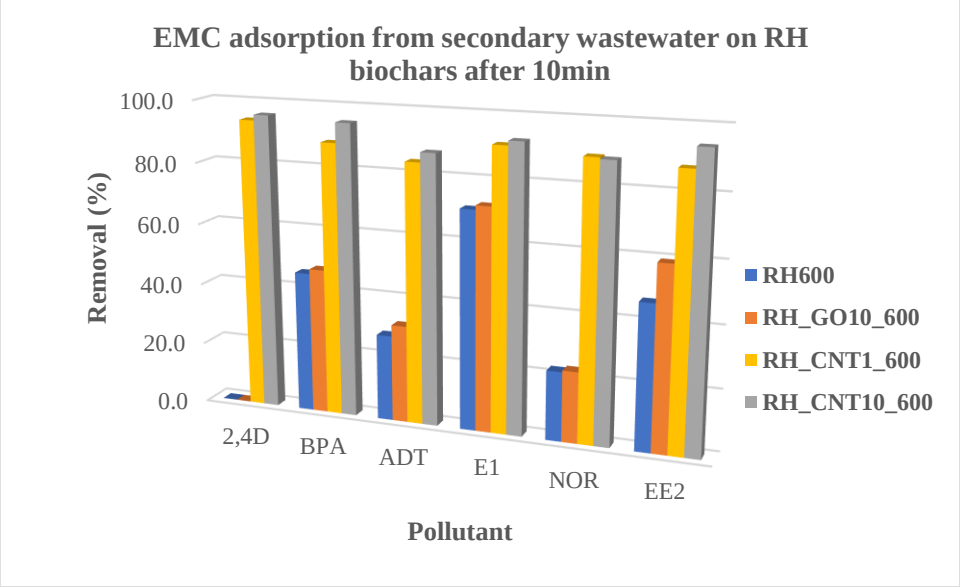

Figure 6.3: Emerging Micro-Contaminant adsorption from secondary wastewater on RH biochar and biochar nanocomposites, after 10min of contact time

A similar trend was observed concerning the SS samples in wastewater, which are presented in Figure 6.4. CNT-doped biochar nanocomposites were the most effective in this case as well, but in this case, GO-doped biochar nanocomposites were also more effective compared to conventional SS biochar. The differences among the two CNT doses of 1% and 10% w/w were minimal on EMC adsorption from wastewater, except for 2.4D where the higher dose (10% w/w) was 18% more efficient by achieving a 97% pollutant removal. CNT-doped samples achieved >80% pollutant removal in all cases, except for ADT and NOR, where SS_CNT1_600 achieved removal rates of 77% and 79% accordingly. Conventional biochar sample SS600 could sufficiently adsorb only the two estrogens, by 77% for E1 and 60% for EE2, while the

rest of EMCs were removed in percentages lower than 21%. GO-doped biochar nanocomposites presented a better behaviour compared to SS600, but they were also not sufficiently effective concerning half of the investigated EMCs.

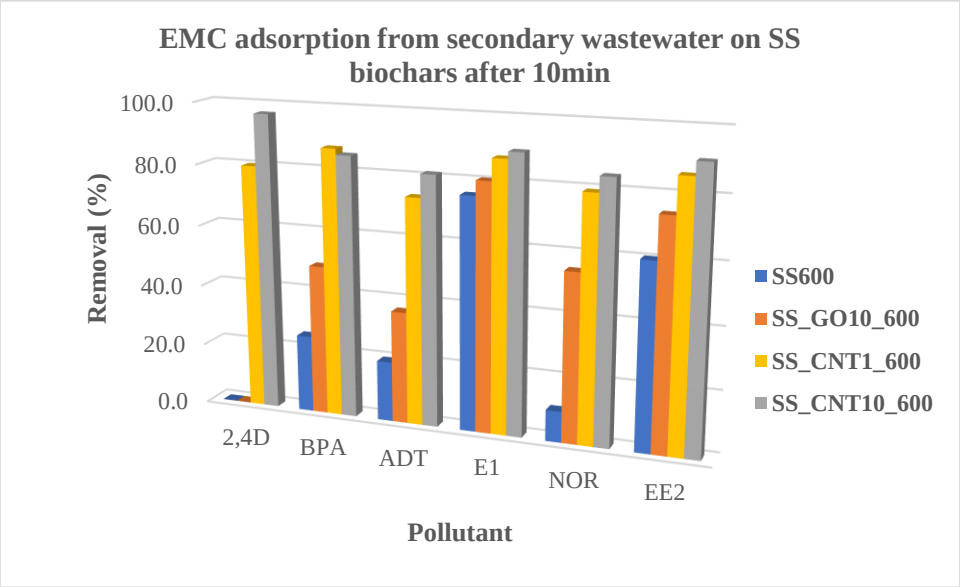

Figure 6.4: Emerging Micro-Contaminant adsorption from secondary wastewater on SS biochar and biochar nanocomposites, after 10min of contact time

The important parameter that made CNT-doped biochar nanocomposites the most effective adsorbents for the removal of EMCs from water and wastewater was the addition of -COOH functionalized CNTs that provided valuable O- functional groups on biochar nanocomposite surface that favoured π-π EDA interaction between the pollutants and the adsorbents, resulting in higher removal rates. The importance of these functional groups was highlighted by the fact that results were similar among the two different investigated nanomaterial doses (1% and 10%), proving that even a low nanomaterial dosage can provide the desirable effect on the performance of the produced biochar nanocomposite. Biochar surface functional groups play a very important role in the mechanisms that will be involved in the adsorption of different pollutants, based on their structure. The investigated organic EMCs were adsorbed quicker and in higher rates by the CNT-doped biochar nanocomposites due to the C- and O- surface functional groups found on their surface, leading to the conclusion that biochar functionalization with the addition of these groups could be a promising solution to mitigate this problem at bigger scale.

7. Overall conclusion

This PhD thesis tried to thoroughly investigate the potential of using biochar technology towards the creation of advanced sorptive materials that could be effectively implemented for the decontamination of water and wastewater from difficult-to-manage Emerging Micro-Contaminants.

The first experimental cycle investigated the properties of biochar from different agronomic or waste-derived biomasses in two pyrolytic temperatures, to evaluate them as candidates for agronomic and environmental applications. Results showed that lower pyrolytic temperature (400°C) was preferable for agronomic applications due to higher fertilizing potential, while higher pyrolytic temperature (600°C) was more suitable for environmental applications as an adsorbent for contaminated soil remediation or for water and wastewater decontamination, due to the higher carbon content and more porous structure.

Rice Husks and Sewage Sludge were the two biomass feedstocks that were chosen to proceed with to the next experimental cycle that focused on the production, characterization and application of Graphene Oxide-doped biochar nanocomposites for the removal of six Emerging Micro-Contaminants from water and wastewater. Graphene Oxide (GO) was produced at the laboratory and was then implemented into the two biomass samples, in two doses (1% and 10% w/w) to produce GO-doped biochar nanocomposites at two pyrolytic temperatures (400°C and 600°C). Samples were characterized thoroughly, leading to the result that biomass type and pyrolysis temperature played a more important role in biochar nanocomposite final structure and properties that GO functionalization itself. EMC adsorption was slightly improved by the application of biochar nanocomposites, being sufficiently achieved after 30min in the case of RH, compared to the conventional biochar samples that needed 60min of contact time. In the wastewater experiments though, the competitive adsorptive phenomena limited the adsorption efficiency of all samples, where biochar nanocomposites again showed higher efficiency. Sample RH_GO10_600 showed the most favourable results, especially in terms of C content and specific surface area, as long as EMC adsorption efficiency.

The last experimental cycle involved the production of CNT-doped biochar nanocomposites by implementing commercially available -COOH functionalized Carbon NanoTubes (CNTs) into the selected biomasses in order to produce efficient biochar nanocomposites that are rich in C- and O- containing surface functional groups, which would favour EMC adsorption from

water and wastewater in a significant manner. Results showed that CNT-doped biochar nanocomposites showed more of the abovementioned surface functional groups on their surface. This was confirmed by the adsorption experiments, where these samples were able to sufficiently remove the investigated EMCs from water and wastewater after 10min of contact time. RH based samples provided sufficient removal rates after just 5min of contact time in both water and wastewater experiments, being the most efficient. This was attributed to the abundance of O- functional groups that favoured adsorbent-pollutant π-π EDA interaction and provided these favourable results.

Based on the above, this PhD thesis suggests that CNTs can successfully be implemented into any type of waste biomass in small portions, to create advanced adsorptive materials named biochar nanocomposites. These nanocomposites can be applied for water and wastewater tertiary treatment, providing at the same time a sustainable solution regarding the rising problem of EMC detection in water and wastewater.

8. PhD thesis dissemination

8.1 Scientific journal publications

1) Pellera, F. M., Regkouzas, P., Manolikaki, I., & Diamadopoulos, E. (2021). Biochar production from waste biomass: Characterization and evaluation for agronomic and environmental applications. *Detritus*, *17*, 15-29. https://doi.org/10.31025/2611-4135/2021.15146
2) Regkouzas, P., Sygellou, L., & Diamadopoulos, E. (2023). Production and characterization of graphene oxide-engineered biochars and application for organic micro-pollutant adsorption from aqueous solutions. *Environmental Science and Pollution Research*, *30*(37), 87810-87829. https://doi.org/10.1007/s11356-023-28549-y
3) Regkouzas, P., Sygellou, L., & Diamadopoulos, E. Emerging Micro-Contaminant adsorption from water and wastewater using CNT-doped biochar nanocomposites from rice husks and sewage sludge. *Submitted to a scientific journal*

8.2 Book chapter publications

1) Regkouzas, P., & Diamadopoulos, E. (2022, October). Production of Nanobiochar from Sewage Sludge for the Adsorption of Emerging Contaminants (ECs) from Water and Wastewater. In *EURECA-PRO Conference on Responsible Consumption and Production* (pp. 351-357). Cham: Springer International Publishing.

8.3 Scientific conference participation

1) IWA Specialist Conference on Sludge Management: SludgeTech, London, 9-13 July 2017. Biochar from sewage sludge: Production, characterization and use for EDCs removal from treated municipal wastewater. P. Regkouzas, E. Diamadopoulos.
2) 6th International Conference on Industrial and Hazardous Waste Management, Chania, September 2018. Use of biochars produced from waste biomass for removing nickel

from aqueous solutions. R.N. Mourgela, F.M. Pellera, P. Regkouzas, E. Diamadopoulos.

3) European Geosciences Union, Vienna, May 2020. Adsorption of six organic micropollutants from water and wastewater using Graphene Oxide-coated biochars. P. Regkouzas, E. Diamadopoulos.
4) European Geosciences Union, Vienna, May 2020. Biochar production from waste biomass: Characterization and evaluation for potential applications. F. M. Pellera, P. Regkouzas, I. Manolikaki, E. Diamadopoulos.
5) 1st EURECA-PRO conference, online, October 2021. Biochar production from sewage sludge and rice husks for organic micro-pollutant adsorption from water and wastewater. P. Regkouzas, E. Diamadopoulos
6) 2nd EURECA-PRO conference, Leon, October 2022. Production of nanobiochar from sewage sludge for the adsorption of Emerging Contaminants (ECs) from water and wastewater. P. Regkouzas, E. Diamadopoulos
7) 3rd EURECA-PRO conference, Chania, Greece, October 2023. Emerging Contaminant adsorption from water using rice husk biochar nanocomposites. P. Regkouzas, E. Diamadopoulos
8) IEES conference on Closed Cycles and the Circular Economy, Chania, Greece, October 2023. Production and characterization of Carbon Nanotubes and Graphene Oxide biochar nanocomposites from rice husks and sewage sludge and adsorption tests on six Emerging Contaminants from wastewater. P. Regkouzas, E. Diamadopoulos

9. Acknowledgements

We acknowledge the financial support of this work by the project INVALOR: Research Infrastructure for Waste Valorization and Sustainable Management" (MIS 5002495) which was implemented under the Action "Reinforcement of the Research and Innovation Infrastructure", funded by the Operational Programme "Competitiveness, Entrepreneurship and Innovation" (NSRF 2014-2020) and co-financed by Greece and the European Union (European Regional Development Fund).

Special acknowledgements are required concerning my supervising professor, Evan Diamadopoulos, for his continuous support since my pre-graduate studies, for believing in me, consulting me and for making this PhD journey a reality.

I would also like to thank all the supervising committee members for their individual support and counselling regarding the scientific content of this work. Special thanks to Dr Nikolaos Xekoukoulotakis for his help and guidance concerning the production of Graphene Oxide at his laboratory. I would also like to express my gratitude to Dr Labrini Sygelou for her assistance and labor concerning the XPS analyses that took place at the Institute of Chemical Engineering Sciences of the Foundation of Research and Technology Hellas in Rio, Greece. Special thanks Dr Alexandros Stefanakis for urging me to complete this academic cycle and for pressuring me to further evolve in academia.

I would also like to thank all the members of the Laboratory of Environmental Engineering and Management of Technical University of Crete for the cooperation, support and friendship that was built during all these years. Special thanks to Elisavet Koukouraki, the 'lab queen', who was the most valuable human resource that I could ask for and became a member of my family. Special thanks to Dr Francesca-Maria Pellera as well, for our beautiful cooperation and friendship, along with her significant role in the content and scientific background of this work.

Finally, I would like to thank my family, friends and individuals that may have had a positive or even negative effect on this journey. After all, everything in life should be a valuable lesson!

10.References

Abbas, Z., Ali, S., Rizwan, M., Zaheer, I. E., Malik, A., Riaz, M. A., Shahid, M. R., Rehman, M. Z. & Al-Wabel, M. I. (2018). A critical review of mechanisms involved in the adsorption of organic and inorganic contaminants through biochar. Arabian Journal of Geosciences, 11, 1-23. https://doi.org/10.1007/s12517-018-3790-1

Abdul, G., Zhu, X., & Chen, B. (2017). Structural characteristics of biochar-graphene nanosheet composites and their adsorption performance for phthalic acid esters. Chemical Engineering Journal, 319, 9-20. https://doi.org/10.1016/j.cej.2017.02.074

Abou Rjeily, M., Gennequin, C., Pron, H., Abi-Aad, E., & Randrianalisoa, J. H. (2021). Pyrolysis-catalytic upgrading of bio-oil and pyrolysis-catalytic steam reforming of biogas: a review. *Environmental Chemistry Letters*, *19*(4), 2825-2872. https://doi.org/10.1007/s10311-021-01190-2

Agrafioti, E., Bouras, G., Kalderis, D., & Diamadopoulos, E. (2013). Biochar production by sewage sludge pyrolysis. Journal of Analytical and Applied Pyrolysis, 101, 72-78. https://doi.org/10.1016/j.jaap.2013.02.010

Ahmad, M., Lee, S.S., Dou, X., Mohan, D., Sung, J.K., Yang, J.E., & Ok, Y.S. (2012). Effects of pyrolysis temperature on soybean stover- and peanut shell-derived biochar properties and TCE adsorption in water. Bioresource Technology, 118, 536-544. https://doi.org/10.1016/j.biortech.2012.05.042

Ahmad, M., Rajapaksha, A.U., Lim, J.E., Zhang, M., Bolan, N., Mohan, D., Vithanage, M., Lee, S.S., & Ok, Y.S. (2014). Biochar as a sorbent for contaminant management in soil and water: A review. Chemosphere, 99, 19-23. https://doi.org/10.1016/j.chemosphere.2013.10.071

Ahmed, M. B., Zhou, J. L., Ngo, H. H., Guo, W., & Chen, M. (2016). Progress in the preparation and application of modified biochar for improved contaminant removal from water and wastewater. Bioresource technology, 214, 836-851. https://doi.org/10.1016/j.biortech.2016.05.057.

Ahmedna, M., Johns, M.M., Clarke, S.J., Marshall, W.E., & Rao, R.M. (1997). Potential of agricultural by-product-based activated carbons for use in raw sugar decolourisation. Journal of the Science of Food and Agriculture, 75(1), 117-124. https://doi.org/10.1002/(SICI)1097-0010(199709)75:1<117::AID-JSFA850>3.0.CO;2-M

Akbarian, A., Andooz, A., Kowsari, E., Ramakrishna, S., Asgari, S., & Cheshmeh, Z. A. (2022). Challenges and opportunities of lignocellulosic biomass gasification in the path of circular bioeconomy. *Bioresource Technology*, 127774. https://doi.org/10.1016/j.biortech.2022.127774

Aller, M.F. (2016). Biochar properties: Transport, fate, and impact. Critical Reviews in Environmental Science and Technology, 46(14-15), 1183-1296. https://doi.org/10.1080/10643389.2016.1212368

Al-Wabel, M.I., Al-Omran, A., El-Naggar, A.H., Nadeem, M., & Usman, A.R.A. (2013). Pyrolysis temperature induced changes in characteristics and chemical composition of biochar produced from conocarpus wastes. Bioresource Technology, 131, 374-379. https://doi.org/10.1016/j.biortech.2012.12.165

Amalina, F., Abd Razak, A. S., Krishnan, S., Sulaiman, H., Zularisam, A. W., & Nasrullah, M. (2022). Advanced techniques in the production of biochar from lignocellulosic biomass and environmental applications. *Cleaner Materials*, 100137. https://doi.org/10.1016/j.clema.2022.100137

Ambaye, T. G., Vaccari, M., van Hullebusch, E. D., Amrane, A., & Rtimi, S. (2021). Mechanisms and adsorption capacities of biochar for the removal of organic and inorganic pollutants from industrial wastewater. International Journal of Environmental Science and Technology, 1-22. https://doi.org/10.1007/s13762-020-03060-w

Amenaghawon, A. N., Anyalewechi, C. L., Okieimen, C. O., & Kusuma, H. S. (2021). Biomass pyrolysis technologies for value-added products: a state-of-the-art review. *Environment, Development and Sustainability*, *23*(10), 14324-14378. https://doi.org/10.1007/s10668-021-01276-5

Antoniou, C. V., Koukouraki, E. E., & Diamadopoulos, E. (2009). Analysis of selected pharmaceutical compounds and endocrine disruptors in municipal wastewater using solid-phase microextraction and gas chromatography. Water Environment Research, 81(7), 664-669, DOI: 10.2175/106143008x390834.

APHA. (1992). Method 2540G. Standard Methods for the Examination of Water and Wastewater.

ASTM D1762-84 (2004). Standard Test Method for Chemical Analysis of Wood Charcoal. ASTM International, West Conshohocken, PA, 2004.

ASTM E897-88 (2004). Standard Test Method for Volatile Matter in the Analysis Sample of Refuse-Derived Fuel. ASTM International, West Conshohocken, PA, 2004.

Barquilha, C. E., & Braga, M. C. (2021). Adsorption of organic and inorganic pollutants onto biochars: Challenges, operating conditions, and mechanisms. *Bioresource Technology Reports*, *15*, 100728. https://doi.org/10.1016/j.biteb.2021.100728

Belyaeva, O.N., Haynes, R.J., & Sturm, E.C. (2012). Chemical, physical and microbial properties and microbial diversity in manufactured soils produced from co-composting green waste and biosolids. Waste Management, 32(12), 2248-2257. https://doi.org/10.1016/j.wasman.2012.05.034

Bhoi, P. R., Ouedraogo, A. S., Soloiu, V., & Quirino, R. (2020). Recent advances on catalysts for improving hydrocarbon compounds in bio-oil of biomass catalytic pyrolysis. *Renewable and Sustainable Energy Reviews*, *121*, 109676. https://doi.org/10.1016/j.rser.2019.109676

Buss, W., Graham, M.C., Shepherd, J.G., & Mašek, O. (2016). Risks and benefits of marginal biomass-derived biochars for plant growth. Science of the Total Environment, 569–570, 496-506. https://doi.org/10.1016/j.scitotenv.2016.06.129

Buss, W., & Mašek, O. (2014). Mobile organic compounds in biochar–a potential source of contamination–phytotoxic effects on cress seed (Lepidium sativum) germination. Journal of Environmental Management, 137, 111-119. https://doi.org/10.1016/j.jenvman.2014.01.045

Cao, X., & Harris, W. (2010). Properties of dairy-manure-derived biochar pertinent to its potential use in remediation. Bioresource Technology, 101(14), 5222-5228. https://doi.org/10.1016/j.biortech.2010.02.052

Chausali, N., Saxena, J., & Prasad, R. (2021). Nanobiochar and biochar based nanocomposites: advances and applications. *Journal of Agriculture and Food Research*, *5*, 100191. https://doi.org/10.1016/j.jafr.2021.100191

Chen, B., Zhou, D., & Zhu, L. (2008). Transitional adsorption and partition of nonpolar and polar aromatic contaminants by biochars of pine needles with different pyrolytic temperatures. Environmental Science & Technology, 42(14), 5137-5143. https://doi.org/10.1021/es8002684

Chen, T., Zhang, Y., Wang, H., Lu, W., Zhou, Z., Zhang, Y., & Ren, L. (2014). Influence of pyrolysis temperature on characteristics and heavy metal adsorptive performance of biochar derived from municipal sewage sludge. Bioresource Technology, 164, 47-54. https://doi.org/10.1016/j.biortech.2014.04.048

Chen, Q., Zhang, Q., Yang, Y., Wang, Q., He, Y., & Dong, N. (2021a). Synergetic effect on methylene blue adsorption to biochar with gentian violet in dyeing and printing wastewater under competitive adsorption mechanism. Case Studies in Thermal Engineering, 101099. https://doi.org/10.1016/j.csite.2021.101099

Chen, X., Lewis, S., Heal, K. V., Lin, Q., & Sohi, S. P. (2021b). Biochar engineering and ageing influence the spatiotemporal dynamics of soil pH in the charosphere. *Geoderma*, *386*, 114919. https://doi.org/10.1016/j.geoderma.2020.114919

Cheng, N., Wang, B., Wu, P., Lee, X., Xing, Y., Chen, M., & Gao, B. (2021). Adsorption of emerging contaminants from water and wastewater by modified biochar: A review. *Environmental Pollution*, *273*, 116448. https://doi.org/10.1016/j.envpol.2021.116448

Chu, G., Zhao, J., Liu, Y., Lang, D., Wu, M., Pan, B., & Steinberg, C. E. (2019). The relative importance of different carbon structures in biochars to carbamazepine and bisphenol A sorption. Journal of hazardous materials, 373, 106-114. https://doi.org/10.1016/j.jhazmat.2019.03.078

Coates, J. (2000). Interpretation of Infrared Spectra, A Practical Approach. Encyclopedia of Analytical Chemistry, 12, 10815-10837. https://doi.org/10.1002/9780470027318.a5606

Colantoni, A., Evic, N., Lord, R., Retschitzegger, S., Proto, A.R., Gallucci, F., & Monarca, D. (2016). Characterization of biochars produced from pyrolysis of pelletized agricultural residues. Renewable and Sustainable Energy Reviews, 64, 187-194. https://doi.org/10.1016/j.rser.2016.06.003

Danish, A., Mosaberpanah, M. A., Salim, M. U., Ahmad, N., Ahmad, F., & Ahmad, A. (2021). Reusing biochar as a filler or cement replacement material in cementitious composites: A review. Construction and Building Materials, 300, 124295. https://doi.org/10.1016/j.conbuildmat.2021.124295

De Marchi, L., Pretti, C., Gabriel, B., Marques, P. A., Freitas, R., & Neto, V. (2018). An overview of graphene materials: Properties, applications and toxicity on aquatic environments.

Science of the Total Environment, 631, 1440-1456. https://doi.org/10.1016/j.scitotenv.2018.03.132

Demirbas, A., & Arin, G. (2002). An overview of biomass pyrolysis. *Energy sources*, *24*(5), 471-482. https://doi.org/10.1080/00908310252889979

Dimiev, A. M., & Tour, J. M. (2014). Mechanism of graphene oxide formation. ACS nano, 8(3), 3060-3068. https://doi.org/10.1021/nn500606a

Domene, X., Enders, A., Hanley, K., & Lehmann, J. (2015). Ecotoxicological characterization of biochars: Role of feedstock and pyrolysis temperature. Science of the Total Environment, 512-513, 552-561. https://doi.org/10.1016/j.scitotenv.2014.12.035

EBC (2012). 'European Biochar Certificate - Guidelines for a Sustainable Production of Biochar.' European Biochar Foundation (EBC), Arbaz, Switzerland. http://www.european-biochar.org/en/download.Version 6.3E of 14th August 2017.

EC. European Commission. Directive 86/278/EEC on the protection of the environment and in particular of the soil. When sewage sludge is used in agriculture, 2009. https://eur-lex.europa.eu/eli/dir/1986/278/2009-04-20

Elkhalifa, S., Al-Ansari, T., Mackey, H.R., & McKay, G. (2019). Food waste to biochars through pyrolysis: A review. Resources, Conservation and Recycling, 144, 310-320. https://doi.org/10.1016/j.resconrec.2019.01.024

Enaime, G., & Lübken, M. (2021). Agricultural waste-based biochar for agronomic applications. *Applied Sciences*, *11*(19), 8914. https://doi.org/10.3390/app11198914

Enders, A., Hanley, K., Whitman, T., Joseph, S., & Lehmann, J. (2012). Characterization of biochars to evaluate recalcitrance and agronomic performance. Bioresource Technology, 114, 644-653. https://doi.org/10.1016/j.biortech.2012.03.022

Essandoh, M., Wolgemuth, D., Pittman, C. U., Mohan, D., & Mlsna, T. (2017). Adsorption of metribuzin from aqueous solution using magnetic and nonmagnetic sustainable low-cost biochar adsorbents. *Environmental Science and Pollution Research*, *24*, 4577-4590. https://doi.org/10.1007/s11356-016-8188-6

EUROSTAT (2020). Available at: https://ec.europa.eu/eurostat (last visited on 8/7/2020)

Fan, Q., Sun, J., Chu, L., Cui, L., Quan, G., Yan, J., Hussain, Q., & Iqbal, M. (2018). Effects of chemical oxidation on surface oxygen-containing functional groups and adsorption behavior of biochar. *Chemosphere*, *207*, 33-40. https://doi.org/10.1016/j.chemosphere.2018.05.044

Fan, J., Li, Y., Yu, H., Li, Y., Yuan, Q., Xiao, H., Li, F., & Pan, B. (2020). Using sewage sludge with high ash content for biochar production and Cu (II) sorption. Science of The Total Environment, 136663. https://doi.org/10.1016/j.scitotenv.2020.136663.

Fountoulakis, M.S., Drakopoulou, S., Terzakis, S., Georgaki, E., & Manios, T. (2008). Potential for methane production from typical Mediterranean agro-industrial by-products. Biomass and Bioenergy 32, 155-161. https://doi.org/10.1016/j.biombioe.2007.09.002

Fryda, L., Visser, R., & Schmidt, J. (2019). Biochar replaces peat in horticulture: environmental impact assessment of combined biochar & bioenergy production. Detritus, 5, 132-149. https://doi.org/10.31025/2611-4135/2019.13778

Gai, X., Wang, H., Liu, J., Zhai, L., Liu, S., Ren, T., & Liu, H. (2014). Effects of feedstock and pyrolysis temperature on biochar adsorption of ammonium and nitrate. PLoS ONE, 9(12), 1-19. https://doi.org/10.1371/journal.pone.0113888

Gao, N., Kamran, K., Quan, C., & Williams, P. T. (2020). Thermochemical conversion of sewage sludge: A critical review. *Progress in Energy and Combustion Science*, *79*, 100843. https://doi.org/10.1016/j.pecs.2020.100843

Gao, Y., Chen, Y., Song, T., Su, R., & Luo, J. (2022). Activated peroxymonosulfate with ferric chloride-modified biochar to degrade bisphenol A: Characteristics, influencing factors, reaction mechanism and reuse performance. Separation and Purification Technology, 300, 121857. https://doi.org/10.1016/j.seppur.2022.121857.

Gell, K., van Groenigen, J.W., & Cayuela, M.L. (2011). Residues of bioenergy production chains as soil amendments: Immediate and temporal phytotoxicity. Journal of Hazardous Materials, 186(2-3), 2017-2025. https://doi.org/10.1016/j.jhazmat.2010.12.105

Ghaffar, A., & Younis, M. N. (2014). Adsorption of organic chemicals on graphene coated biochars and its environmental implications. Green Processing and Synthesis, 3(6), 479-487. https://doi.org/10.1515/gps-2014-0071

Gogoi, A., Mazumder, P., Tyagi, V. K., Chaminda, G. T., An, A. K., & Kumar, M. (2018). Occurrence and fate of emerging contaminants in water environment: A review. Groundwater for Sustainable Development, 6, 169-180, DOI: https://doi.org/10.1016/j.gsd.2017.12.009.

Gómez, N., Rosas, J.G., Cara, J., Martínez, O., Alburquerque, J.A., & Sánchez, M.E. (2016). Slow pyrolysis of relevant biomasses in the Mediterranean basin. Part 1. Effect of temperature on process performance on a pilot scale. Journal of Cleaner Production, 120, 181-190. https://doi.org/10.1016/j.jclepro.2014.10.082

Guedes, R. E., Luna, A. S., & Torres, A. R. (2018). Operating parameters for bio-oil production in biomass pyrolysis: A review. *Journal of analytical and applied pyrolysis*, *129*, 134-149. https://doi.org/10.1016/j.jaap.2017.11.019

Gunarathne, V., Ashiq, A., Ramanayaka, S., Wijekoon, P., & Vithanage, M. (2019). Biochar from municipal solid waste for resource recovery and pollution remediation. Environmental Chemistry Letters, 1-11. https://doi.org/10.1007/s10311-019-00866-0

Hossain, M.K., Strezov, V., Chan, K.Y., Ziolkowski, A., & Nelson, P.F. (2011). Influence of pyrolysis temperature on production and nutrient properties of wastewater sludge biochar. Journal of Environmental Management, 92(1), 223-228. https://doi.org/10.1016/j.jenvman.2010.09.008

Huang, D., Wang, X., Zhang, C., Zeng, G., Peng, Z., Zhou, J., Cheng, M., Wang, R., Hu, Z., Qin, X. (2017). Sorptive removal of ionizable antibiotic sulfamethazine from aqueous solution by graphene oxide-coated biochar nanocomposites: influencing factors and mechanism. Chemosphere, 186, 414-421. https://doi.org/10.1016/j.chemosphere.2017.07.154

Hummers Jr, W. S., & Offeman, R. E. (1958). Preparation of graphitic oxide. Journal of the american chemical society, 80(6), 1339-1339, https://doi.org/10.1021/ja01539a017.

IBI (2015). Standardized Product Definition and Product Testing Guidelines for Biochar That Is Used in Soil. International Biochar Initiative, Version 2.1, (November 23rd 2015). https://www.biochar-international.org/wp-content/uploads/2018/04/IBI_Biochar_Standards_V2.1_Final.pdf

Ibn Ferjani, A., Jeguirim, M., Jellali, S., Limousy, L., Courson, C., Akrout, H., Thevenin, N., Ruidavets, L. Muller, A., & Bennici, S. (2019). The use of exhausted grape marc to produce

biofuels and biofertilizers: Effect of pyrolysis temperatures on biochars properties. Renewable and Sustainable Energy Reviews, 107, 425-433. https://doi.org/10.1016/j.rser.2019.03.034

Ihsanullah, I., Khan, M. T., Zubair, M., Bilal, M., & Sajid, M. (2022). Removal of pharmaceuticals from water using sewage sludge-derived biochar: A review. *Chemosphere*, *289*, 133196. https://doi.org/10.1016/j.chemosphere.2021.133196

Inguanzo, M., Domínguez, A., Menéndez, J.A., Blanco, C.G., & Pis, J.J. (2002). On the Pyrolysis of Sewage Sludge: The Influence of Pyrolysis Temperature on Biochar, Liquid and Gas Fractions. Journal of Analytical and Applied Pyrolysis, 63(1), 209-222. https://doi.org/10.1016/S0165-2370(01)00155-3

Inyang, M., Gao, B., Zimmerman, A., Zhang, M., & Chen, H. (2014). Synthesis, characterization, and dye sorption ability of carbon nanotube–biochar nanocomposites. Chemical Engineering Journal, 236, 39-46. https://doi.org/10.1016/j.cej.2013.09.074

Inyang, M., & Dickenson, E. (2015). The potential role of biochar in the removal of organic and microbial contaminants from potable and reuse water: a review. Chemosphere, 134, 232-240. https://doi.org/10.1016/j.chemosphere.2015.03.072

Inyang, M., Gao, B., Zimmerman, A., Zhou, Y., & Cao, X. (2015). Sorption and cosorption of lead and sulfapyridine on carbon nanotube-modified biochars. *Environmental Science and Pollution Research*, *22(3)*, 1868-1876. https://doi.org/10.1007/s11356-014-2740-z

Intani, K., Latif, S., Islam, M. S., & Müller, J. (2018). Phytotoxicity of corncob biochar before and after heat treatment and washing. Sustainability (Switzerland), 11(1). https://doi.org/10.3390/su11010030

Janu, R., Mrlik, V., Ribitsch, D., Hofman, J., Sedláček, P., Bielská, L., & Soja, G. (2021). Biochar surface functional groups as affected by biomass feedstock, biochar composition and pyrolysis temperature. *Carbon Resources Conversion*, *4*, 36-46. https://doi.org/10.1016/j.crcon.2021.01.003

Ji, J., Yuan, X., Zhao, Y., Jiang, L., & Wang, H. (2022). Mechanistic insights of removing pollutant in adsorption and advanced oxidation processes by sludge biochar. *Journal of Hazardous Materials*, *430*, 128375. https://doi.org/10.1016/j.jhazmat.2022.128375

Jimoh, O. A., Otitoju, T. A., Hussin, H., Ariffin, K. S., & Baharun, N. (2017). Understanding the precipitated calcium carbonate (PCC) production mechanism and its characteristics in the

liquid–gas system using milk of lime (MOL) suspension. South African Journal of Chemistry, 70, 1-7. http://dx.doi.org/10.17159/0379-4350/2017/v70a1

Jin, H., Capareda, S., Chang, Z., Gao, J., Xu, Y., & Zhang, J. (2014). Biochar pyrolytically produced from municipal solid wastes for aqueous As(V) removal: Adsorption property and its improvement with KOH activation. Bioresource Technology, 169, 622-629. https://doi.org/10.1016/j.biortech.2014.06.103

Jin, J., Li, Y., Zhang, J., Wu, S., Cao, Y., Liang, P., Zhang, J., Wong, M. H., Wang, M., Shan, S., & Christie, P. (2016). Influence of pyrolysis temperature on properties and environmental safety of heavy metals in biochars derived from municipal sewage sludge. Journal of Hazardous Materials, 320, 417-426. https://doi.org/10.1016/j.jhazmat.2016.08.050

Jin, X., Liu, R., Wang, H., Han, L., Qiu, M., & Hu, B. (2022). Functionalized porous nanoscale Fe 3 O 4 particles supported biochar from peanut shell for Pb (II) ions removal from landscape wastewater. Environmental Science and Pollution Research, 1-11. https://doi.org/10.1007/s11356-021-18432-z

Kah, M., Sun, H., Sigmund, G., Hüffer, T., & Hofmann, T. (2016). Pyrolysis of waste materials: Characterization and prediction of sorption potential across a wide range of mineral contents and pyrolysis temperatures. Bioresource Technology, 214, 225-233. https://doi.org/10.1016/j.biortech.2016.04.091

Kah, M., Sigmund, G., Xiao, F., & Hofmann, T. (2017). Sorption of ionizable and ionic organic compounds to biochar, activated carbon and other carbonaceous materials. *Water research*, *124*, 673-692. https://doi.org/10.1016/j.watres.2017.07.070

Kalderis, D., Kayan, B., Akay, S., Kulaksız, E., & Gözmen, B. (2017). Adsorption of 2, 4-dichlorophenol on paper sludge/wheat husk biochar: process optimization and comparison with biochars prepared from wood chips, sewage sludge and hog fuel/demolition waste. Journal of environmental chemical engineering, 5(3), 2222-2231. https://doi.org/10.1016/j.jece.2017.04.039

Kan, T., Strezov, V., & Evans, T. J. (2016). Lignocellulosic biomass pyrolysis: A review of product properties and effects of pyrolysis parameters. *Renewable and sustainable energy reviews*, *57*, 1126-1140. https://doi.org/10.1016/j.rser.2015.12.185

Khan, R., Shukla, S., Kumar, M., Zuorro, A., & Pandey, A. (2023). Sewage sludge derived biochar and its potential for sustainable environment in circular economy: Advantages and challenges. *Chemical Engineering Journal*, 144495. https://doi.org/10.1016/j.cej.2023.144495

Kończak, M., & Huber, M. (2022). Application of the engineered sewage sludge-derived biochar to minimize water eutrophication by removal of ammonium and phosphate ions from water. *Journal of Cleaner Production*, *331*, 129994. https://doi.org/10.1016/j.jclepro.2021.129994

Kong, L., Liu, J., Zhou, Q., Sun, Z., & Ma, Z. (2019). Sewage sludge derived biochars provoke negative effects on wheat growth related to the PTEs. Biochemical Engineering Journal, 152, 107386. https://doi.org/10.1016/j.bej.2019.107386

Kumar, A., Singh, E., Mishra, R., & Kumar, S. (2021). Biochar as environmental armour and its diverse role towards protecting soil, water and air. *Science of The Total Environment*, *150444*. https://doi.org/10.1016/j.scitotenv.2021.150444

Lan, W., Chen, G., Zhu, X., Wang, X., & Xu, B. (2015). Progress in techniques of biomass conversion into syngas. *Journal of the Energy Institute*, *88*(2), 151-156. https://doi.org/10.1016/j.joei.2014.05.003

Lee, C.W., Mahendra, S., Zodrow, K., Li, D., Tsai, Y.C., Braam, J., & Alvarez, P.J.J. (2010). Developmental phytotoxicity of metal oxide nanoparticles to Arabidopsis thaliana. Environmental Toxicology and Chemistry: An International Journal, 29(3), 669-675. https://doi.org/10.1002/etc.58

Legan, M., Gotvajn, A. Ž., & Zupan, K. (2022). Potential of biochar use in building materials. Journal of Environmental Management, 309, 114704. https://doi.org/10.1016/j.jenvman.2022.114704

Leontakianakos, G., Baziotis, I., Papandreou, A., Kanellopoulou, D., Stathopoulos, V.N., & Tsimas, S. (2015). A comparative study of the physicochemical properties of Mg-rich and Ca-rich quicklimes and their effect on reactivity. Materials and Structures/Materiaux et Constructions, 48(11), 3735-3753. https://doi.org/10.1617/s11527-014-0436-y

Li, D.-C., & Jiang, H. (2017). The thermochemical conversion of non-lignocellulosic biomass to form biochar: A review on characterizations and mechanism elucidation. Bioresource Technology, 246, 57-68. https://doi.org/10.1016/j.biortech.2017.07.029

Li, H., Dong, X., da Silva, E.B., de Oliveira, L.M., Chen, Y., & Ma, L.Q. (2017). Mechanisms of metal sorption by biochars: Biochar characteristics and modifications. Chemosphere, 178, 466-478. https://doi.org/10.1016/j.chemosphere.2017.03.072

Li, R., Wang, J. J., Gaston, L. A., Zhou, B., Li, M., Xiao, R., Wang, Q., Zhang, Z., Huang, H., Liang, W., Huang, H., Zhang, X. (2018). An overview of carbothermal synthesis of metal–biochar composites for the removal of oxyanion contaminants from aqueous solution. Carbon, 129, 674-687. https://doi.org/10.1016/j.carbon.2017.12.070 Li, M., Tang, Y., Ren, N., Zhang, Z., & Cao, Y. (2018). Effect of mineral constituents on temperature-dependent structural characterization of carbon fractions in sewage sludge-derived biochar. *Journal of cleaner production*, *172*, 3342-3350. https://doi.org/10.1016/j.jclepro.2017.11.090

Li, Y., Xing, B., Ding, Y., Han, X., & Wang, S. (2020). A critical review of the production and advanced utilization of biochar via selective pyrolysis of lignocellulosic biomass. *Bioresource Technology*, *312*, 123614. https://doi.org/10.1016/j.biortech.2020.123614

Lin, S. L., Zhang, H., Chen, W. H., Song, M., & Kwon, E. E. (2023). Low-temperature biochar production from torrefaction for wastewater treatment: A review. *Bioresource technology*, 129588. https://doi.org/10.1016/j.biortech.2023.129588

Liu, W. J., Jiang, H., & Yu, H. Q. (2015). Development of biochar-based functional materials: toward a sustainable platform carbon material. Chemical Reviews, 115(22), 12251-12285. https://doi.org/10.1021/acs.chemrev.5b00195.

Liu, T., Gao, B., Fang, J., Wang, B., & Cao, X. (2016). Biochar-supported carbon nanotube and graphene oxide nanocomposites for Pb (II) and Cd (II) removal. Rsc Advances, 6(29), 24314-24319. https://doi.org/10.1039/C6RA01895E

Liu, F., Wang, S., Zhao, C., & Hu, B. (2023). Constructing coconut shell biochar/MXenes composites through self-assembly strategy to enhance U (VI) and Cs (I) immobilization capability. Biochar, 5(1), 31. https://doi.org/10.1007/s42773-023-00231-z

Liu, M., Almatrafi, E., Zhang, Y., Xu, P., Song, B., Zhou, C., Zheng, G., Zhu, Y. (2021). A critical review of biochar-based materials for the remediation of heavy metal contaminated environment: Applications and practical evaluations. *Science of The Total Environment, 150531*. https://doi.org/10.1016/j.scitotenv.2021.150531

Lu, H., Zhang, W., Wang, S., Zhuang, L., Yang, Y., & Qiu, R. (2013). Characterization of sewage sludge-derived biochars from different feedstocks and pyrolysis temperatures. Journal of Analytical and Applied Pyrolysis, 102, 137-143. https://doi.org/10.1016/j.jaap.2013.03.004

Luo, F., Song, J., Xia, W., Dong, M., Chen, M., & Soudek, P. (2014). Characterization of contaminants and evaluation of the suitability for land application of maize and sludge biochars. Environmental Science and Pollution Research, 21(14), 8707-8717. https://doi.org/10.1007/s11356-014-2797-8

Luo, Z., Yao, B., Yang, X., Wang, L., Xu, Z., Yan, X., Tian, L., Zhou, H., & Zhou, Y. (2022). Novel insights into the adsorption of organic contaminants by biochar: a review. *Chemosphere*, *287*, 132113. https://doi.org/10.1016/j.chemosphere.2021.132113

Manolikaki, I.I., Mangolis, A., & Diamadopoulos, E. (2016). The impact of biochars prepared from agricultural residues on phosphorus release and availability in two fertile soils. Journal of Environmental Management, 181, 536-543. https://doi.org/10.1016/j.jenvman.2016.07.012

Melia, P. M., Busquets, R., Ray, S., & Cundy, A. B. (2018). Agricultural wastes from wheat, barley, flax and grape for the efficient removal of Cd from contaminated water. RSC advances, 8(70), 40378-40386. https://doi.org/10.1039/C8RA07877G

Méndez, A., Gómez, A., Paz-Ferreiro, J., & Gascó, G. (2012). Effects of sewage sludge biochar on plant metal availability after application to a Mediterranean soil. Chemosphere, 89(11), 1354-1359. https://doi.org/10.1016/j.chemosphere.2012.05.092

Mer, K., Sajjadi, B., Egiebor, N. O., Chen, W. Y., Mattern, D. L., & Tao, W. (2021). Enhanced degradation of organic contaminants using catalytic activity of carbonaceous structures: A strategy for the reuse of exhausted sorbents. Journal of Environmental Sciences, 99, 267-273. https://doi.org/10.1016/j.jes.2020.06.030

Mitchell, K., Trakal, L., Sillerova, H., Avelar-González, F.J., Guerrero-Barrera, A.L., Hough, R., & Beesley, L. (2018). Mobility of As, Cr and Cu in a contaminated grassland soil in response to diverse organic amendments; a sequential column leaching experiment. Applied Geochemistry, 88, 95-102. https://doi.org/10.1016/j.apgeochem.2017.05.020

Mosa, A., El-Ghamry, A., & Tolba, M. (2018). Functionalized biochar derived from heavy metal rich feedstock: phosphate recovery and reusing the exhausted biochar as an enriched soil amendment. Chemosphere, 198, 351-363. https://doi.org/10.1016/j.chemosphere.2018.01.113

Mosa, A., El-Ghamry, A., & Tolba, M. (2020). Biochar-supported natural zeolite composite for recovery and reuse of aqueous phosphate and humate: batch sorption–desorption and bioassay investigations. Environmental Technology & Innovation, 19, 100807. https://doi.org/10.1016/j.eti.2020.100807

Moyo, G. G., Hu, Z., & Getahun, M. D. (2020). Decontamination of xenobiotics in water and soil environment through potential application of composite maize stover/rice husk (MS/RH) biochar. A review. Environmental Science and Pollution Research, 27(23), 28679-28694. https://doi.org/10.1007/s11356-020-09163-8

Mukherjee, A., Zimmerman, A.R., & Harris W. (2011). Surface chemistry variations among a series of laboratory-produced biochars. Geoderma, 163(3-4), 247-255. https://doi.org/10.1016/j.geoderma.2011.04.021

Mumme, J., Getz, J., Prasad, M., Lüder, U., Kern, J., Mašek, O., & Buss, W. (2018). Toxicity screening of biochar-mineral composites using germination tests. Chemosphere, 207, 91-100. https://doi.org/10.1016/j.chemosphere.2018.05.042

Nanda, S., Dalai, A. K., Berruti, F., & Kozinski, J. A. (2016). Biochar as an exceptional bioresource for energy, agronomy, carbon sequestration, activated carbon and specialty materials. *Waste and Biomass Valorization*, *7*(2), 201-235. https://doi.org/10.1007/s12649-015-9459-z

Naqvi, S. R., Tariq, R., Hameed, Z., Ali, I., Taqvi, S. A., Naqvi, M., Niazi, M., B., K., Noor, T., & Farooq, W. (2018). Pyrolysis of high-ash sewage sludge: Thermo-kinetic study using TGA and artificial neural networks. *Fuel*, *233*, 529-538. https://doi.org/10.1016/j.fuel.2018.06.089

Nasir, M., Rahmawati, T., & Dara, F. (2019). Synthesis and characterization of biochar from crab shell by pyrolysis. IOP Conference Series: Materials Science and Engineering, 553(1). https://doi.org/10.1088/1757-899X/553/1/012031

Neeli, S. T., & Ramsurn, H. (2018). Synthesis and formation mechanism of iron nanoparticles in graphitized carbon matrices using biochar from biomass model compounds as a support. Carbon, 134, 480-490. https://doi.org/10.1016/j.carbon.2018.03.079

Nieto, A., Gascó, G., Paz-Ferreiro, J., Fernández, J. M., Plaza, C., & Méndez, A. (2016). The effect of pruning waste and biochar addition on brown peat based growing media properties. Scientia Horticulturae, 199, 142-148. https://doi.org/10.1016/j.scienta.2015.12.012

Nikolaou, I. E., Jones, N., & Stefanakis, A. (2021). Circular economy and sustainability: the past, the present and the future directions. *Circular Economy and Sustainability*, *1*(1), 1-20. https://doi.org/10.1007/s43615-021-00030-3

Oh, T.-K., Choi, B., Shinogi, Y., & Chikushi, J. (2012a). Characterization of biochar derived from three types of biomass. J. Fac. Agric. Kyushu Univ., 57(1), 61-66. https://doi.org/10.5109/22049

Oh, T. K., Choi, B., Shinogi, Y., & Chikushi, J. (2012b). Effect of pH conditions on actual and apparent fluoride adsorption by biochar in aqueous phase. Water, Air, & Soil Pollution, 223(7), 3729-3738. https://doi.org/10.1007/s11270-012-1144-2

Oh, S. Y., & Seo, Y. D. (2016). Sorption of halogenated phenols and pharmaceuticals to biochar: affecting factors and mechanisms. Environmental Science and Pollution Research, 23(2), 951-961. https://doi.org/10.1007/s11356-015-4201-8

Oleszczuk, P., & Hollert, H. (2011). Comparison of sewage sludge toxicity to plants and invertebrates in three different soils. Chemosphere, 83(4), 502-509. https://doi.org/10.1016/j.chemosphere.2010.12.061

Oni, B. A., Oziegbe, O., & Olawole, O. O. (2019). Significance of biochar application to the environment and economy. *Annals of Agricultural Sciences*, *64*(2), 222-236. https://doi.org/10.1016/j.aoas.2019.12.006

Palansooriya, K. N., Yang, Y., Tsang, Y. F., Sarkar, B., Hou, D., Cao, X., Meers, E., Rinklebe, J., Kim, K. H., Ok, Y. S. (2019). Occurrence of contaminants in drinking water sources and the potential of biochar for water quality improvement: A review. Critical Reviews in Environmental Science and Technology, 1-63. https://doi.org/10.1080/10643389.2019.1629803.

Palansooriya, K. N., Yang, Y., Tsang, Y. F., Sarkar, B., Hou, D., Cao, X., Meers, E., Rinklebe, J, Kim, K. H., Ok, Y. S. (2020). Occurrence of contaminants in drinking water sources and the potential of biochar for water quality improvement: A review. *Critical Reviews in*

Environmental Science and Technology, *50(6)*, 549-611. https://doi.org/10.1080/10643389.2019.1629803

Pariyar, P., Kumari, K., Jain, M. K., & Jadhao, P.S. (2020). Evaluation of change in biochar properties derived from different feedstock and pyrolysis temperature for environmental and agricultural application. Science of the Total Environment, 713, 136433. https://doi.org/10.1016/j.scitotenv.2019.136433

Pellera, F.-M., & Gidarakos, E. (2015). Effect of dried olive pomace – derived biochar on the mobility of cadmium and nickel in soil. Journal of Environmental Chemical Engineering, 3(2), 1163-1176. https://doi.org/10.1016/j.jece.2015.04.005

Pellera, F. M., Regkouzas, P., Manolikaki, I., & Diamadopoulos, E. (2021). Biochar production from waste biomass: Characterization and evaluation for agronomic and environmental applications. *Detritus*, *17*, 15-29. https://doi.org/10.31025/2611-4135/2021.15146

Phoungthong, K., Zhang, H., Shao, L. M., & He, P. J. (2018). Leaching characteristics and phytotoxic effects of sewage sludge biochar. Journal of Material Cycles and Waste Management, 20(4), 2089-2099. https://doi.org/10.1007/s10163-018-0763-0.

Pituello, C., Francioso, O., Simonetti, G., Pisi, A., Torreggiani, A., Berti, A., & Morari, F. (2015). Characterization of chemical–physical, structural and morphological properties of biochars from biowastes produced at different temperatures. Journal of Soils and Sediments, 15(4), 792-804. https://doi.org/10.1007/s11368-014-0964-7

Plaza, D., Artigas, J., Ábrego, J., Gonzalo, A., Sánchez, J. L., Dro, A. D., & Richardson, Y. (2019). Design and operation of a small-scale carbonization kiln for cashew nutshell valorization in Burkina Faso. Energy for Sustainable Development, 53, 71-80. https://doi.org/10.1016/j.esd.2019.10.005

Qiu, M., Hu, B., Chen, Z., Yang, H., Zhuang, L., & Wang, X. (2021). Challenges of organic pollutant photocatalysis by biochar-based catalysts. Biochar, 3(2), 117-123. https://doi.org/10.1007/s42773-021-00098-y

Qiu, M., Liu, L., Ling, Q., Cai, Y., Yu, S., Wang, S., Fu, D., Hu, B., & Wang, X. (2022a). Biochar for the removal of contaminants from soil and water: a review. Biochar, 4(1), 19. Rajapaksha, A. U., Chen, S. S., Tsang, D. C., Zhang, M., Vithanage, M., Mandal, S., Gao, B., Bolan, N. S., & Ok, Y. S. (2016). Engineered/designer biochar for contaminant

removal/immobilization from soil and water: potential and implication of biochar modification. Chemosphere, 148, 276-291. https://doi.org/10.1016/j.chemosphere.2016.01.043

Qiu, B., Shao, Q., Shi, J., Yang, C., & Chu, H. (2022b). Application of biochar for the adsorption of organic pollutants from wastewater: Modification strategies, mechanisms and challenges. *Separation and Purification Technology*, 121925. https://doi.org/10.1016/j.seppur.2022.121925

Rajkovich, S., Enders, A., Hanley, K., Hyland, C., Zimmerman, A. R., & Lehmann, J. (2012). Corn growth and nitrogen nutrition after additions of biochars with varying properties to a temperate soil. Biology and Fertility of Soils, 48(3), 271-284. DOI: 10.1007/s00374-011-0624-7.

Ramos, A., Monteiro, E., & Rouboa, A. (2022). Biomass pre-treatment techniques for the production of biofuels using thermal conversion methods–A review. *Energy Conversion and Management*, *270*, 116271. https://doi.org/10.1016/j.enconman.2022.116271

Randolph, P., Bansode, R.R., Hassan, O.A., Rehrah, D., Ravella, R., Reddy, M.R., Watts, D.W., Novak, J.M., & Ahmedna, M. (2017). Effect of biochars produced from solid organic municipal waste on soil quality parameters. Journal of Environmental Management, 192, 271-280. https://doi.org/10.1016/j.jenvman.2017.01.061

Rangabhashiyam, S., dos Santos Lins, P. V., de Magalhães Oliveira, L. M., Sepulveda, P., Ighalo, J. O., Rajapaksha, A. U., & Meili, L. (2022). Sewage sludge-derived biochar for the adsorptive removal of wastewater pollutants: A critical review. *Environmental Pollution*, *293*, 118581. https://doi.org/10.1016/j.envpol.2021.118581

Rathi, B. S., Kumar, P. S., & Show, P. L. (2021). A review on effective removal of emerging contaminants from aquatic systems: Current trends and scope for further research. *Journal of Hazardous Materials*, *409*, 124413. https://doi.org/10.1016/j.jhazmat.2020.124413

Rathi, B. S., & Kumar, P. S. (2021). Application of adsorption process for effective removal of emerging contaminants from water and wastewater. Environmental Pollution, 280, 116995. https://doi.org/10.1016/j.envpol.2021.116995

Regkouzas, P., & Diamadopoulos, E. (2019). Adsorption of selected organic micro-pollutants on sewage sludge biochar. *Chemosphere*, *224*, 840-851. https://doi.org/10.1016/j.chemosphere.2019.02.165

Regkouzas, P., Sygellou, L., & Diamadopoulos, E. (2023). Production and characterization of graphene oxide-engineered biochars and application for organic micro-pollutant adsorption from aqueous solutions. *Environmental Science and Pollution Research, 30*(37), 87810-87829. https://doi.org/10.1007/s11356-023-28549-y

Rehrah, D., Reddy, M.R., Novak, J.M., Bansode, R.R., Schimmel, K.A., Yu, J., Watts, D.W., & Ahmedna, M. (2014). Production and characterization of biochars from agricultural by-products for use in soil quality enhancement. Journal of Analytical and Applied Pyrolysis, 108, 301-309. https://doi.org/10.1016/j.jaap.2014.03.008

Rehrah, D., Bansode, R.R., Hassan, O., & Ahmedna, M. (2016). Physico-chemical characterization of biochars from solid municipal waste for use in soil amendment. Journal of Analytical and Applied Pyrolysis, 118, 42-53. https://doi.org/10.1016/j.jaap.2015.12.022

Richardson, S. D., & Kimura, S. Y. (2019). Water analysis: emerging contaminants and current issues. Analytical chemistry, 92(1), 473-505. https://doi.org/10.1021/acs.analchem.9b05269

Roy, J., Ghosh, S., Ojha, P. K., & Roy, K. (2019). Predictive quantitative structure–property relationship (QSPR) modeling for adsorption of organic pollutants by carbon nanotubes (CNTs). *Environmental Science: Nano, 6(1)*, 224-247. https://doi.org/10.1039/C8EN01059E

Rucińska-Sobkowiak, R. (2016). Water relations in plants subjected to heavy metal stresses. Acta Physiologiae Plantarum, 38. https://doi.org/10.1007/s11738-016-2277-5

Rybova K., Burcin B., Slavik, J. (2018). Spatial and non-spatial analysis of socio-demographic aspects influencing municipal solid waste generation in the czech republic. Detritus, 1(1), 3 - 7. https://doi.org/10.26403/detritus/2018.2

Severo, F. F., da Silva, L. S., Moscôso, J. S. C., Sarfaraz, Q., Rodrigues Júnior, L. F., Lopes, A. F., Marzari, L. B., & Molin, G. D. (2020). Chemical and physical characterization of rice husk biochar and ashes and their iron adsorption capacity. *SN Applied Sciences*, *2*, 1-9. https://doi.org/10.1007/s42452-020-3088-2

Shen, Y., Wang, J., Ge, X., & Chen, M. (2016). By-products recycling for syngas cleanup in biomass pyrolysis–An overview. *Renewable and Sustainable Energy Reviews, 59*, 1246-1268. https://doi.org/10.1016/j.rser.2016.01.077

Shen, Z., Zhang, Y., McMillan, O., Jin, F., & Al-Tabbaa, A. (2017). Characteristics and mechanisms of nickel adsorption on biochars produced from wheat straw pellets and rice husk.

Environmental Science and Pollution Research, 24(14), 12809-12819. https://doi.org/10.1007/s11356-017-8847-2

Singh, B., Dolk, M.M., Shen, Q., & Camps-Arbestain, M. (2017). Biochar pH, electrical conductivity and liming potential. In Biochar: A Guide to Analytical Methods, Balwant Singh, et al. (Eds), Csiro Publishing, Clayton, Australia, 23-38. https://doi.org/10.1071/9781486305100

Singh, S., Kumar, V., Dhanjal, D. S., Datta, S., Bhatia, D., Dhiman, J., Samuel, J., Prassad, R., & Singh, J. (2020). A sustainable paradigm of sewage sludge biochar: valorization, opportunities, challenges and future prospects. *Journal of Cleaner Production*, *269*, 122259. https://doi.org/10.1016/j.jclepro.2020.122259

Singh, E., Mishra, R., Kumar, A., Shukla, S. K., Lo, S. L., & Kumar, S. (2022). Circular economy-based environmental management using biochar: Driving towards sustainability. *Process Safety and Environmental Protection*, *163*, 585-600. https://doi.org/10.1016/j.psep.2022.05.056

Sivaranjanee, R., & Kumar, P. S. (2021). A review on remedial measures for effective separation of emerging contaminants from wastewater. *Environmental Technology & Innovation*, *23*, 101741. https://doi.org/10.1016/j.eti.2021.101741

Sizmur, T., Fresno, T., Akgül, G., Frost, H., & Moreno-Jiménez, E. (2017). Biochar modification to enhance sorption of inorganics from water. Bioresource technology, 246, 34-47. https://doi.org/10.1016/j.biortech.2017.07.082

Song, W., & Guo, M. (2012). Quality variations of poultry litter biochar generated at different pyrolysis temperatures. Journal of Analytical and Applied Pyrolysis, 94, 138-145. https://doi.org/10.1016/j.jaap.2011.11.018

Stefaniuk, M., & Oleszczuk, P. (2015). Characterization of biochars produced from residues from biogas production. Journal of Analytical and Applied Pyrolysis, 115, 157-165. https://doi.org/10.1016/j.jaap.2015.07.011

Stylianou, M., Christou, A., Dalias, P., Polycarpou, P., Michael, C., Agapiou, A., Papanastasiou, P., & Fatta-Kassinos, D. (2020). Physicochemical and structural characterization of biochar derived from the pyrolysis of biosolids, cattle manure and spent

coffee grounds. Journal of the Energy Institute, 93(5), 2063-2073. https://doi.org/10.1016/j.joei.2020.05.002

Suliman, W., Harsh, J.B., Abu-Lail, N.I., Fortuna, A.-M., Dallmeyer, I., & Garcia-Perez, M. (2016). Influence of feedstock source and pyrolysis temperature on biochar bulk and surface properties. Biomass and Bioenergy, 84, 37-48. https://doi.org/10.1016/j.biombioe.2015.11.010

Swat, A. A. A., Saleh, T. A., Ganiyu, S. A., Siddiqui, M. N., & Alhooshani, K. R. (2017). Preparation of activated carbon, zinc oxide and nickel oxide composites for potential application in the desulfurization of model diesel fuels. Journal of Analytical and Applied Pyrolysis, 128, 246-256. https://doi.org/10.1016/j.jaap.2017.10.004

Sygellou, L., Paterakis, G., Galiotis, C., & Tasis, D. (2016). Work function tuning of reduced graphene oxide thin films. The Journal of Physical Chemistry C, 120(1), 281-290. https://doi.org/10.1021/acs.jpcc.5b09234

Tag, A.T., Duman, G., Ucar, S., & Yanik, J. (2016). Effects of feedstock type and pyrolysis temperature on potential applications of biochar. Journal of Analytical and Applied Pyrolysis, 120, 200-206. https://doi.org/10.1016/j.jaap.2016.05.006

Taheran, M., Naghdi, M., Brar, S. K., Verma, M., & Surampalli, R. Y. (2018). Emerging contaminants: here today, there tomorrow!. *Environmental nanotechnology, monitoring & management*, *10*, 122-126. https://doi.org/10.1016/j.enmm.2018.05.010

Taherymoosavi, S., Verheyen, V., Munroe, P., Joseph, S., & Reynolds, A. (2017). Characterization of organic compounds in biochars derived from municipal solid waste. Waste Management, 67, 131-142. https://doi.org/10.1016/j.wasman.2017.05.052

Tan, X., Liu, Y., Zeng, G., Wang, X., Hu, X., Gu, Y., & Yang, Z. (2015). Application of biochar for the removal of pollutants from aqueous solutions. Chemosphere, 125, 70-85. https://doi.org/10.1016/j.chemosphere.2014.12.058

Tan, X. F., Liu, Y. G., Gu, Y. L., Xu, Y., Zeng, G. M., Hu, X. J., Liu, S. B., Wang, X., Liu, S. M., Li, J. (2016). Biochar-based nano-composites for the decontamination of wastewater: a review. Bioresource technology, 212, 318-333. https://doi.org/10.1016/j.biortech.2016.04.093

Tang, J., Lv, H., Gong, Y., & Huang, Y. (2015). Preparation and characterization of a novel graphene/biochar composite for aqueous phenanthrene and mercury removal. Bioresource technology, 196, 355-363. https://doi.org/10.1016/j.biortech.2015.07.047

Taskin, E., de Castro Bueno, C., Allegretta, I., Terzano, R., Rosa, A.H., & Loffredo, E. (2019). Multianalytical characterization of biochar and hydrochar produced from waste biomasses for environmental and agricultural applications. Chemosphere, 233, 422-430. https://doi.org/10.1016/j.chemosphere.2019.05.204

Tiwari, S. K., Bystrzejewski, M., De Adhikari, A., Huczko, A., & Wang, N. (2022). Methods for the conversion of biomass waste into value-added carbon nanomaterials: Recent progress and applications. *Progress in Energy and Combustion Science*, *92*, 101023. https://doi.org/10.1016/j.pecs.2022.101023

Tong, Y., McNamara, P. J., & Mayer, B. K. (2019). Adsorption of organic micropollutants onto biochar: a review of relevant kinetics, mechanisms and equilibrium. *Environmental Science: Water Research & Technology*, *5*(5), 821-838. https://doi.org/10.1039/C8EW00938D

Trakal, L., Raya-Moreno, I., Mitchell, K., & Beesley, L. (2017). Stabilization of metal(loid)s in two contaminated agricultural soils: Comparing biochar to its non-pyrolysed source material. Chemosphere, 181, 150-159. https://doi.org/10.1016/j.chemosphere.2017.04.064

Tran, H. N., You, S. J., & Chao, H. P. (2016). Effect of pyrolysis temperatures and times on the adsorption of cadmium onto orange peel derived biochar. Waste Management & Research, 34(2), 129-138. https://doi.org/10.1177/0734242X15615698

Tran, H. N., Tomul, F., Ha, N. T. H., Nguyen, D. T., Lima, E. C., Le, G. T., Chang, C. T., Masindi, V., & Woo, S. H. (2020). Innovative spherical biochar for pharmaceutical removal from water: Insight into adsorption mechanism. *Journal of hazardous materials*, *394*, 122255. https://doi.org/10.1016/j.jhazmat.2020.122255

Tripathi, M., Sahu, J. N., & Ganesan, P. (2016). Effect of process parameters on production of biochar from biomass waste through pyrolysis: a review. Renewable and Sustainable Energy Reviews, 55, 467-481. https://doi.org/10.1016/j.rser.2015.10.122

Uchimiya, M., Klasson, K.T., Wartelle, L.H., & Lima, I.M. (2011a). Influence of soil properties on heavy metal sequestration by biochar amendment: 1. Copper sorption isotherms and the release of cations. Chemosphere, 82(10), 1431-1437. https://doi.org/10.1016/j.chemosphere.2010.11.050

Uchimiya, M., Wartelle, L. H., Klasson, K. T., Fortier, C. A., & Lima, I. M. (2011b). Influence of pyrolysis temperature on biochar property and function as a heavy metal sorbent in soil.

Journal of agricultural and food chemistry, 59(6), 2501-2510. https://doi.org/10.1021/jf104206c.

Uddin, M. N., Techato, K., Taweekun, J., Rahman, M. M., Rasul, M. G., Mahlia, T. M. I., & Ashrafur, S. M. (2018). An overview of recent developments in biomass pyrolysis technologies. *Energies*, *11*(11), 3115. https://doi.org/10.3390/en11113115

US EPA (1986). Method 9081. Cation exchange capacity of soils (sodium acetate).

Varsha, M., Kumar, P. S., & Rathi, B. S. (2021). A review on recent trends in the removal of emerging contaminants from aquatic environment using low-cost adsorbents. *Chemosphere, 132270*. https://doi.org/10.1016/j.chemosphere.2021.132270

Velli, P., Manolikaki, I., & Diamadopoulos, E. (2021). Effect of biochar produced from sewage sludge on tomato (Solanum lycopersicum L.) growth, soil chemical properties and heavy metal concentrations. *Journal of Environmental Management*, *297*, 113325. https://doi.org/10.1016/j.jenvman.2021.113325

Wang, Y., Xiao, X., & Chen, B. (2018). Biochar Impacts on Soil Silicon Dissolution Kinetics and their Interaction Mechanisms. Scientific Reports, 8(1), 1-11. https://doi.org/10.1038/s41598-018-26396-3

Wang, X., Chi, Q., Liu, X., & Wang, Y. (2019). Influence of pyrolysis temperature on characteristics and environmental risk of heavy metals in pyrolyzed biochar made from hydrothermally treated sewage sludge. Chemosphere, 216, 698-706. https://doi.org/10.1016/j.chemosphere.2018.10.189

Wang, J., & Wang, S. (2019). Preparation, modification and environmental application of biochar: a review. Journal of Cleaner Production, 227, 1002-1022. https://doi.org/10.1016/j.jclepro.2019.04.282

Wang, J., & Zhang, M. (2020). Adsorption characteristics and mechanism of bisphenol A by magnetic biochar. *International journal of environmental research and public health*, *17*(3), 1075. https://doi.org/10.3390/ijerph17031075

Weber, K., & Quicker, P. (2018). Properties of biochar. *Fuel*, *217*, 240-261. https://doi.org/10.1016/j.fuel.2017.12.054

Wei, L., Huang, Y., Li, Y., Huang, L., Mar, N. N., Huang, Q., & Liu, Z. (2017). Biochar characteristics produced from rice husks and their sorption properties for the acetanilide

herbicide metolachlor. *Environmental Science and Pollution Research*, *24*, 4552-4561. https://doi.org/10.1007/s11356-016-8192-x

Xie, Y., Wang, L., Li, H., Westholm, L. J., Carvalho, L., Thorin, E., Yu, Z., Yu, X., & Skreiberg, Ø. (2022). A critical review on production, modification and utilization of biochar. *Journal of Analytical and Applied Pyrolysis*, *161*, 105405. https://doi.org/10.1016/j.jaap.2021.105405

Xiong, S., Wu, Z., & Li, Z. (2021). Facile fabrication of robust, versatile, and recyclable biochar-graphene oxide composite monoliths for efficient removal of different contaminants in water. Chemosphere, 132418. https://doi.org/10.1016/j.chemosphere.2021.132418

Yao, Y., Gao, B., Inyang, M., Zimmerman, A.R., Cao, X., Pullammanappallil, P., & Yang, L. (2011). Biochar derived from anaerobically digested sugar beet tailings: Characterization and phosphate removal potential. Bioresource Technology, 102(10), 6273-6278. https://doi.org/10.1016/j.biortech.2011.03.006

Yargicoglu, E.N., Sadasivam, B.Y., Reddy, K.R., Spokas, K. (2015). Physical and chemical characterization of waste wood derived biochars. Waste Management, 36, 256-268. https://doi.org/10.1016/j.wasman.2014.10.029

Yi, S., Gao, B., Sun, Y., Wu, J., Shi, X., Wu, B., & Hu, X. (2016). Removal of levofloxacin from aqueous solution using rice-husk and wood-chip biochars. Chemosphere, 150, 694-701. https://doi.org/10.1016/j.chemosphere.2015.12.112

Yin, W., Guo, Z., Zhao, C., & Xu, J. (2019). Removal of Cr (VI) from aqueous media by biochar derived from mixture biomass precursors of Acorus calamus Linn. and feather waste. Journal of Analytical and Applied Pyrolysis, 140, 86-92. https://doi.org/10.1016/j.jaap.2019.04.024.

Zeng, X., Xiao, Z., Zhang, G., Wang, A., Li, Z., Liu, Y., Wang, H., Zeng, Q., Liang, Y., & Zou, D. (2018). Speciation and bioavailability of heavy metals in pyrolytic biochar of swine and goat manures. Journal of Analytical and Applied Pyrolysis, 132, 82–93. https://doi.org/10.1016/j.jaap.2018.03.012

Zhang, K., Sun, P., Faye, M.C.A., & Zhang, Y. (2018). Characterization of biochar derived from rice husks and its potential in chlorobenzene degradation. Carbon, 130, 730-740. https://doi.org/10.1016/j.carbon.2018.01.036

Zhang, M., Gao, B., Yao, Y., Xue, Y., & Inyang, M. (2012). Synthesis, characterization, and environmental implications of graphene-coated biochar. Science of the Total Environment, 435, 567-572. https://doi.org/10.1016/j.scitotenv.2012.07.038

Zhang, Y., Cao, B., Zhao, L., Sun, L., Gao, Y., Li, J., & Yang, F. (2018). Biochar-supported reduced graphene oxide composite for adsorption and coadsorption of atrazine and lead ions. Applied Surface Science, 427, 147-155. https://doi.org/10.1016/j.apsusc.2017.07.237

Zhang, X., Zhang, P., Yuan, X., Li, Y., & Han, L. (2020). Effect of pyrolysis temperature and correlation analysis on the yield and physicochemical properties of crop residue biochar. Bioresource technology, 296, 122318. https://doi.org/10.1016/j.biortech.2019.122318

Zhao, S.-X., Ta, N., & Wang, X.-D. (2017). Effect of temperature on the structural and physicochemical properties of biochar with apple tree branches as feedstock material. Energies, 10(9), 1293. https://doi.org/10.3390/en10091293

Zhao, D., Luo, Y., Feng, Y. Y., He, Q. P., Zhang, L. S., Zhang, K. Q., & Wang, F. (2021). Enhanced adsorption of phosphorus in soil by lanthanum-modified biochar: improving phosphorus retention and storage capacity. Environmental Science and Pollution Research, 28(48), 68982-68995. https://doi.org/10.1007/s11356-021-15364-6

Zheng, X., Shi, T., Song, W., Xu, L., & Dong, J. (2019). Biochar of distillers' grains anaerobic digestion residue: Influence of pyrolysis conditions on its characteristics and ammonium adsorptive optimization. Waste Management & Research, 0734242X19893021. https://doi.org/10.1177/0734242X19893021

Zhou, J., Chen, H., Thring, R. W., & Arocena, J. M. (2019). Chemical pretreatment of rice straw biochar: effect on biochar properties and hexavalent chromium adsorption. *International Journal of Environmental Research*, *13*, 91-105. https://doi.org/10.1007/s41742-018-0156-1

Zhou, Y., Qin, S., Verma, S., Sar, T., Sarsaiya, S., Ravindran, B., Anil, K. P., Parameswaran, B., Sunita, V., Reeta, R. S., Zengqiang, Z., Awasthi, M. K. (2021). Production and beneficial impact of biochar for environmental application: A comprehensive review. *Bioresource Technology, 125451*. https://doi.org/10.1016/j.biortech.2021.125451